SAND76-8232
Unlimited Release

Momentum and Energy Transport in the Accelerated Fully Rough Turbulent Boundary Layer

H. W. Coleman

Prepared by Sandia Laboratories, Albuquerque, New Mexico 87115 and Livermore, California 94550 for the United States Energy Research and Development Administration under Contract AT (29-1) 789

Printed June 1976

Sandia Laboratories

2900 Q(7-73)

When printing a copy of any digitized SAND Report, you are required to update the markings to current standards.

Issued by Sandia Laboratories, operated for the United States Energy Research and Development Administration by Sandia Corporation.

NOTICE

This report was prepared as an account of work sponsored by the United States Government. Neither the United States nor the United States Energy Research and Development Administration, nor any of their employees, nor any of their contractors, subcontractors, or their employees, makes any warranty, express or implied, or assumes any legal liability or responsibility for the accuracy, completeness or usefulness of any information, apparatus, product or process disclosed, or represents that its use would not infringe privately owned rights.

SAND76-8232
Unlimited Release
Printed June 1976

MOMENTUM AND ENERGY TRANSPORT IN THE ACCELERATED FULLY ROUGH TURBULENT BOUNDARY LAYER

H. W. Coleman
Combustion Research Division 8115
Sandia Laboratories, Livermore

ABSTRACT

The behavior of the fully rough turbulent boundary layer subjected to favorable pressure gradients was investigated experimentally using a porous test surface composed of densely packed spheres of uniform size. Measurements of profiles of mean velocity, mean temperature and the components of the Reynolds stress tensor are reported for both unblown and blown layers. Stanton numbers were determined from energy balances on the test surface and skin friction coefficients from measurements of the Reynolds shear stress and mean velocity.

A new acceleration parameter, K_r, for fully rough layers is defined and shown to be dependent on a characteristic roughness dimension but independent of molecular viscosity. For K_r constant and the blowing fraction, F, constant and greater than or equal to zero, it is shown that the fully rough turbulent boundary layer reaches an equilibrium state in which profiles of the mean velocity and the Reynolds stress tensor components are similar in the flow direction and skin friction coefficient, momentum thickness, boundary layer shape factor, and the Clauser shape factor and pressure gradient parameter all become constant. The thermal data indicate the possibility that such a layer, with wall temperature constant, may approach a state of equilibrium in the thermal sense, also. Such a state would be characterized by Stanton number becoming constant, enthalpy thickness approaching an asymptote, and temperature profiles exhibiting similarity in the flow direction.

For fully rough turbulent flow, acceleration causes an increase in Stanton number compared to zero pressure gradient values at the same enthalpy thickness, Reynolds number, or position. For the present range of accelerations, these increases were approximately 10 and 20% for the unblown and blown cases, respectively. Data for variable test surface temperature cases

show that nondimensionally equivalent positive axial gradients of freestream velocity and temperature potential across the boundary layer have identical effects on Stanton number. The fully rough Stanton number behavior observed in this study is contrary to that previously reported for unblown accelerated smooth wall layers.

Acceleration of a fully rough layer decreases the normalized turbulent kinetic energy and makes the turbulence field much less isotropic in the inner region (for F equal zero) compared to zero pressure gradient fully rough layers. The values of the Reynolds shear stress correlation coefficients, however, are unaffected by acceleration or blowing and are identical with values previously reported for zero pressure gradient smooth and rough wall flows. Increasing values of roughness Reynolds number with acceleration indicate that the fully rough layer does not tend toward the transitionally rough or smooth wall state when accelerated.

An integral prediction method is presented which successfully describes Stanton number behavior in a fully rough turbulent flow with variable velocity, wall temperature, and blowing using only a kernel function determined from zero pressure gradient flow with an unheated starting length.

Preface

This report is the doctoral thesis of the author, who attended Stanford University on Sandia's Doctoral Study Program from June 1973 to August 1975. The research program at Stanford was supported by the Office of Naval Research, Contract N00014-67-A-0112-0072.

The author wishes to acknowledge the support of the members of his committee at Stanford--Professors R. J. Moffat, W. M. Kays and W. C. Reynolds--and the many people at Sandia who made possible the author's participation in the Doctoral Study Program.

TABLE OF CONTENTS

	Page
Preface	iii
Abstract	iv
Table of Contents	vi
List of Figures	viii
Nomenclature	xi
Chapter	
1 INTRODUCTION	1
1.1 Background	2
1.2 Objectives	4
1.3 The Experiment	5
1.4 General Organization	7
2 THE EQUILIBRIUM FULLY ROUGH TURBULENT BOUNDARY LAYER WITH PRESSURE GRADIENT AND TRANSPIRATION	10
2.1 Previous Studies of Equilibrium Turbulent Boundary Layers	11
2.2 Conditions for Equilibrium in the Fully Rough Turbulent Boundary Layer with Pressure Gradient and Transpiration	13
2.3 Choice of Length Scale in Acceleration Parameter K_r	16
3 EXPERIMENTAL RESULTS	19
3.1 Zero Pressure Gradient Data	20
3.2 Data with Acceleration	24
3.2.1 Integral Quantities	26
3.2.2 Mean Velocity and Temperature Profiles	29
3.2.3 Reynolds Stress Tensor Components	33
3.2.4 Turbulent Prandtl Number and Related Quantities	39
3.3 Heat Transfer Predictions and Supplementary St Data	44
4 EFFECTS OF ACCELERATION ON THE FULLY ROUGH TURBULENT BOUNDARY LAYER	81
5 CONCLUSIONS	87
References	90
Appendices	
I DESCRIPTION OF EXPERIMENTAL APPARATUS AND MEASUREMENT TECHNIQUES	96
II QUALIFICATION TESTS	105

Appendices		Page
III	INDUCED TRANSPIRATION EFFECTS ON ACCELERATION DATA	108
IV	TABULATION OF EXPERIMENTAL DATA	110

LIST OF FIGURES

Figure		Page
1-1	Schematic of the Experimental Apparatus	8
1-2	Closeup Photograph of the Rough Test Surface	9
3-1	Zero Pressure Gradient Stanton Number Data	49
3-2	Zero Pressure Gradient Skin Friction Coefficient Data . .	49
3-3	Typical Mean Velocity Profile for Fully Rough, Zero Pressure Gradient Flow	50
3-4	Components of Turbulent Kinetic Energy for Fully Rough, Zero Pressure Gradient Flow	50
3-5	Summary Data for $K_r = 0.15 \times 10^{-3}$, F = 0 Equilibrium Acceleration Case	51
3-6	Summary Data for $K_r = 0.29 \times 10^{-3}$, F = 0 Equilibrium Acceleration Case	52
3-7	Summary Data for $K_r = 0.29 \times 10^{-3}$, F = 0.0039 Equilibrium Acceleration Case	53
3-8	Summary Data for $K = 0.28 \times 10^{-6}$, F = 0 Nonequilibrium Acceleration Case	54
3-9	Comparison of Enthalpy Thickness Data and Solution for Equilibrium Enthalpy Thickness Behavior	55
3-10	Equilibrium Acceleration Stanton Number Data vs. (Enthalpy Thickness/Sphere Radius)	55
3-11	Skin Friction Coefficient Data vs. (Momentum Thickness/Sphere Radius)	56
3-12	Thermal and Velocity Boundary Layer Thicknesses Variation with Axial Distance	57
3-13	Enthalpy Thickness Variation with Axial Distance	58
3-14	Roughness Reynolds Number Variation with Axial Distance	59
3-15	Mean Velocity Profiles Illustrating Similarity in Flow Direction ($K_r = 0.15 \times 10^{-3}$)	60
3-16	Mean Velocity Profiles Illustrating Similarity in Flow Direction ($K_r = 0.29 \times 10^{-3}$, F = 0)	60
3-17	Mean Velocity Profiles Illustrating Similarity in Flow Direction ($K_r = 0.29 \times 10^{-3}$, F = 0.0039)	61
3-18	Mean Velocity Profiles Illustrating Lack of Similarity in Flow Direction ($K = 0.28 \times 10^{-6}$)	61
3-19	Mean Velocity Profile Plotted Using Shifted Wall Position ($K_r = 0.15 \times 10^{-3}$)	62

Figure		Page
3-20	Mean Velocity Profile Plotted Using Shifted Wall Position ($K_r = 0.29 \times 10^{-3}$, F = 0)	62
3-21	Comparison of Blown and Unblown Mean Velocity Profiles at Same Axial Position ($K_r = 0.29 \times 10^{-3}$)	63
3-22	Nondimensional Mean Temperature Profiles Illustrating Similarity in Flow Direction ($K_r = 0.15 \times 10^{-3}$)	63
3-23	Nondimensional Mean Temperature Profiles Illustrating Similarity in Flow Direction ($K_r = 0.29 \times 10^{-3}$, F = 0) .	64
3-24	Nondimensional Mean Temperature Profiles Illustrating Similarity in Flow Direction, $K_r = 0.29 \times 10^{-3}$, F = 0.0039)	64
3-25	Nondimensional Mean Temperature Profiles for Non-equilibrium Acceleration Run ($K = 0.28 \times 10^{-6}$)	65
3-26	Nondimensional Mean Temperature Plotted versus Non-dimensional Mean Velocity ($K_r = 0.15 \times 10^{-3}$)	65
3-27	Comparison of Blown and Unblown Nondimensional Mean Temperature Profiles at Same Axial Position ($K_r = 0.29 \times 10^{-3}$)	66
3-28	Profiles of Turbulent Kinetic Energy Components Illustrating Similarity in Flow Direction ($K_r = 0.15 \times 10^{-3}$).	66
3-29	Profiles of Reynolds Shear Stress Compared at Two Axial Positions ($K_r = 0.15 \times 10^{-3}$)	67
3-30	$\overline{u'^2}/U_\infty^2$ Profiles Compared for $K_r = 0$ and $K_r = 0.15 \times 10^{-3}$	67
3-31	Profiles of Components of Turbulent Kinetic Energy Compared for $K_r = 0$ and $K_r = 0.15 \times 10^{-3}$	68
3-32	Profiles of Components of Turbulent Kinetic Energy Compared for $K_r = 0$ and $K_r = 0.29 \times 10^{-3}$, F = 0 . . .	68
3-33	Profiles of Components of Turbulent Kinetic Energy Compared for $K_r = 0$ and $K = 0.28 \times 10^{-6}$	69
3-34	Profiles of Components of Turbulent Kinetic Energy Compared for $K_r = 0$, F = 0.0039 and $K_r = 0.29 \times 10^{-3}$, F = 0.0039	69
3-35	Comparison of Blown and Unblown Profiles of $\overline{u'^2}/U_\infty^2$ for Unaccelerated ($K_r = 0$) and Accelerated ($K_r = 0.29 \times 10^{-3}$) Cases	70
3-36	Comparison of Reynolds Shear Stress Profiles for $K_r = 0$ and $K_r = 0.15 \times 10^{-3}$	70
3-37	Distribution of Reynolds Shear Stress Correlation Coefficients through the Boundary Layer	71
3-38	Comparison of Turbulent Prandtl Numbers Measured by Pimenta[2] and Calculated by Present Method for $K_r = 0$.	72

Figure		Page
3-39	Turbulent Prandtl Number Distributions for the Acceleration Cases of the Present Study	72
3-40	Mixing Length Distributions for the Equilibrium Acceleration Cases of the Present Study	73
3-41	τ^+ and Q^+ Distributions for the $K_r = 0.29 \times 10^{-3}$, $F = 0$ and $F = 0.0039$ Runs	74
3-42	Comparison of the Unblown $\overline{v't'}/U_\tau T_\tau$ Profiles for the Equilibrium Accelerations of the Present Study with the Unaccelerated Profiles for Smooth and Rough Wall Layers	75
3-43	Calculated Distribution of the Nondimensional Turbulent Kinetic Energy Production for $K_r = 0$ and $K_r = 0.15 \times 10^{-3}$	76
3-44	Comparison of St Data and Interpolation Expression for U_∞, T_w and F Constant	77
3-45	Comparison of Unheated Starting Length St Data with Results of Kernel Solution for U_∞ and F Constant	77
3-46	Comparison of St Data and Prediction for a Bilinear Variation of T_w with U_∞ Constant, $F = 0$	78
3-47	Comparison of St Data and Predictions for $K = 0.28 \times 10^{-6}$, $F = 0$ Run Both With and Without an Unheated Starting Length	78
3-48	Comparison of St Data and Prediction for $K_r = 0.50 \times 10^{-3}$, $F = 0$ Run with T_w Constant	79
3-49	Comparison of St Data and Predictions for Arbitrary U_∞ Variation with Steps in F, F Variable and T_w Constant	80
3-50	Comparison of St Data and Predictions for Arbitrary U_∞ Variation with Steps in F, F Variable and a Step in T_w in the Blowing Region	80
I-1	Cross-Section of Typical Test Plate -- Casting Configuration	103
I-2	Schematic of the Horizontal Hot-Wire Probe Configuration	103
I-3	Schematic of the Rotatable Slant Hot-Wire Probe Configuration	104
I-4	Coordinate Systems for Analysis of Slant-Wire Directional Characteristics	104

NOMENCLATURE

B_h	Blowing parameter, F/St
$C_f/2$	Skin friction coefficient, $\tau_w/(\rho U_\infty^2)$
C_p	Specific heat of fluid
E	Turbulent kinetic energy, $\rho q^2/2$
e'	Fluctuating voltage
F	Blowing fraction, $\rho_w v_o/\rho_\infty U_\infty$
G	Clauser shape factor, Equation 2.1
H	Shape factor, δ_1/δ_2
I	Total enthalpy referenced to freestream, $(i + U^2/2) - (i_\infty + U_\infty^2/2)$
i	Static enthalpy
k	Thermal conductivity
k_s	Equivalent sand grain roughness
K	Smooth wall acceleration parameter, $(\nu/U_\infty^2)(dU_\infty/dx)$
K_r	Fully rough acceleration parameter, $(r/U_\infty)(dU_\infty/dx)$

ℓ	Mixing length
ℓ	x-position of step in wall temperature
P	Mean pressure
p'	Fluctuating pressure
$\mathcal{P}$	Turbulent kinetic energy production, Equation 3.27
Pr_T	Turbulent Prandtl number, $\varepsilon_M/\varepsilon_H$
$\dot{q}''$	Heat flux
q^2	$\overline{u'^2} + \overline{v'^2} + \overline{w'^2}$
Q^+	$\dot{q}''/\dot{q}''_w$
r	Radius of spheres comprising test surface
Re_k	Roughness Reynolds number, $k_s\ U_\tau/\nu$
Re_{δ_2}	Momentum thickness Reynolds number, $\delta_2\ U_\infty/\nu$
Re_{Δ_2}	Enthalpy thickness Reynolds number, $\Delta_2\ U_\infty/\nu$
R_{uv}	$-\overline{u'v'} \Big/ \sqrt{\overline{u'^2}\ \overline{v'^2}}$
R_{q^2}	$-\overline{u'v'}/q^2$
St	Stanton number, $\dot{q}''_w/[\rho_\infty\ U_\infty\ C_p\ (T_w - T_{\infty,o})]$
St_o	Stanton number for U_∞, T_w, F constant
t'	Fluctuating temperature

T	Mean temperature
T_w	Wall temperature
$T_{\infty,o}$	Total freestream temperature
ΔT	$(T_w - T_{\infty,o})$
T_τ	$(\Delta T)\ St/\sqrt{C_f/2}$
u	Instantaneous longitudinal velocity
u'	Longitudinal velocity fluctuation
u_{eff}	Instantaneous effective velocity sensed by the hot wire
U	Mean longitudinal velocity
U_∞	Freestream velocity
U_τ	Friction velocity, $U_\infty \sqrt{C_f/2}$
v	Instantaneous velocity normal to surface
v'	Normal velocity fluctuation
v_o	Velocity of transpired fluid at the wall
w	Instantaneous transverse velocity
w'	Transverse velocity fluctuation
x	Longitudinal coordinate
y	Coordinate normal to surface

Δy	y-coordinate shift
z	Transverse coordinate
α	Thermal diffusivity
β	Pressure gradient parameter, Equation 2.2
Δ	Thermal boundary layer thickness, $(T_w - T)/(T_w - T_\infty) = 0.99$
Δ_2	Enthalpy thickness, $\int_0^\infty \frac{\rho U}{\rho_\infty U_\infty} \left(\frac{T - T_\infty}{T_w - T_\infty}\right) dy$
δ	Momentum boundary layer thickness, $U/U_\infty = 0.99$
δ_1	Displacement thickness, $\int_0^\infty \left(1 - \frac{\rho U}{\rho_\infty U_\infty}\right) dy$
δ_2	Momentum thickness, $\int_0^\infty \frac{\rho U}{\rho_\infty U_\infty} \left(1 - \frac{U}{U_\infty}\right) dy$
ε_H	Eddy diffusivity for heat, Equation 3.21
ε_M	Eddy diffusivity for momentum, Equation 3.20
κ	Karman constant
ν	Kinematic viscosity
ρ	Density
τ	Shear stress
τ^+	τ/τ_w

Subscripts

a	Position where K or K_r becomes constant
w	Wall
∞	Freestream

Superscripts

$\overline{}$	Mean (time-averaged) value

CHAPTER 1. INTRODUCTION

Although turbulent flow has been a prime area of both theoretical and experimental research for the past several decades, the present understanding of the behavior and basic mechanisms of tubulence fields is rather tenuous, at best. Experimental data on turbulent boundary layers is either very limited or nonexistent for many classes of boundary conditions. With the recent advent of more sophisticated prediction schemes and turbulence models, requirements for more detailed data on the turbulence field have increased. Measurements of skin friction, Stanton number, and mean temperature and velocity fields no longer provide a sufficient data base from which turbulence behavior may be examined. Additional measurements of the turbulence quantities (fluctuations, correlations) are required.

An experimental study of the effects of roughness on the fluid dynamics and heat transfer in the turbulent boundary layer has been in progress at Stanford for the past several years. Results of this investigation for zero pressure gradient flows have been reported previously [1,2]. The present study considers the effects of acceleration on a turbulent boundary layer in the fully rough state. This subject was investigated not only because of its importance in the flow in nozzles and over turbine blades and reentry vehicles, but also to provide more information on the nature of turbulence by observing the response of the turbulence field to the imposed perturbations (roughness and acceleration).

1.1 Background

Discussions of the literature on turbulent flows over rough surfaces have been presented previously by Healzer [1] and Pimenta [2] and will not be repeated here. In this section a brief introduction on the effects of roughness on a turbulent boundary layer will be made, followed by brief reviews of the zero pressure gradient results reported previously for the present rough surface, the results of accelerated smooth wall turbulent boundary layer studies, and the few previous investigations of accelerated turbulent flow over rough surfaces.

The influence of surface roughness on turbulent flows is usually divided into three regimes, which are characterized by the magnitude of the "roughness Reynolds number," Re_k, where

$$Re_k = \frac{k_s U_\tau}{\nu} \tag{1.1}$$

The equivalent sand grain roughness parameter, k_s, is a commonly used, single-length-scale descriptor of rough surfaces determined by comparison with Nikuradse's [3] classic rough pipe flow experiments. For $Re_k \leq 5$, the roughness elements are contained entirely within the viscous sublayer and the flow is termed "smooth." For $5 < Re_k < 55\text{-}70$ some of the elements protrude through the sublayer, and the flow is called "transitionally rough". For $Re_k > 55\text{-}70$ the viscous sublayer is effectively destroyed, and the flow is termed "fully rough".

In general, skin friction coefficients and Stanton numbers are greater in a turbulent boundary layer influenced by roughness than in a smooth wall layer at the same Reynolds number. This causes larger temperature and velocity defects through the layer and hence thicker boundary layers, since more freestream fluid is entrained.

Experimental results for zero pressure gradient turbulent boundary layers on the present rough surface were reported by Healzer [1] and Pimenta [2]. Healzer constructed the present experimental apparatus and reported $C_f/2$ and St data both with and without blowing for several velocities which included the transitionally rough and fully rough flow regimes. He confirmed that, for fully rough flow over the present surface, both $C_f/2$ and St were independent of Reynolds number, i.e.

$$C_f/2 = f\left(\frac{\delta_2}{r}, F\right) \tag{1.2}$$

$$St = g\left(\frac{\Delta_2}{r}, F\right) \tag{1.3}$$

Pimenta [2] reported results of an extensive investigation of the fluid dynamics and heat transfer in both transitionally rough and fully rough zero pressure gradient layers both with and without blowing. His observations on the fully rough state included:

(1) The effect of roughness on the turbulence field structure extends over most of the layer.

(2) Blowing makes the layer behave as if the surface has physically larger roughness elements.

(3) For very large enthalpy thicknesses, the Stanton number appears to converge to an asymptotic value.

(4) Reynolds shear stress correlation coefficients are unchanged from the values reported for smooth wall flows.

The response of smooth wall boundary layers to acceleration is discussed in the summary report by Kays and Moffat [4]. Briefly, smooth wall layer accelerations are characterized by the acceleration parameter, $K = \frac{\nu}{U_\infty^2}\frac{dU_\infty}{dx}$.

Above a certain value of K, the turbulent layer develops toward a state resembling laminar flow. For a given Reynolds number, Stanton number decreases with increasing K, and the profiles of u'^2/U_∞^2 are lowered with acceleration [5]. In a constant K flow, the smooth wall turbulent boundary layer reaches an asymptotic state where mean profiles are similar, Re_{δ_2} and $C_f/2$ are constant, and boundary layer thickness decreases.

Previously published studies of the combined effects of acceleration and roughness on the turbulent boundary layer have reported only values of wall heat flux. Reshotko, et al. [6], and Banerian and McKillop [7] investigated nozzle wall flows, while Chen [8] cited experimental results for flow over hemispheres. No boundary layer information was obtained in any of these studies.

1.2 Objectives

This investigation was undertaken to determine the effects of acceleration on the fluid dynamics and heat transfer in the fully rough turbulent boundary layer. Specific objectives were:

(1) To define and experimentally verify the conditions required for equilibrium in the fully rough turbulent boundary layer with pressure gradient and transpiration.

(2) To obtain a comprehensive fluid dynamic and thermal data set for both equilibrium and nonequilibrium accelerations of the fully rough turbulent boundary layer.

(3) To examine the behavior of the mean and turbulence fields in the accelerated fully rough turbulent boundary layer .

(4) To investigate the effect of blowing on the equilibrium accelerated layer.

1.3 The Experiment

A brief description of the experimental apparatus and measurement techniques will be given in this section. Additional information is provided in Appendix I.

The Stanford Roughness Rig (Figure 1-1) is a closed-loop wind tunnel using air as both the primary and transpiration fluids. Air temperature is controlled using water-cooled heat exchangers in both the primary and transpiration loops. The eight-foot long, 20-inch wide test section is four inches high at its entrance. A flexible plexiglass upper wall (constructed in five sections connected by thin plexiglass joints) can be adjusted to give the desired variation in U_∞.

The test surface consists of 24 plates each four inches in the axial direction. The plates (Figure 1-2) are 0.5 inch thick and uniformly porous. They are constructed of 11 layers of 0.050-inch diameter Oxygen-Free High Conductivity (OFHC) copper spheres packed in the most dense array and brazed together. This configuration produces a rough test surface which is uniform and deterministic.

Each plate has individual electrical power and transpiration air controls and thermocouples for determining plate temperature. Stanton number is determined by subtracting the plate losses (known from energy balance qualification tests) from the measured power input. Uncertainty of the St data is within ± 0.0001 Stanton number units (i.e., if St = 0.00200, the uncertainty is within ± 5%).

The Stanton number data reported here were taken with a wall-to-freestream temperature difference of approximately 30°F to maintain a constant property boundary layer. Unless specifically stated otherwise, all St data presented are for constant wall temperature. The freestream

velocity at the test section inlet was a nominal 88 ft/sec, and all data were taken with a 1/2" wide, 1/32" high phenolic trip installed three inches inside the nozzle exit. The turbulent boundary layer was in a fully rough state for all cases reported.

Mean temperature profiles were measured with a 0.003-inch diameter, butt-welded, Chromel-constantan thermocouple mounted in a traversing probe holder. The design was similar to that of Blackwell [9].

All velocity measurements were made in an isothermal flow using linearized, constant temperature hot-wire anemometry. Measurements of U and $\overline{u'^2}$ were obtained using a horizontal wire, while measurements of $\overline{v'^2}$, $\overline{w'^2}$ and $\overline{u'v'}$ were made with a rotatable, 45° slant wire.

The physical size of the Roughness Rig and the porosity of the plates imposed limitations on the strengths of the accelerations which could be investigated. The height of the tunnel (four inches at the nozzle exit) limited both the length and severity of the acceleration region since interference of the top wall boundary layer with that on the test surface was carefully avoided. Also, since the plates were porous, the pressure gradient in the axial direction induced flow through the plates even with the transpiration supply valves closed. An analysis and discussion of this effect is presented in Appendix III. No effects of the induced transpiration were apparent in the data. It was concluded that the quantitative effect of the induced transpiration was negligible, certainly for the mildest and also the blown acceleration runs, and that the qualitative trends in all the data (and the conclusions drawn from them) were unaffected.

1.4 General Organization

The general organization of the results presented in the following chapters is described below. In Chapter 2 the concept of "equilibrium" in turbulent boundary layers is discussed, and the requirements for establishing equilibrium in the fully rough turbulent boundary layer with pressure gradient and transpiration are developed. The experimental data are presented in Chapter 3, and characteristics and trends are discussed. An integrated discussion of the effects of acceleration on the fully rough turbulent boundary layer is given in Chapter 4, and Chapter 5 contains the conclusions of the study.

Additional information and tabular data listings are contained in Appendices I - IV.

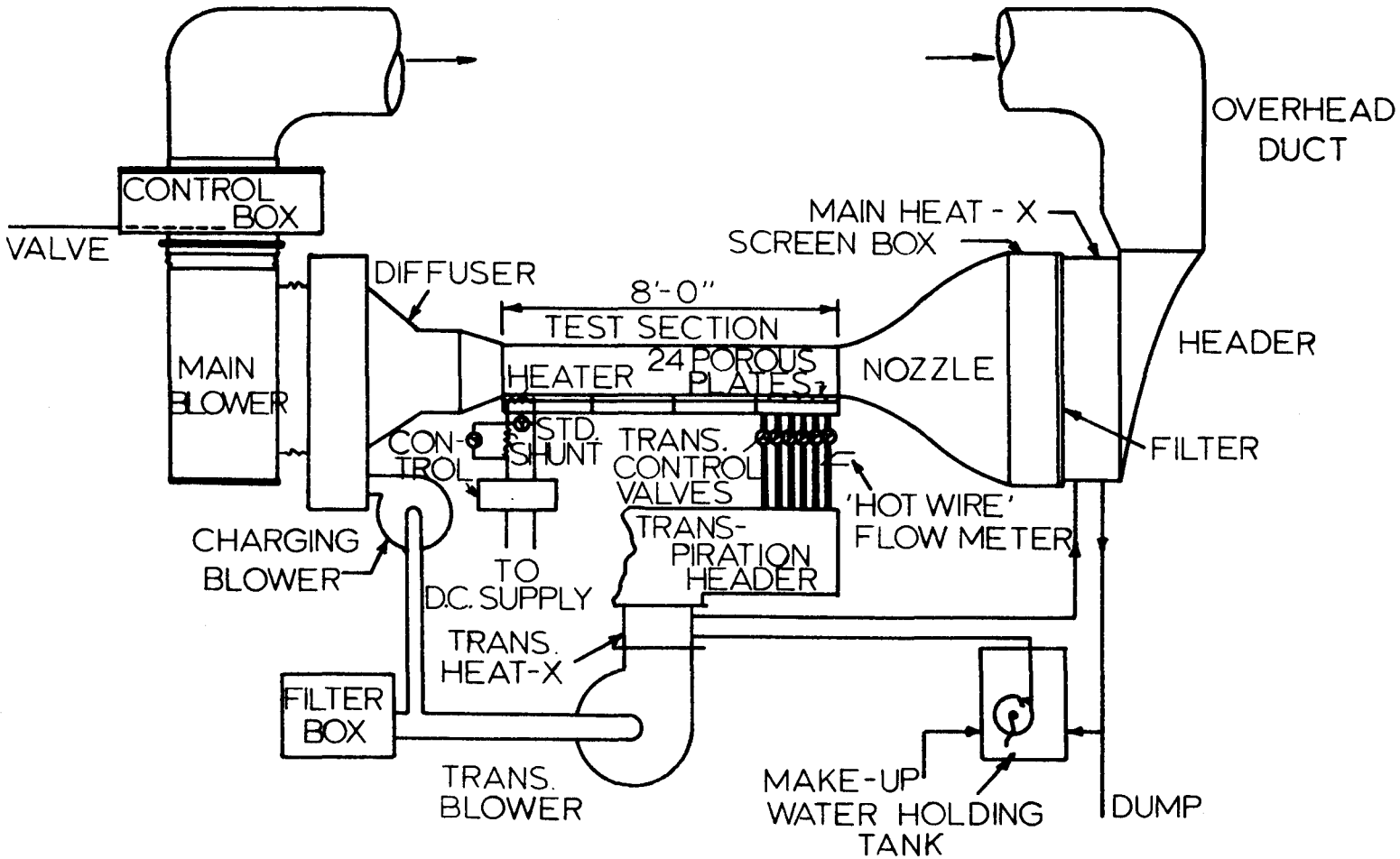

Figure 1-1. Schematic of the Experimental Apparatus

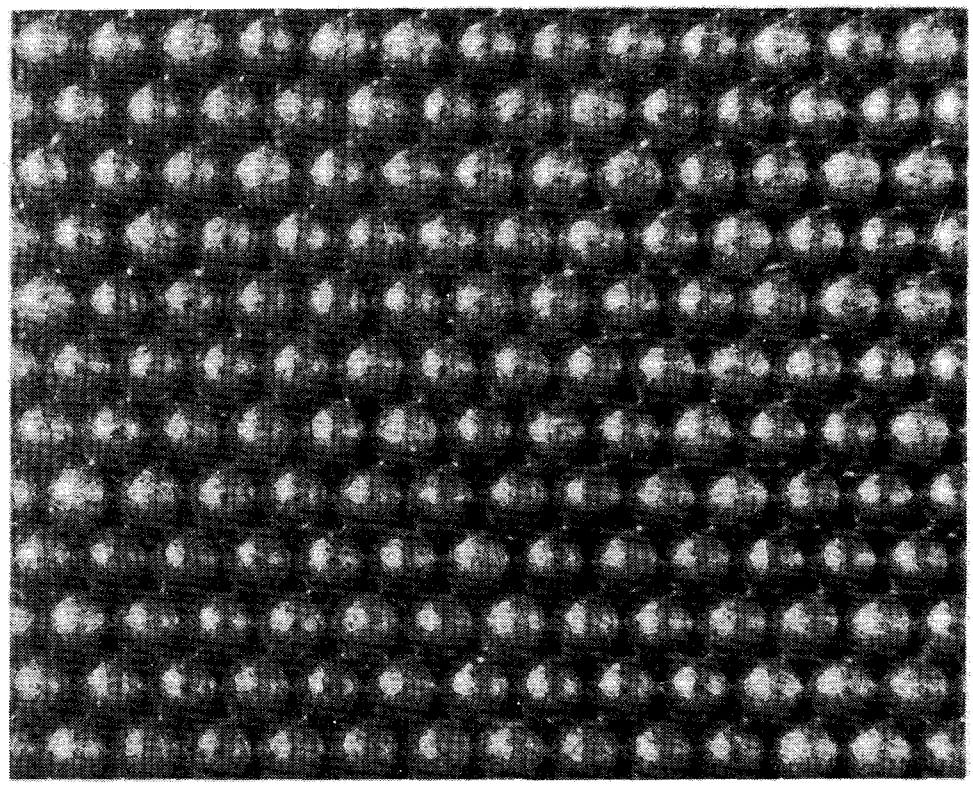

Figure 1-2. Closeup Photograph of the Rough Test Surface

CHAPTER 2

THE EQUILIBRIUM FULLY ROUGH TURBULENT BOUNDARY LAYER WITH PRESSURE GRADIENT AND TRANSPIRATION

The definition of conditions for which a turbulent boundary layer becomes similar in the flow direction in some non-dimensional sense has been a subject of interest for a number of years. Such similar behavior is usually termed an "equilibrium" flow in the literature. The term "equilibrium" flow is sometimes used in the sense of similarity of properly normalized mean velocity profiles; however, truly equilibrium turbulent flow exhibits similarity not only in mean profiles, but also in the turbulence quantities themselves.

The analytical and experimental work in equilibrium layers has been prompted in part by the desire to follow the systematic method of fixing as many variables as possible in a given problem. This allows one to obtain a better understanding of the sensitivity of the problem to the uncontrolled variables. In the specific case addressed here, that of the fully rough turbulent boundary layer, the approach described above is the logical one to follow. If the behavior of the fully rough turbulent boundary layer subjected to pressure gradient and transpiration can be examined in the equilibrium case, one can then proceed to an examination of the more realistic non-equilibrium cases with more confidence and understanding.

In this chapter the previous work in describing and establishing the conditions for which equilibrium exists in turbulent boundary layers is

discussed. Following this, an analysis of the fully rough layer is presented. The analysis yields a definition of the proper acceleration parameter for fully rough flows and a description of the conditions required to establish equilibrium in the fully rough turbulent boundary layer with pressure gradient and transpiration.

2.1 Previous Studies of Equilibrium Turbulent Boundary Layers

In 1950 Rotta [10] presented an examination of the conditions which would yield a smooth wall turbulent boundary layer in which the velocity profile is distorted only affinely in the flow direction. He termed such flows similar and showed that, neglecting the viscous wall region, the equations describing the flow become ordinary differential equations if $C_f/2$ = constant and $U_\infty = ax^m$, where a and m are constants. For a layer where the friction coefficient is almost independent of x, similar solutions exist which depend only on m and $C_f/2$, and the boundary layer thickness increases linearly with x.

In 1954 Clauser [11] presented experimental verification of the existence of similar turbulent boundary layer flows on smooth walls for two different adverse pressure gradients. He termed such behavior "equilibrium" and defined it as the case where both

$$G = \left(\frac{H-1}{H}\right)\left(\frac{1}{\sqrt{C_f/2}}\right) \tag{2.1}$$

and

$$\beta = \frac{\delta'}{\tau_w}\frac{dP}{dx}$$

were independent of x. In a later paper, Clauser [12] showed that the correct choice of the length scale δ' was the displacement thickness, so that

$$\beta = \frac{\delta_1}{\tau_w}\frac{dP}{dx} . \tag{2.2}$$

It should be noted that Clauser's definition of the shape parameter G is identical with that presented earlier by Rotta [10,13]. Additional theoretical treatments of equilibrium turbulent boundary layers were presented by Townsend [14] and Coles [15].

The most definitive work on equilibrium turbulent boundary layer flow was presented by Rotta [16] in 1962. He showed that the conditions required for exact equilibrium behavior (reduction of the equations of motion to an ordinary differential equation) are:

$$\left.\begin{aligned} C_f/2 &= \text{constant} \\ \frac{d\delta_1}{dx} &= \text{constant} \\ \text{and} \qquad \beta = \frac{\delta_1}{\tau_w}\frac{dP}{dx} &= \text{constant} \end{aligned}\right\} \tag{2.3}$$

Two flows obeying these constraints exactly were shown to be flow over a smooth wall with $U_\infty \sim \frac{1}{x_o - x}$ where $x_o > x$ and flow over a uniformly rough wall with $U_\infty \sim \exp\left(\frac{x}{U_\infty}\frac{dU_\infty}{dx}\right)$. Other variations of U_∞ were shown to either require a given roughness variation with x or not to satisfy exactly the conditions required above.

There are indications based on experimental rough wall studies that exact equilibrium cases exist for conditions not corresponding to the velocity and roughness criteria above. Perry, et al. [17], found that a

zero pressure gradient turbulent boundary layer developing over a two-dimensional cavity type roughness of constant height conformed to Rotta's conditions for precise self-preserving flow. Pimenta [2] also found indications in his work on zero pressure gradient flow over the rough surface used in this study that the boundary layer was approaching such an equilibrium state.

2.2 Conditions for Equilibrium in the Fully Rough Turbulent Boundary Layer with Pressure Gradient and Transpiration

In order to determine the conditions for which equilibrium will be obtained in the fully rough turbulent boundary layer with pressure gradient and transpiration, consider the two-dimensional momentum integral equation

$$\frac{C_f}{2} + F = \frac{d\delta_2}{dx} + \delta_2(2 + H)\frac{1}{U_\infty}\frac{dU_\infty}{dx} \tag{2.4}$$

where the variation of ρ_∞ with x has been neglected, as have the normal Reynolds stresses. For the zero pressure gradient fully rough state, it has been shown [1,2] that the skin friction is independent of Reynolds number and can be functionally represented as

$$C_f/2 = f\left(\frac{\delta_2}{r}, F\right) \tag{2.5}$$

where r is a length scale characteristic of the roughness elements.

For the present deterministic rough wall where height and distribution are describable by a single length scale, r is taken as the radius of the spheres comprising the surface. In the most general case, of course, one length scale describing height and one describing distribution in addition

to a parameter describing roughness element form are necessary for the description of a rough surface. Most investigators in the past have used the "equivalent sand grain roughness" scale, k_s, determined by comparison with Nikuradse's [3] classic pipe flow experiments, in order to obtain a single length scale description of roughness.

One condition necessary for equilibrium is that $C_f/2$ be constant. Additionally, consider only the case for constant F and assume that the functional form of Equation (2.5) will remain valid for flows with pressure gradient. Under these conditions, δ_2 is constant and Equation (2.4) becomes

$$C_f/2 + F = (2 + H) \frac{\delta_2}{U_\infty} \frac{dU_\infty}{dx} = \text{constant} \tag{2.6}$$

Defining a pressure gradient parameter for fully rough flow as

$$K_r \equiv \frac{L}{U_\infty} \frac{dU_\infty}{dx} \tag{2.7}$$

where L is a length scale yet to be specified, Equation (2.6) can be written as

$$K_r = \frac{(C_f/2 + F)}{(2 + H)(\delta_2/L)} = \text{constant} \tag{2.8}$$

for an equilibrium condition.

The choice of the proper length scale L to use in (2.7) is not immediately obvious. One might use an integral scale of the flow (δ, δ_1, δ_2) or a roughness scale (r, k_s). The roughness element radius, r, will be used in this development. A discussion of the arguments for this choice will be deferred to a later section. Thus,

$$K_r \equiv \frac{r}{U_\infty}\frac{dU_\infty}{dx} \tag{2.9}$$

For a fully rough flow with constant F and K_r, the layer could be expected to exhibit an equilibrium state for which $C_f/2$, δ_2, H, and β are all independent of x. This expectation has been experimentally verified in the present investigation for positive K_r and F. For $K_r < 0$ (adverse pressure gradients) Equation (2.8) indicates equilibrium flow is possible only for $F < 0$ (suction). Fully rough flows with K_r constant are equilibrium flows in the strictest sense since all of the conditions of (2.3) are satisfied.

The freestream velocity variation required for an equilibrium flow is found by integration of Equation (2.9) with K_r = constant to be

$$\frac{U_\infty}{U_{\infty,o}} = e^{K_r(x-x_o)/r} \tag{2.10}$$

where the subscript o indicates the position at which the velocity variation begins. This agrees with Rotta's [16] result, but from the development above it is clear that fully rough flow is required for the velocity variation (2.10) to give an equilibrium flow. For transitionally rough flow, $C_f/2$ is a function not only of δ_2/r and F, but also of U_∞. Thus,a constant K_r flow would not be an equilibrium flow for a transitionally rough turbulent boundary layer.

For F and K_r constant, it can also be shown that

$$\beta = -\left(\frac{H}{H+2}\right)\left(\frac{C_f/2 + F}{C_f/2}\right) \tag{2.11}$$

and

$$C_f/2 = (H + 2)\ K_r(\delta_2/r) - F \tag{2.12}$$

The definition of K_r for fully rough flows is analogous to that of the smooth wall acceleration parameter

$$K = \frac{\nu}{U_\infty^2}\frac{dU_\infty}{dx} \tag{2.13}$$

An accelerating turbulent flow on a smooth wall with K = constant yields a boundary layer with Re_{δ_2} constant that is equilibrium in the sense that mean velocity profiles become similar and G and β are constant. Such a flow is not truly an equilibrium flow in the sense of equations (2.3) since $\frac{d\delta_1}{dx} \sim \frac{1}{U_\infty^2} \neq$ constant. A comparison of the asymptotic accelerated states for smooth wall and fully rough turbulent boundary layers is presented in Table 2.1.

2.3 Choice of Length Scale in Acceleration Parameter K_r

The choice of the correct length scale to be used in the fully rough acceleration parameter K_r is not obvious from the development in Section 2.2. A scale based on roughness size (r, k_s) or a local scale of the boundary layer (δ, δ_1, δ_2) could be chosen. The near wall scale used in smooth wall layers, $\frac{\nu}{U_\tau}$, should not be considered because the turbulence field of the fully rough layer is independent of viscous effects, at least for regions outside the roughness elements [2].

One requirement which should be imposed is that when K_r is constant, an equilibrium condition should result. This requirement leads to the choice of roughness size as the proposed scale. Define:

$$K_r = \frac{r}{U_\infty}\frac{dU_\infty}{dx} \tag{2.9}$$

$$K_r' = \frac{\delta_1}{U_\infty}\frac{dU_\infty}{dx} \tag{2.14}$$

and

$$K_r^* = \frac{\delta_2}{U_\infty}\frac{dU_\infty}{dx} \tag{2.15}$$

for convenience in the discussion to follow. If the fully rough flow is in an equilibrium state, δ_1 and δ_2 are both constant and thus K_r, K_r', and K_r^* are all constant and meet the requirement above. However, consider a case where a non-equilibrium acceleration is imposed on a surface of constant roughness. It is possible, in principle, that an acceleration could be imposed such that the product of $\left(\frac{1}{U_\infty}\frac{dU_\infty}{dx}\right)$ and δ_1 or δ_2 would be constant. Thus, in principle, K_r' or K_r^* could be maintained constant in a non-equilibrium fully rough flow. Therefore, it appears that a local scale of the layer is not suitable for use in defining K_r.

In choosing a roughness length scale for use in K_r, one is assuming that if r (or k_s) is doubled, then $\left(\frac{1}{U_\infty}\frac{dU_\infty}{dx}\right)$ must be halved to achieve the same effect for both the cases $r = r_1$ and $r = 2r_1$. Confirmation of this behavior must await further experimental work. However, it is obvious that some wall scale effect must be included in K_r, otherwise the smooth wall parameter, K, would adequately describe rough wall accelerations.

Since the equivalent sand grain roughness of the present rough surface according to Schlichting [18] is 1.25 r, the conversion of the K_r values reported to values based on k_s is easily made if desired.

Table 2.1

COMPARISON OF ASYMPTOTIC ACCELERATED STATES FOR SMOOTH AND FULLY ROUGH TURBULENT BOUNDARY LAYERS

	Smooth	Rough
Acceleration Parameter	$K = \frac{\nu}{U_\infty^2} \frac{dU_\infty}{dx}$	$K_r = \frac{r}{U_\infty} \frac{dU_\infty}{dx}$
Re_{δ_2}	Constant	Increases
δ_2	Decreases	Constant
$U_\infty/U_{\infty,o}$	$\frac{1}{1 - \frac{KU_{\infty,o}}{\nu}(x - x_o)}$	$e^{-K_r(x - x_o)/r}$
β	$-\left(\frac{H}{H+1}\right)\left(\frac{C_f/2 + F}{C_f/2}\right)$	$-\left(\frac{H}{H+2}\right)\left(\frac{C_f/2 + F}{C_f/2}\right)$
$C_f/2$	$\frac{\delta_2(H+1)}{U_\infty} \frac{dU_\infty}{dx} - F$	$\frac{\delta_2(H+2)}{U_\infty} \frac{dU_\infty}{dx} - F$

Note: Subscript o indicates point where acceleration begins.

CHAPTER 3

EXPERIMENTAL RESULTS

The experimental data obtained in this study will be presented in this chapter and trends, similarities, and comparisons will be noted and discussed briefly. An integrated discussion and description of the effects of acceleration on the fully rough turbulent boundary layer will be presented in Chapter 4.

The experimental program covered five different cases:

(1)	$K_r = 0$	$F = 0$	
(2)	$K_r = 0.15\text{x}10^{-3}$	$F = 0$	(equilibrium)
(3)	$K_r = 0.29\text{x}10^{-3}$	$F = 0$	(equilibrium)
(4)	$K_r = 0.29\text{x}10^{-3}$	$F = 0.0039$	(equilibrium)
(5)	$K = 0.28\text{x}10^{-6}$	$F = 0$	(non-equilibrium)

Case 1 was run as a baseline set and to compare the present data with those of Pimenta [2] for identical conditions. Cases 2, 3, and 4 are equilibrium acceleration runs for the fully rough turbulent boundary layer. In Case 5 the smooth wall acceleration parameter $K = \frac{\nu}{U_\infty^2}\frac{dU_\infty}{dx}$ was maintained constant. This represents a non-equilibrium run for the fully rough layer.

In setting up each of the equilibrium runs, the value of K_r and the x-position at which the acceleration was begun were matched with the δ_2, H,

and $C_f/2$ data taken at that position for $K_r = 0$, using Equation (2.8). Thus, the boundary layer entered the region of acceleration near the equilibrium state for the K_r applied, and the length of the equilibrium flow established was maximized.

Measurements included Stanton numbers and profiles of T, U, $\overline{u'^2}$, $\overline{v'^2}$, $\overline{w'^2}$, $\overline{u'v'}$. These data allowed calculation of skin friction coefficient $C_f/2$, turbulent Prandtl number Pr_T, mixing length ℓ, and profiles of Q^+ and τ^+. The profile measurements were obtained using two hot wires--one horizontal and one rotatable 45° slant--and a butt-welded thermocouple probe similar in design to that used by Blackwell [9]. Details of the measurements and techniques used are presented in Appendix I.

In the following sections the $K_r = 0$ baseline data will be presented first. The four cases with acceleration will then be described with presentation of the data in the following order:

- Summary graphs for each case
- Integral quantities (St, $C_f/2$, δ, Δ, etc.)
- Mean velocity and temperature profiles
- Reynolds stress tensor components
- Turbulent Prandtl number and related quantities

The final section of this chapter will describe a Stanton number prediction technique and some supplementary Stanton number data, including cases with steps in wall temperature, variable wall temperature, and variable blowing with acceleration.

3.1 Zero Pressure Gradient Data

The data for zero pressure gradient were obtained both to provide a baseline set of measurements taken using the same techniques used in

acquiring the accelerated data and also to demonstrate the compatibility of the data with the results of Pimenta [2] for the same conditions and test surface.

Stanton number data are shown in Figure 3-1 for both F = 0 and 0.0039. The data of Pimenta for an untripped layer are also plotted, and the comparison between the two sets is excellent for large $\frac{\Delta_2}{r}$, being well within the data uncertainty of ± 0.0001 Stanton number units. The correlations proposed by Pimenta for interpolation of his data are also shown. These correlations are:

$$St = 0.00317 \left(\frac{\Delta_2}{r}\right)^{-0.175} \tag{3.1}$$

for F = 0 and $4 < \frac{\Delta_2}{r} < 15$ and

$$\left.\frac{St}{St_o}\right|_{\Delta_2} = \left[\frac{\ln(1+B_h)}{B_h}\right]^{1.175} (1+B_h)^{0.175} \tag{3.2}$$

for $0 < F < 0.0040$, where:

St_o is the Stanton number for F = 0 and the same Δ_2

$B_h = F/St$ is the blowing parameter.

Figure 3-2 presents the skin friction coefficients obtained for F = 0 by Healzer [1], Pimenta [2], and the present author. Healzer differentiated his momentum thickness measurements to obtain $C_f/2$, while Andersen's [19] shear stress method for skin friction determination was used in this study and also by Pimenta. The results of Pimenta and the present author show good agreement, while the data of Healzer deviate slightly from the others at the larger values of δ_2/r. The correlation of Pimenta for F = 0 and $1.0 < \frac{\delta_2}{r} < 10.0$

$$C_f/2 = 0.00328 \left(\frac{\delta_2}{r}\right)^{-0.175} \tag{3.3}$$

is also plotted.

All of the skin friction coefficients in this study were calculated using

$$\begin{aligned} U_\infty^2 C_f/2 = {} & \nu \frac{\partial U}{\partial y}\bigg|_{y_1} - \overline{u'v'}\bigg|_{y_1} - U_\infty U_{y_1} F \\ & - \left[\left(\int_0^{y_1} \left(\frac{U}{U_\infty}\right)^2 dy\right) - \frac{y_1}{2}\right]\left[\frac{U_\infty^2}{\rho_\infty}\frac{d\rho_\infty}{dx} + \frac{2U_\infty^2}{r} K_r\right] \\ & + \left[\int_0^{y_1} \frac{U}{U_\infty}\, dy\right]\left[\frac{U_\infty U_{y_1}}{\rho_\infty}\frac{d\rho_\infty}{dx} + \frac{U_{y_1} U_\infty}{r} K_r\right] \\ & - U_\infty^2 \frac{d}{dx}\left[\int_0^{y_1} \frac{U^2}{U_\infty^2}\, dy\right] + U_{y_1} U_\infty \frac{d}{dx}\left[\int_0^{y_1} \frac{U}{U_\infty}\, dy\right] \end{aligned} \tag{3.4}$$

The derivation of (3.4) is straightforward. Briefly, the momentum equation (incorporating the usual boundary layer assumptions but allowing $\rho_\infty = \rho_\infty(x)$) and the continuity equation are integrated from the surface to a position y_1 in the boundary layer. Then, measurement of successive velocity profiles in the x-direction and $\overline{u'v'}$ at $y = y_1$ for each x-position allows calculation of $C_f/2$ versus x, using (3.4). The position y_1 was always 0.130" in this study, since the rotatable slant hot wire used to measure $\overline{u'v'}$ was limited to $y > 0.125$".

A typical velocity profile is plotted versus $(y + \Delta y)/\delta_2$ in Figure 3.3. Since the normal coordinate y is referred to the tops of the spherical

elements comprising the test surface, the "wall shift" Δy gives the location of the "apparent wall" for the mean velocity. This wall shift has been a topic of much discussion by previous workers in roughness and will be discussed in more detail later in this chapter. It is shown in the figure that the present data follow Schlichting's [18] expression for fully rough flow

$$\frac{U}{U_\tau} = \frac{1}{\kappa} \ln \frac{y}{k_s} + 8.5 \tag{3.5}$$

Note that the value of k_s used (0.031") is determined from Schlichting's tabulated values and not by back-fitting Equation (3.5). The smooth wall "law of the wall" is also shown for reference.

Measurements of the three components of the turbulent kinetic energy normalized by U_∞^2 are shown in Figure 3-4 plotted versus y/δ. The present measurements agree with those of Pimenta within the data uncertainty. Comparison of the fully rough data with the $\overline{u'^2}$ data of Klebanoff [20] for a smooth wall shows several important characteristics of fully rough flow (which were noted by Pimenta [2]). First, for fully rough flow the peak in $\overline{u'^2}$ is moved out from the wall, lowered, and spread over a greater portion of the layer than is the case for smooth wall flows. Second, the effect of the roughness is felt across practically the entire layer in the form of increased turbulence energy. Blake [21] also observed this behavior in his fully rough flow data. Thus, the assumption made by some authors [8,17] that the effect of roughness is confined to the near wall region is not valid for the turbulent kinetic energy components. Pimenta showed that this effect was not due to the greater freestream turbulence ($\approx$ 0.4%) in the present tunnel as compared with that of Klebanoff ($\approx$ 0.02%). He also showed that

the use of U_τ^2 as a normalizing velocity did not collapse the smooth and rough wall results, as was suggested by Hinze [22] based on the measurements of Corrsin and Kistler [23] over 2-D roughness elements.

3.2 Data with Acceleration

Summary graphs for the four cases of accelerated flow investigated are shown in Figures 3-5 through 3-8. The purpose of these plots is to show the variation of K_r and the integral quantities $C_f/2$, δ_2, and H which are indicators of equilibrium flow according to the discussion in Chapter 2. The Stanton number variation is also plotted to illustrate the integral behavior of the thermal field. In each figure, the data are plotted versus distance along the test section, x. In the discussion which follows, F = 0 unless specifically stated otherwise.

Data from the $K_r = 0.15 \times 10^{-3}$ run are presented in Figure 3-5. This run had the longest region of K_r constant (x = 44" to 88"), with the velocity increasing from approximately 88 to 115 ft/sec. As seen in the figure, δ_2, H and $C_f/2$ all become constant in the region of K_r constant, indicating that equilibrium flow was established. Stanton numbers in the acceleration region are about 10% larger than for the $K_r = 0$ case and appear to be approximately constant within the data uncertainty. The behavior is different from that observed for accelerated smooth wall layers, where Stanton number is unaffected for small K, then decreases in comparison to the unaccelerated case at the same Reynolds number or same x-position as K increases [4,24,25,26].

Data for $K_r = .29 \times 10^{-3}$ are shown in Figures 3-6 and 3-7 for F = 0 and F = 0.0039, respectively. In both these cases, K_r is constant from x = 24" to 52", U_∞ increases from 88 to 129 ft/sec, and δ_2, $C_f/2$, and H all reach constant values in the acceleration region. Stanton number shows the

same behavior as seen in Figure 3-5 in the region of acceleration, then decreases immediately to the $K_r = 0$ baseline data when the acceleration is removed.

The summary data for the $K = .28 \times 10^{-6}$, nonequilibrium case are presented in Figure 3-8. The smooth wall acceleration parameter K is constant from x = 24" to 52", U_∞ increases from 88 to 150 ft/sec, and K_r varies from $.25 - .50 \times 10^{-3}$ in this region. The shape parameter H decreases along the entire test section, while δ_2 increases as the layer is entering the region of acceleration, then levels off and finally decreases. This δ_2 behavior is similar to that observed in the asymptotic accelerated smooth wall layer [27,28]. Skin friction coefficient shows very little variation, and appears to remain about constant. This is not surprising considering the small variation of δ_2 in the acceleration region. Stanton number shows the same increase over $K_r = 0$ values observed in the equilibrium cases and recovers immediately to unaccelerated baseline values when the acceleration is removed.

It was noted above that Stanton number appears to be approximately constant within the data uncertainty in regions of K_r constant. However, it is impossible to reach a firm conclusion in this regard due to the inherent uncertainty in the data and the relatively short regions of acceleration. An argument that Stanton number for $K_r > 0$ varies as $\Delta_2^{-0.175}$ (as in the $K_r = 0$ case) or some similar weak function of Δ_2 could also be supported by the present data.

If, for the sake of argument, one assumes that St is constant in a region of constant K_r, then the behavior of Δ_2 in such a region can be determined. The 2-D energy integral equation for F = 0, constant properties, and constant wall to freestream temperature difference may be written as [29]

$$St = \frac{d\Delta_2}{dx} + \frac{K_r}{r}\Delta_2 \tag{3.6}$$

If St and K_r are constant from a position x_c to x, then (3.6) can be integrated to yield

$$\Delta_2 = \frac{St_c r}{K_r} + \left[\Delta_{2_c} - \frac{St_c r}{K_r}\right] e^{-K_r(x-x_c)/r} \tag{3.7}$$

Thus the enthalpy thickness will approach an asymptotic value $(St_c r/K_r)$ if a flow is established such that St and K_r are constant.

Equation (3.7) was evaluated for the $K_r = .15 \times 10^{-3}$ case assuming $x_c = 58''$ and $St_c = 0.00242$. The results are shown in Figure 3-9 and compared with the enthalpy thicknesses computed from the mean velocity and temperature profiles. The agreement between the measured values and calculated values assuming St = constant is excellent, thus supporting the observation that Stanton number, if not a constant, is at most a weakly varying function of Δ_2 in an equilibrium accelerated fully rough turbulent boundary layer with constant wall temperature.

As shown in Figure 3-9, for the $K_r = .15 \times 10^{-3}$ run the approach of Δ_2 to the indicated asymptotic value is very slow. In fact, Δ_2 would reach 99% of the asymptotic value only after $(x-x_c) \approx 60$ feet. Since δ_2 is constant in the equilibrium case, the ratio Δ_2/δ_2 would therefore increase for an appreciable distance.

3.2.1 Integral Quantities

The Stanton number data in the accelerated region for the three equilibrium runs are shown versus Δ_2/r in Figure 3-10 compared with unaccelerated data for F = 0 and 0.0039. The accelerated data increase

over the $K_r = 0$ data by ~ 10% for F = 0 and ~ 20% for F = 0.0039. As discussed in the previous section, the Stanton number data in the constant K_r region can be argued to be either approaching a constant value or at the very least to be a weaker function of enthalpy thickness than in the unaccelerated case.

Skin friction coefficients in the acceleration region are plotted versus δ_2/r in Figure 3-11 and compared with the unaccelerated cases. The $K_r = 0$ data for F = 0.0039 are from Pimenta's study. For the three equilibrium cases, both $C_f/2$ and δ_2 are constant in the acceleration region and thus only a single data point for each case appears in these coordinates. In the unblown cases, it appears that acceleration causes a slight increase (~ 5%) in $C_f/2$ over the baseline data. It should be noted that this is within the uncertainty (~ 10%) of the $C_f/2$ data, however. In the blown case (F = 0.0039), the acceleration data point lies approximately 30% above Pimenta's $K_r = 0$ data. In smooth wall flows acceleration also leads to an increase in $C_f/2$ compared with zero pressure gradient values for the same Reynolds number [27,28].

Figure 3-12 shows temperature and velocity boundary layer thicknesses (Δ and δ, respectively) for the five cases investigated. No temperature profiles were taken in the present study for $K_r = 0$, so Δ is not shown for the baseline case. In the three equilibrium accelerated cases, the rate of growth of both δ and Δ decreases in the acceleration region. From the equilibrium conditions developed earlier for the fluid dynamics, one would expect δ to eventually assume a constant value for K_r = constant, and it does appear from Figure 3-12 that δ is approaching an asymptote in the region of K_r constant. After the acceleration is removed in the two $K_r = 0.29 \times 10^{-3}$ runs, the boundary layer thicknesses Δ and δ resume a rate of increase with x similar to that observed for the $K_r = 0$ case. The data for the nonequilibrium

$K = .28 \times 10^{-6}$ run exhibit behavior similar to that observed in smooth wall accelerated flows [24,25,27,28]. Both δ and Δ begin to decrease near the end of the acceleration region. In all four acceleration cases, the temperature boundary layer thickness Δ is greater than δ for all x, but the two thicknesses show the same trends in the acceleration and recovery regions.

A comparison of enthalpy thicknesses obtained from integration of temperature and velocity profiles and from integration of the constant property energy integral equation in the form

$$St + F = \frac{1}{U_\infty (T_w - T_{\infty,o})} \frac{d}{dx} \left[\Delta_2 U_\infty (T_w - T_{\infty,o}) \right] \quad . \tag{3.8}$$

using measured Stanton numbers is shown in Figure 3-13 for the four acceleration cases. Reasonable agreement is found between the two methods, with the maximum discrepancy being about 10%. The behavior of Δ_2 is similar to that observed for Δ in Figure 3-12.

Figure 3-14 presents the variation of roughness Reynolds number with x for all five cases, where

$$Re_k = \frac{k_s U_\tau}{\nu} \tag{3.9}$$

and k_s was taken as 0.031", as noted previously, for the present surface. The roughness Reynolds number increases with acceleration since U_τ $(=\sqrt{C_f/2}\, U_\infty)$ increases and $\frac{k_s}{\nu}$ remains constant.

These results have important implications. The utility of the roughness Reynolds number lies in its magnitude relative to the viscous sublayer thickness. Following the traditional argument, for $Re_k < 5$, the roughness elements do not penetrate the sublayer and the flow retains its smooth wall

characteristics. For $5 < Re_k < 55$ to 70 (depending on the data and/or author) the flow is "transitionally" rough, and for $Re_k > 55$ to 70 the flow is fully rough. These ranges are all for $F = 0$. Since Re_k increases in the acceleration region, the roughness elements protrude further out into the layer (in a nondimensional sense) in this region. There is no viscous sublayer present in the fully rough layer, so the increase in Re_k with acceleration can be viewed as making it more difficult for a viscous sublayer to form.

This observation is important when one considers the behavior of accelerated smooth wall flow. Kays and Moffat [4] note that experimental evidence indicates acceleration of a smooth wall turbulent boundary layer causes an increase in the viscous sublayer thickness. Also, it is well known from the results of many investigations that acceleration of a smooth wall turbulent layer causes the layer to develop toward a state resembling laminar flow. Consideration of these smooth wall accelerated flow characteristics might lead one to expect a fully rough turbulent boundary layer subjected to a favorable pressure gradient to develop first transitionally rough, then finally smooth wall characteristics. The present results indicate that this is not the case. To the contrary, acceleration makes a fully rough flow appear "rougher" in the sense that the roughness elements protrude further, nondimensionally, into the turbulent layer.

3.2.2 Mean Velocity and Temperature Profiles

Figures 3-15 through 3-18 present mean velocity profiles for the four acceleration runs plotted as U/U_∞ versus y/δ_2. In these and subsequent figures, x_a denotes the x position at which the relevant acceleration parameter (K_r or K) becomes constant.

In the graphs for the three equilibrium runs (3-15 through 3-17) the profiles are similar, as expected, after the layer is a sufficient distance into the acceleration region. The similarity extends down to the first point from the surface (y = 0.006"). The nonequilibrium data (Figure 3-18) do not exhibit similarity.

Figures 3-19 and 3-20 present profiles from the $K_r = 0.15 \times 10^{-3}$ and unblown $K_r = 0.29 \times 10^{-3}$ cases, respectively, plotted as U/U_τ vs $(y + \Delta y)/\delta_2$. The smooth wall "law of the wall" and Schlichting's [18] expression for fully rough flow (Equation 3.5) are also shown for comparison. As noted previously in this chapter, the wall shift Δy locates the apparent or virtual location of the surface below the tops of the roughness elements.

The wall shift was determined by the same technique used by Pimenta [2], i.e., the method suggested by Monin and Yaglom [30]. Briefly, if it is assumed that a logarithmic law of the wall region exists in the velocity profile, it can be shown that

$$\frac{U}{U_\tau} = \frac{1}{\kappa} \ln\left(\frac{y + \Delta y}{z_o}\right) \tag{3.10}$$

where

κ = Karman constant (≈ 0.41)

z_o = constant

Δy = constant

The proper wall shifts were determined using a form of (3.10) - Δy was varied until a value was determined for which z_o was constant.

It was found that $\Delta y = 0.006''$ for all the profiles in the present unblown data. Since this is the same value found by Pimenta for his zero pressure gradient data, it can be concluded that, for the K_r range of this study, Δy is unaffected by favorable pressure gradients and does not vary with x. This result is quite different than that reported by Perry, et al. [17], who investigated turbulent boundary layer flow over 2-D roughness elements for both zero and adverse pressure gradients. They found that Δy varied with x, and in fact, was actually larger than the roughness height under some adverse pressure gradient conditions.

Comparison of the present profiles with Schlichting's expression shows that the constant would have to be increased from 8.5 to approximately 9.1 to match the accelerated data. The reason for this shift is not known. The decrease in the value of $\Delta U/U_\tau$ between the smooth wall law of the wall and the present data when acceleration is imposed should not, in the author's opinion, be taken as an indication the flow is tending toward the transitionally rough state. The $\overline{u'^2}$ profiles to be presented later in this chapter exhibit none of the transitionally rough characteristics described by Pimenta [2] for this surface. In addition, the increase of Re_k in the acceleration region indicates a trend away from, rather than toward the transitionally rough state (see Section 3.2.1).

A comparison between the blown and unblown velocity profiles for $K_r = 0.29 \times 10^{-3}$ is presented in Figure 3-21. The behavior is as expected - the injection of low momentum fluid at the wall lowers the mean velocity compared to the unblown case.

Temperature profiles for the three equilibrium acceleration cases are plotted in Figures 3-22 through 3-24 in $(T_w-T)/(T_w-T_\infty)$ vs y/Δ_2 coordinates. Similarity of the profiles is observed in all cases and

extends to the closest data point from the surface (y = 0.013"). Temperature profiles for the $K = 0.28 \times 10^{-6}$ non-equilibrium run are shown in Figure 3-25. The apparent similarity observed here is surprising but can be explained by reference to the behavior of the thermal boundary layer thickness Δ and enthalpy thickness Δ_2 for this case shown in Figures 3-12 and 3-13, respectively. Both Δ and Δ_2 vary little in the acceleration region - they appear to be approaching maxima, and a decrease is actually observed in the data for Δ at the end of the acceleration region. Thus the combination of approximately constant Δ and Δ_2 and approximately constant Stanton number (Figure 3-8) in the region of acceleration leads to similarity in the temperature profiles. This similarity would probably not be maintained if the region of K constant were extended.

Temperature profiles for the $K_r = 0.15 \times 10^{-3}$ run are plotted in Figure 3-26 in $(T_w-T)/(T_w-T_\infty)$ versus U/U_∞ coordinates. Pimenta [2] found these coordinates useful since $K_r = 0$ data are linear when plotted in this manner. The present profile at x = 34" (prior to the acceleration region) exhibits this linearity. The two profiles in the acceleration region, however, are not linear and do not exhibit similarity in these coordinates. It should be noted that the accelerated profiles, if extrapolated to $U/U_\infty = 0$, still show the temperature "jump" condition discussed by Pimenta, indicating that the apparent wall position is different for the temperature and velocity fields.

A comparison of the blown and unblown temperature profiles for $K_r = .29 \times 10^{-3}$ is shown in Figure 3-27. The results are as expected, with the injection of fluid at the wall temperature resulting in higher temperatures in the near wall region.

3.2.3 Reynolds Stress Tensor Components

The behavior of the turbulence quantities will be examined in this section. Due to the physical limitations of the apparatus, only in the $K_r = 0.15 \times 10^{-3}$ run was an acceleration region of sufficient length established to investigate the similarity of the turbulence quantities in the flow direction. The data from this run will form the primary basis for the discussion of the effects of acceleration on the turbulence field. Data from the other runs will be presented as additional support for the points presented; however, a direct comparison of the exact magnitudes between the data of different accelerations is not particularly meaningful due to the variation in the values of $(x-x_a)/\delta$ at which the profiles of the different runs were taken.

In the following discussion, the similarity of turbulence profiles in the flow direction is examined first. Comparisons are then made between the acceleration profiles and those for $K_r = 0$, and finally a comparison of the Reynolds shear stress correlation coefficients for the different runs is presented. A comparison of correlation coefficients between the different acceleration runs is valid due to the demonstrated insensitivity of the coefficients to the boundary conditions imposed.

Figure 3-28 presents, for $K_r = 0.15 \times 10^{-3}$, the three components of the turbulent kinetic energy nondimensionalized by U_∞^2 and plotted versus y/δ_2 for $(x-x_a) = 22$ and 42 inches. Excellent similarity is observed in the u' component, and the agreement in the v' and w' components is within the uncertainty of the data (~ 10%). The Reynolds stress profiles at the two positions are compared in Figure 3-29. The difference between the two profiles is on the order of the data uncertainty. The results shown in Figure 3-28 and 3-29 demonstrate that a state of similarity is being

approached by the turbulence quantities, with the data indicating that $\overline{u'v'}$ possibly requires a greater distance to become truly similar than do the other quantities.

Profiles of $\overline{u'^2}/U_\tau^2$ versus y/δ are shown in Figure 3-30 for the $K_r = 0$ and $.15 \times 10^{-3}$ cases. The decrease in longitudinal turbulence intensity with acceleration is quite evident and similar to the behavior observed with accelerated smooth wall flows [5]. When the profiles in Figure 3-30 are compared with the same two profiles in Figure 3-31 (where the data are normalized by U_∞^2), one observes that the peaks in $\overline{u'^2}$ nearly coincide when U_∞^2 scaling is used but are displaced in level if U_τ^2 scaling is used. This near-coincidence of the $\overline{u'^2}$ peaks when normalized by U_∞^2 provides a convenient reference level when comparing the profiles, and all fluctuation data to follow are presented in this form.

The three components of the turbulent kinetic energy for the $K_r = 0$ and 0.15×10^{-3} cases are compared in Figure 3-31 as $\overline{u_i'}/U_\infty^2$ versus y/δ. As stated above, the level of the u' component in these coordinates is changed very little by acceleration for $y/\delta < 0.1$. The v' and w' components are substantially lower than the $K_r = 0$ data in the region $y/\delta \approx 0.1$, while in the outer region ($y/\delta \gtrsim 0.2$) all three components are lowered on the order of 40% compared to the $K_r = 0$ values. Thus, when compared with the unaccelerated data, acceleration decreases the level of turbulent kinetic energy over the entire layer and makes the turbulence structure much more anisotropic in the inner region. Unfortunately, no measurements of the v' and w' components in a smooth wall accelerated layer are known to the author, so no comparison of rough and smooth wall behavior with acceleration is possible.

Consideration of the turbulent kinetic energy equation and the equations for the energies in the three components allows some insight into

the behavior observed in Figure 3-31. The time averaged turbulent kinetic energy equation for stationary flow and no body forces can be written as [30,31]

$$\frac{\partial}{\partial x_i}\left(E\,U_i + \frac{1}{2}\rho\,\overline{u_j' u_j' u_i'} + \overline{p' u_i'} - \overline{u_j' \sigma_{ij}'}\right) =$$

$$-\rho\,\overline{\sigma_{ij}'\,\frac{\partial u_j'}{\partial x_i}} - \rho\,\overline{u_i' u_j'}\,\frac{\partial U_j}{\partial x_i} \qquad (3.11)$$

where $$E = \frac{1}{2}\rho\,\overline{u_i' u_i'} = \frac{1}{2}\rho\,q^2$$

and

$$\sigma_{ij}' = \rho\,\nu\left(\frac{\partial u_i'}{\partial x_j} + \frac{\partial u_j'}{\partial x_i}\right)$$

The terms on the left side of (3.11) are, respectively, the spatial transfer of E by the mean motion, by the turbulence fluctuations, by the "pressure diffusion", and by the viscous shear stresses of the turbulence field. The terms on the right hand side are the dissipation of E by molecular viscosity and the production of E by the interaction of the Reynolds stress tensor with the mean velocity gradients.

The equations [30] for the three components of E contain terms similar to those in (3.11) and, in addition, the terms $\overline{p'\,\frac{\partial u'}{\partial x}}$, $\overline{p'\,\frac{\partial v'}{\partial y}}$, and $\overline{p'\,\frac{\partial w'}{\partial z}}$ appear on the right hand side of the $\overline{u'^2}$, $\overline{v'^2}$, and $\overline{w'^2}$ equations, respectively. Since these three additional terms sum to zero by continuity, they do not appear in the equation for the total turbulent kinetic energy. Thus these pressure fluctuation-turbulence field interaction terms transfer energy

among the components of E, but play no direct role in the spatial transfer of turbulence energy.

In the flows of this investigation, all the terms of the production $\overline{u_i'u_j'}\ \frac{\partial U_j}{\partial x_i}$ are negligible except $\overline{u'v'}\ \frac{\partial U}{\partial y}$ (see Section 3.2.4). Therefore the entire turbulent kinetic energy production goes into the $\overline{u'^2}$ component of E, and the $\overline{v'^2}$ and $\overline{w'^2}$ components receive energy only through the pressure fluctuation-turbulence field interaction terms described above. Since the effect of acceleration is to make the fully rough layer much more anisotropic in the inner region, acceleration must decrease the sum of the pressure fluctuation transfer (source) and dissipation (sink) terms in the $\overline{v'^2}$ and $\overline{w'^2}$ equations. This argument can be carried further only if one assumes the dissipation is affected only slightly by acceleration--under this assumption, it would have to be true that the correlations between p' and $\frac{\partial v'}{\partial y}$, $\frac{\partial w'}{\partial z}$ are decreased significantly by acceleration.

Profiles for the components of q^2 are presented in Figures 3-32 and 3-33 for the $K_r = 0.29 \times 10^{-3}$, F = 0, and $K = 0.28 \times 10^{-6}$ cases, respectively. The behavior observed in each case is similar to that already shown in Figure 3-31 for the $K_r = 0.15 \times 10^{-3}$ data.

The effects of acceleration on the components of q^2 in a fully rough layer with blowing are shown in Figure 3-34. The data points are for the $K_r = 0.29 \times 10^{-3}$, F = 0.0039 case of the present study, while the solid lines for $K_r = 0$, F = 0.0039 are from Pimenta [2]. Comparison of the two sets of data yields several important points. First acceleration decreases all components of q^2 in the outer region much as it does in the unblown layers. However, the behavior in the inner region is quite different from that in the unblown cases. The degree of anisotropy in the accelerated data is about the same at $y/\delta \approx 0.2$ as in the zero pressure gradient data.

Unfortunately, the probe size restrictions prevented acquisition of v' and w' data for $y/\delta < 0.1$ and the trends inside this region are undetermined.

In the unblown cases, the general shapes of the profiles with and without acceleration were similar. However, in Figure 3-34 one sees that in the blown layer acceleration alters the basic shape of the profiles. The curvature of the $\overline{u'^2}$ profile in the outer region is completely changed, and the peaks in the $\overline{v'^2}$ and $\overline{w'^2}$ profiles for $K_r = 0$ are suppressed. In fact, the profiles from the blown accelerated layer look much more like the unblown $K_r = 0$ profiles than the profiles from the blown $K_r = 0$ case. This can be seen in Figure 3-35 where the $\overline{u'^2}$ component is shown.

The Reynolds shear stress nondimensionalized by U_τ^2 is shown in Figure 3-36 for the $K_r = 0$ and 0.15×10^{-3} cases. The behavior of $\overline{u'v'}$ with acceleration is similar to that calculated for the smooth wall accelerated layer [25]. No measurements of this term in the smooth wall accelerated layer have been published to the knowledge of the author. The observed decrease in $-\overline{u'v'}/U_\tau^2$ with acceleration would lead one to expect a probable decrease in the production of turbulent kinetic energy with acceleration (in a nondimensional sense). This point will be expanded in the following section.

Figure 3-37 presents the measured correlation coefficients R_{uv} and R_{q^2} where

$$R_{uv} = -\overline{u'v'} \Big/ \sqrt{\overline{u'^2}}\,\sqrt{\overline{v'^2}} \tag{3.12}$$

and

$$R_{q^2} = -\overline{u'v'}/q^2 \tag{3.13}$$

The measured values for all four acceleration cases are in excellent agreement with those ($R_{uv} \approx 0.45$, $R_{q2} \approx 0.15$) reported for both smooth wall layers [32,33,34] and zero pressure gradient rough wall layers [2]. It thus appears that the relationship between the Reynolds shear stress and the diagonal components of the tensor is truly universal and independent of boundary conditions.

Since the turbulent shear and turbulent kinetic energy are primarily generated during periods of bursting [35,36,37], it is logical to propose that the universal values of R_{uv} and R_{q2} observed result from a universal attribute of the bursting and decay process itself. Grass [38], who reported results of a hydrogen bubble technique investigation of a turbulent water channel flow over a pebble-type rough surface, observed that the bursting process appeared more vigorous in the fully rough than the smooth wall case. The inrushing fluid interacted with the fluid among the roughness elements (which is more energetic than that in the viscous sublayer on a smooth wall), and in the ejection phase of the process the fluid moved almost vertically upward. These results are consistent with Pimenta's results of higher turbulence energy throughout the layer in the fully rough state. Thus, the levels of shear stress and energy are influenced by the vigor of the bursting process and, by extension, the boundary conditions. However, it appears from all the data available that in any flow where the level of turbulence is generated and maintained by the bursting process, the relationship between the components of the Reynolds stress tensor is fixed by some basic attribute of the bursting and decay mechanisms and is independent of boundary conditions.

3.2.4 Turbulent Prandtl Number and Related Quantities

The results discussed in this section were obtained from calculations using St, $C_f/2$, U, and T data and the energy, momentum, and continuity equations integrated to a position y_1 in the boundary layer. These integrations yield

$$\begin{aligned}\tau = \tau_w &+ \rho_\infty U_\infty U F + \left(U_\infty^2 \frac{d\rho_\infty}{dx} + \frac{2\rho_\infty U_\infty^2}{r} K_r\right)\left[\left(\int_0^{y_1} \left(\frac{U}{U_\infty}\right)^2 dy\right) - \frac{y_1}{2}\right] \\ &- \left(U_\infty \frac{d\rho_\infty}{dx} + \frac{\rho_\infty U_\infty}{r} K_r\right)\left(U \int_0^{y_1} \frac{U}{U_\infty}\, dy\right) \\ &+ \rho_\infty U_\infty^2 \frac{d}{dx}\left[\int_0^{y_1} \left(\frac{U}{U_\infty}\right)^2 dy\right] \\ &- \rho_\infty U_\infty U \frac{d}{dx}\left(\int_0^{y_1} \frac{U}{U_\infty}\, dy\right)\end{aligned} \tag{3.14}$$

for the shear stress distribution and

$$\begin{aligned}\dot{q}''/\dot{q}''_w = 1 &+ \frac{\tau U}{\dot{q}''_w} + \frac{F}{St}\left(1 - \frac{I}{I_w}\right) \\ &+ \left(\frac{I}{\dot{q}''_w} \int_0^{y_1} \frac{\rho U}{\rho_\infty U_\infty}\, dy\right) \frac{d}{dx}(\rho_\infty U_\infty) \\ &+ \left(\frac{I}{\dot{q}''_w} \rho_\infty U_\infty\right) \frac{d}{dx}\left(\int_0^{y_1} \frac{\rho U}{\rho_\infty U_\infty}\, dy\right) \\ &- \left(\frac{1}{\dot{q}''_w} \int_0^{y_1} \frac{\rho U I}{\rho_\infty U_\infty I_w}\, dy\right) \frac{d}{dx}(\rho_\infty U_\infty I_w) \\ &- \left(\frac{\rho_\infty U_\infty I_w}{\dot{q}''_w}\right) \frac{d}{dx}\left(\int_0^{y_1} \frac{\rho U I}{\rho_\infty U_\infty I_w}\, dy\right)\end{aligned} \tag{3.15}$$

for the heat flux distribution. Since the fluid dynamics data were taken under isothermal conditions, Equation (3.14) assumes $\rho = \rho_\infty(x)$, while Equation (3.15) retains $\rho = \rho(x,y)$. (Although these variations were included in the analysis, numerically they were insignificant in all cases.)

The shear stress and heat flux contain both turbulent and laminar contributions and may be written as

$$\tau = -\rho_\infty \overline{u'v'} + \rho_\infty \nu \frac{\partial U}{\partial y} \tag{3.16}$$

and

$$\dot{q}'' = \rho C_p \overline{v't'} - k\frac{\partial T}{\partial y} \tag{3.17}$$

If the turbulent contributions are modeled using eddy diffusivities for momentum and heat, Equations (3.16) and (3.17) become

$$\tau = \rho\ (\varepsilon_m + \nu)\ \frac{\partial U}{\partial y} \tag{3.18}$$

and

$$\dot{q}'' = -\ \rho\ C_p\ (\varepsilon_H + \alpha)\ \frac{\partial T}{\partial y} \tag{3.19}$$

where

$$-\ \overline{u'v'} = \varepsilon_m \frac{\partial U}{\partial y} \tag{3.20}$$

and

$$-\ \overline{v't'} = \varepsilon_H \frac{\partial T}{\partial y} \tag{3.21}$$

Alternatively, if the turbulent shear stress is modeled using the mixing length approach, a mixing length ℓ may be defined as

$$\varepsilon_m = \ell^2 \left|\frac{\partial U}{\partial y}\right| \tag{3.22}$$

or, using Equation (3.20)

$$\ell = \sqrt{-\overline{u'v'}} \Big/ \left|\frac{\partial U}{\partial y}\right| \tag{3.23}$$

The turbulent Prandtl number is defined as the ratio of the eddy diffusivities for momentum and heat:

$$Pr_T = \varepsilon_m/\varepsilon_H \tag{3.24}$$

In order to demonstrate the consistency of the Pr_T results calculated using the method outlined above with the Pr_T data obtained by Pimenta [2] from measurements of $\overline{u'v'}$, $\overline{v't'}$, and dT/dU, values of Pr_T were calculated using the present method for the unaccelerated, unblown U_∞ = 89 ft/sec case reported by Pimenta. Results of this calculation are compared in Figure 3-38 with the measured values of Pr_T reported by Pimenta. The two methods give results which agree well in the inner region. The calculated data are very uncertain in the outer region where $\frac{\partial U}{\partial y}$ and $\frac{\partial T}{\partial y}$ approach zero since the uncertainty in the numerical calculations of the derivatives approaches infinity as $y \to \delta$. Pimenta avoided this increase in uncertainty by calculating dT/dU from the linear $(T_w-T)/(T_w-T_\infty)$ vs. U/U_∞ plots discussed previously.

Calculated values of Pr_T for the four acceleration cases of this study are presented in Figure 3-39. Also shown are the bounds on the smooth wall acceleration data reported by Kearney for $K \leq 2.5 \times 10^{-6}$ and the calculated data for Pimenta's $K_r = 0$ case. The rough wall data lie at the lower edge of the smooth wall data range. It appears from the present data that the use of a constant $Pr_T = 0.7 - 0.8$ would be a reasonable assumption in a prediction method modeling accelerated flow over the present rough surface. Comparison of the present data with those of Pimenta indicates that for fully rough flow the turbulent Prandtl number is decreased slightly by acceleration.

Mixing lengths calculated using Equation (3.23) are presented in Figure 3-40. In the determination of ℓ, values of $\overline{u'v'}$ calculated from Equations (3.14) and (3.16) were used since comparison with the measured values showed agreement within a few percent and the calculations yielded values of $\overline{u'v'}$ closer to the surface than were possible to obtain with the probes. The plot shows that in the inner region $\ell/(y+\Delta y)$ is slightly lower than the unaccelerated values of 0.40 - 0.41 found by Pimenta. The behavior of ℓ/δ in the outer region is in agreement with that observed by Pimenta for $K_r = 0$.

Calculations of the nondimensional shear stress, τ^+, and nondimensional heat flux, Q^+, are presented in Figure 3-41 for the $K_r = 0.29 \times 10^{-3}$, $F = 0$ and 0.0039 runs. The trends observed are similar to those for smooth wall accelerated flows [25], indicating that the effect of roughness on these nondimensional distributions is small. The turbulent contributions to τ^+ and Q^+ are also shown (denoted with the subscript T). Comparison of the total values with the turbulent ones shows that the laminar contribution to both shear stress and heat flux was extremely small throughout the region of measurement.

Also plotted in Figure 3-41 are Couette flow approximations calculated using

$$\dot{q}''_c = \dot{q}''_w + \tau U + \frac{F\dot{q}''_w}{St}(1 - I/I_w) \tag{3.25}$$

and

$$\tau_c = \tau_w + F\rho_\infty U_\infty U - \frac{y}{2}\left(U_\infty^2 \frac{d\rho_\infty}{dx} + \frac{2\rho_\infty U_\infty^2}{r} K_r\right) \tag{3.26}$$

The expression for $\dot{q}''_c$ is the one normally found by assuming all $\frac{\partial}{\partial x}$ terms to be zero. However, in Equation (3.26) for τ_c only the first two terms on the right hand side are the ones normally retained for the Couette flow approximation. The additional term can be viewed as a correction term for the effects of the pressure gradient. Thus the expression for τ_c might be more accurately labeled a "near-wall" approximation rather than a Couette flow approximation. In any case, it can be observed from the figure that Equations (3.25) and (3.26) provide accurate representations of the behavior of τ^+ and Q^+ in the region very near the wall.

Values of $\overline{v't'}$ for the two unblown equilibrium runs calculated from Equations (3.15) and (3.17) are shown in Figure 3-42 as $\overline{v't'}/U_\tau T_\tau$ vs y/δ. Comparison of these values with the unaccelerated data measured by Pimenta [2] and Orlando [34] on rough and smooth walls, respectively, indicates that the distribution of $\overline{v't'}/U_\tau T_\tau$ is independent of acceleration and surface condition, at least within the ranges of the data available.

Figure 3-43 shows results of calculation of the turbulent kinetic energy production for Pimenta's [2] zero pressure gradient data and the present $K_r = 0.15 \times 10^{-3}$ data. From Equation (3.11), the production term can be written (using the standard boundary layer assumptions) as

$$P = -\overline{u'v'}\frac{\partial U}{\partial y} - \overline{u'^2}\frac{\partial U}{\partial x} + \overline{v'^2}\frac{\partial U}{\partial x} \tag{3.27}$$

The second and third terms are normally neglected in zero pressure gradient flows. In the calculations presented in Figure 3-43, the last term in Equation (3.27) was neglected since measurements of $\overline{u'^2}$ were made much closer to the wall than those of $\overline{v'^2}$. Thus the results shown present an upper bound on the effect of the pressure gradient through the $\frac{\partial U}{\partial x}$ terms.

In a boundary layer subjected to a favorable pressure gradient, the second term in (3.27) is negative and thus appears as a sink for turbulent kinetic energy. Hinze [22] notes that one should expect a decrease in q^2 as a result. Such a decrease in turbulence energy was noted in the present accelerated data (see Figure 3-31, for example). However, the results shown in Figure 3-43 indicate that for the present data the production is decreased with acceleration primarily because of changes in the distributions of $-\overline{u'v'}$ and $\frac{\partial U}{\partial y}$, while the sink term remains of negligible magnitude.

3.3 Heat Transfer Predictions and Supplementary St Data

The Stanton number data discussed in previous sections were all for constant F, constant T_w boundary conditions. In the period following the investigation reported by Pimenta [2] and in the course of the present study, additional St cases were run for conditions of variable of T_w and F. A prediction method for rough wall heat transfer with variable velocity, wall temperature and blowing was developed using these data. In this section, the prediction method is described and some typical comparisons of data and predictions are presented. Additional cases of St with variable boundary conditions, not presented in the Figures, are tabulated in Appendix IV.

For smooth walls the variable wall temperature case was dealt with by Reynolds, et al. [39], using superposition based on a kernel function describing the downstream effects of a step change in wall temperature. Whitten [40] extended this to include variable blowing and Orlando [34] used this same method for variable wall temperatures in adverse pressure gradients. However, Orlando found that smooth wall Stanton numbers were not affected by the adverse pressure gradients investigated when presented in enthalpy thickness coordinates.

It was shown by Healzer [1] and Pimenta [2] over a range of free stream velocities that for a fully rough turbulent boundary layer flow on the present surface, with constant U_∞, T_w and F

$$St = f(\Delta_2/r, F) \tag{3.28}$$

from which it follows that

$$\Delta_2 = f(x/r, F) \tag{3.29}$$

where r is the radius of the spheres comprising the test surface. Thus there is a unique curve of St vs x/r for each value of F, so long as both U_∞ and T_w are uniform. The present data for constant U_∞ and ΔT confirm this, being well represented by the interpolation expression

$$\log_{10} St_o = A + B \log_{10}(x/r) + C \log_{10}^2(x/r) \tag{3.30}$$

where

$$A = -1.36 + 48.2\ F$$

$$B = -0.61 - 57.4\ F$$

$$C = 0.0675 + 3.69\ F$$

for $0 \leq F \leq 0.004$. Figure 3-44 shows the St_o data and interpolation curves from Equation (3.30) for three values of F. The F = 0.002 data are from Pimenta's [2] study and were untripped, while the data for F = 0 and 0.0039 are from the present study which did use a boundary layer trip.

Now consider the case of an unheated starting length with constant F and U_∞. Reynolds, et al. [39], showed that for turbulent flow over a smooth wall with F = 0 the Stanton number downstream of a step increase in wall temperature could be predicted by

$$\frac{St}{St_o} = \left[1 - \left(\frac{\ell}{x}\right)^m\right]^n \qquad x > \ell \tag{3.31}$$

where ℓ is the x-position of the temperature step, m = 9/10 and n = -1/9. This expression was then used as the kernel function in a superposition integral for predictions with arbitrarily varying ΔT, as follows:

$$\frac{St_x}{St_o} = \frac{1}{\Delta T_x} \int_o^x \left[1 - \left(\frac{\xi}{x}\right)^m\right]^n \frac{d[\Delta T(\xi)]}{d\xi}\, d\xi \tag{3.32}$$

A kernel function of the same type can be developed for the present rough wall unheated starting length results, and the data are well represented using m = 1 and n = -0.22. Thus, for fully rough turbulent flow with unheated starting length and U_∞, F and ΔT constant

$$\frac{St_x}{St_o} = \left[1 - \left(\frac{\ell}{x}\right)\right]^{-0.22} \qquad x > \ell \tag{3.33}$$

where St_o is evaluated at the same F and x as St_x. Figure 3-45 shows the unheated starting length St data and curves evaluated using Equation (3-33) for two cases with F = 0 and one case with F = 0.0039.

As shown previously, for a fully rough turbulent boundary layer a positive value of dU_∞/dx gives a higher Stanton number than the constant velocity case at the same x or Δ_2. Thus, the response of Stanton number to positive dU_∞/dx is the same as to positive values of dT_w/dx. Also, consideration of the energy integral equation (with constant properties) in the form

$$St + F = \frac{1}{U_\infty \Delta T} \frac{d}{dx} (\Delta_2 U_\infty \Delta T) \tag{3.34}$$

shows that the variables U_∞ and ΔT always appear in the product form as $(U_\infty \Delta T)$. (Of course, Equation 3.34 is a conservation equation obeyed by both smooth and rough wall flows. The different response of smooth and fully rough layers to positive dU_∞/dx is evidently related to the effect of the viscous sublayer present in smooth wall layers on the rate equations.)

These observations lead to the following proposed prediction method for cases of variable U_∞, ΔT and F in a fully rough flow:

$$\frac{St_x}{St_o} = \frac{1}{(U_\infty \Delta T)_x} \int_o^x \frac{1}{(1-\xi/x)^{.22}} \frac{d}{d\xi} [U_\infty(\xi)\ \Delta T(\xi)]\ d\xi \quad x > \xi \tag{3.35}$$

where St_o is evaluated at the same x and F as St_x. The predictions which follow were obtained by numerically integrating Equation (3.35). For these calculations, the integral was expanded to a sum of two integrals and the $dU_\infty(\xi)$ term was approximated by assuming a linear variation of U_∞ with ξ across each integration step.

It was found that Equation (3.35) worked well except in cases where there were steps in F. Obviously, St cannot change instantaneously after a

step; therefore, modification of the method is required to account for the "lag" in St after such a step. A simple and satisfactory approach is to define a new St_o which is modified by the kernel function, giving

$$St_o^* = St_o - \sum_{i=1}^{N} \Delta St_{o_i} \left[1 - \left(1 - \frac{\ell_i}{x} \right)^{0.22} \right] \quad x > \ell_i \tag{3.36}$$

where $St_{o_i} = St_o(\ell_i^+) - St_o(\ell_i^-)$ and ℓ_i is the position of the ith step. Thus, when there are steps in F, use of St_o^* in place of St_o in Equation (3.35) accounts for the "lag" in St caused by the step.

Figure 3-46 presents data and predictions for constant U_∞, F = 0 and a bilinear variation of wall temperature; Figure 3-47 shows cases for the $K = .28 \times 10^{-6}$ nonequilibrium run both with and without unheated starting length; and in Figure 3-48 data and predictions for an unblown, $K_r = .50 \times 10^{-3}$ equilibrium run are presented. In all three figures the agreement between the data and predictions is very good.

Figures 3-49 and 3-50 present data from two cases designed to provide a test of any prediction method proposing to calculate heat transfer in the fully rough turbulent boundary layer. The flow is accelerated arbitrarily and subjected to a step in F, followed by a variable F and then a step back to F = 0. Figure 3-49 presents the ΔT constant case, while Figure 3-50 shows results when a step in ΔT is imposed in the region of variable F. In both figures the dashed line is the prediction using Equation (3.35), while the solid line shows the prediction including the modification for the steps in F (Equation (3.36)). It is evident that the lag introduced by the steps in F must be taken into account, but once this is done the present predictions are in excellent agreement with the data.

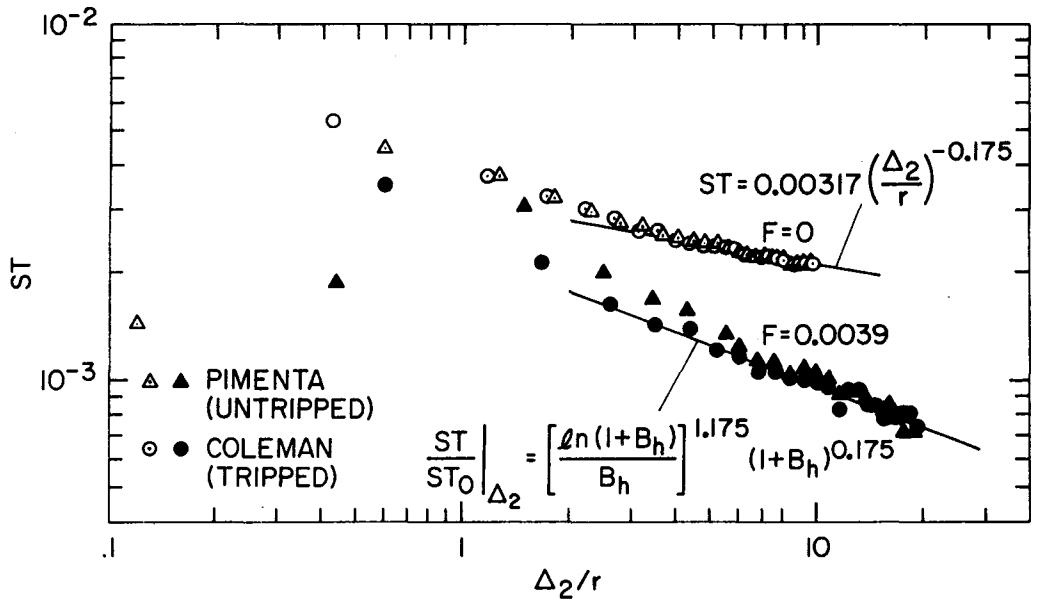

Figure 3-1. Zero Pressure Gradient Stanton Number Data

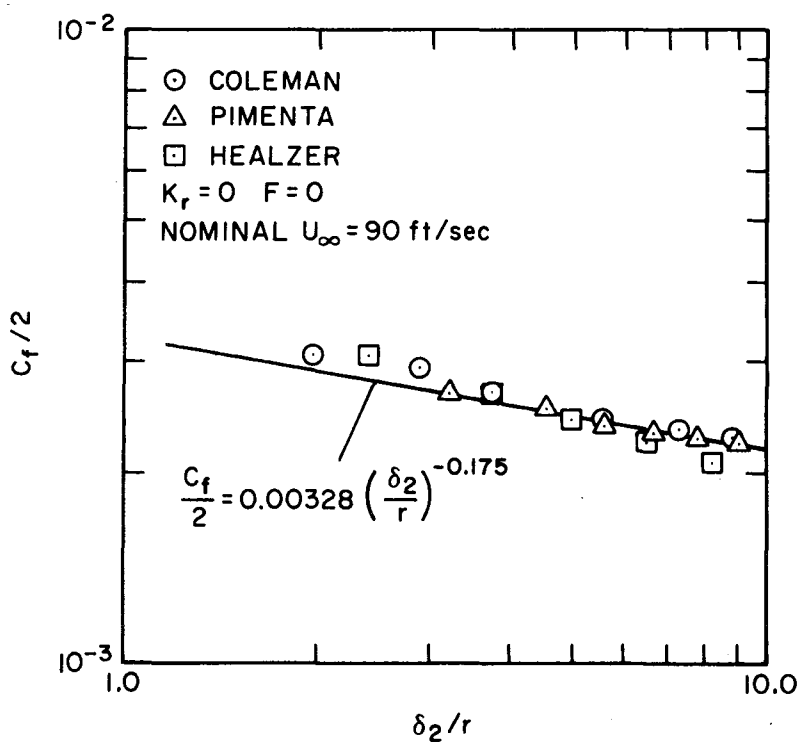

Figure 3-2. Zero Pressure Gradient Skin Friction Coefficient Data

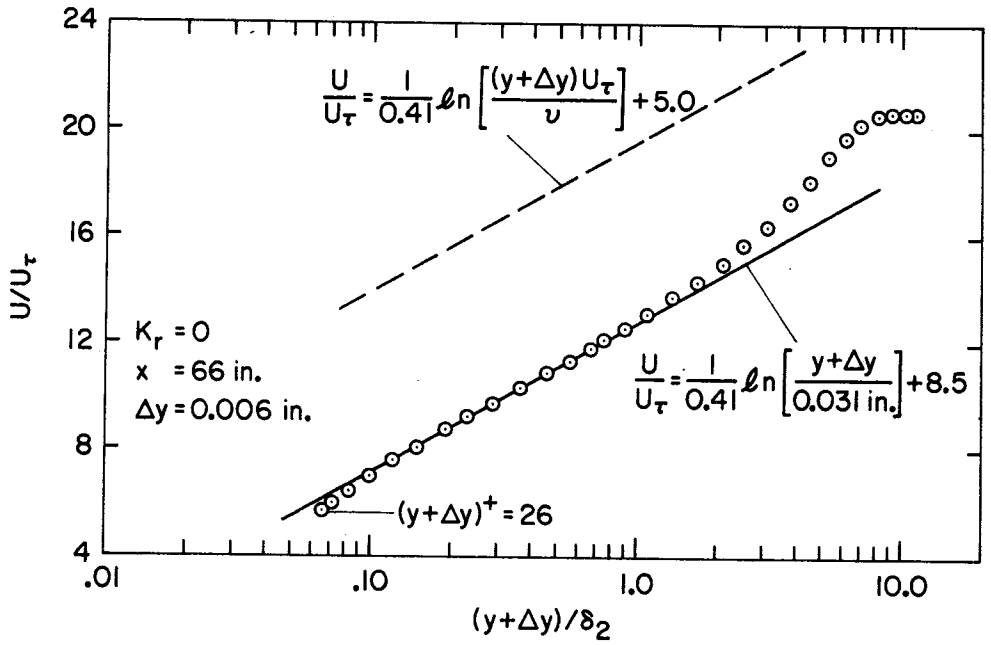

Figure 3-3. Typical Mean Velocity Profile for Fully Rough, Zero Pressure Gradient Flow

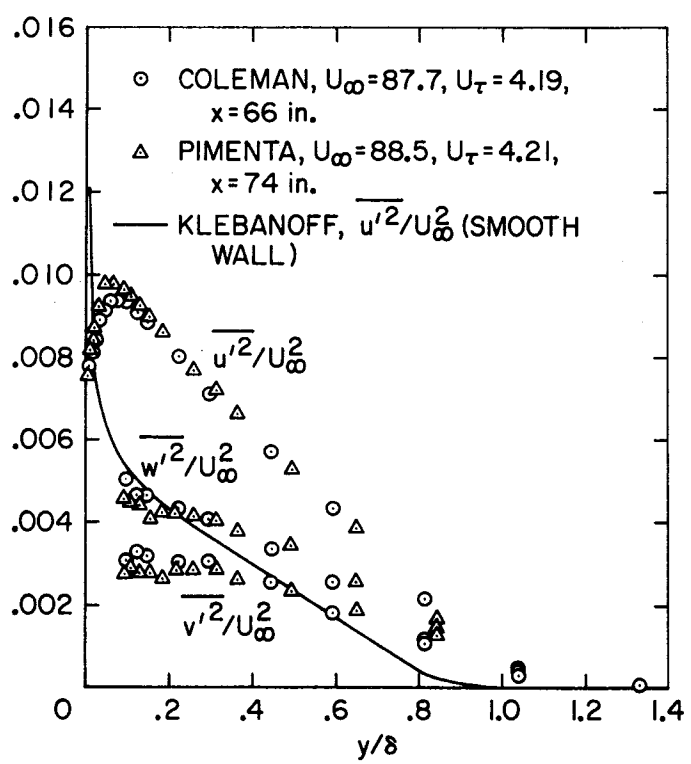

Figure 3-4. Components of Turbulent Kinetic Energy for Fully Rough, Zero Pressure Gradient Flow

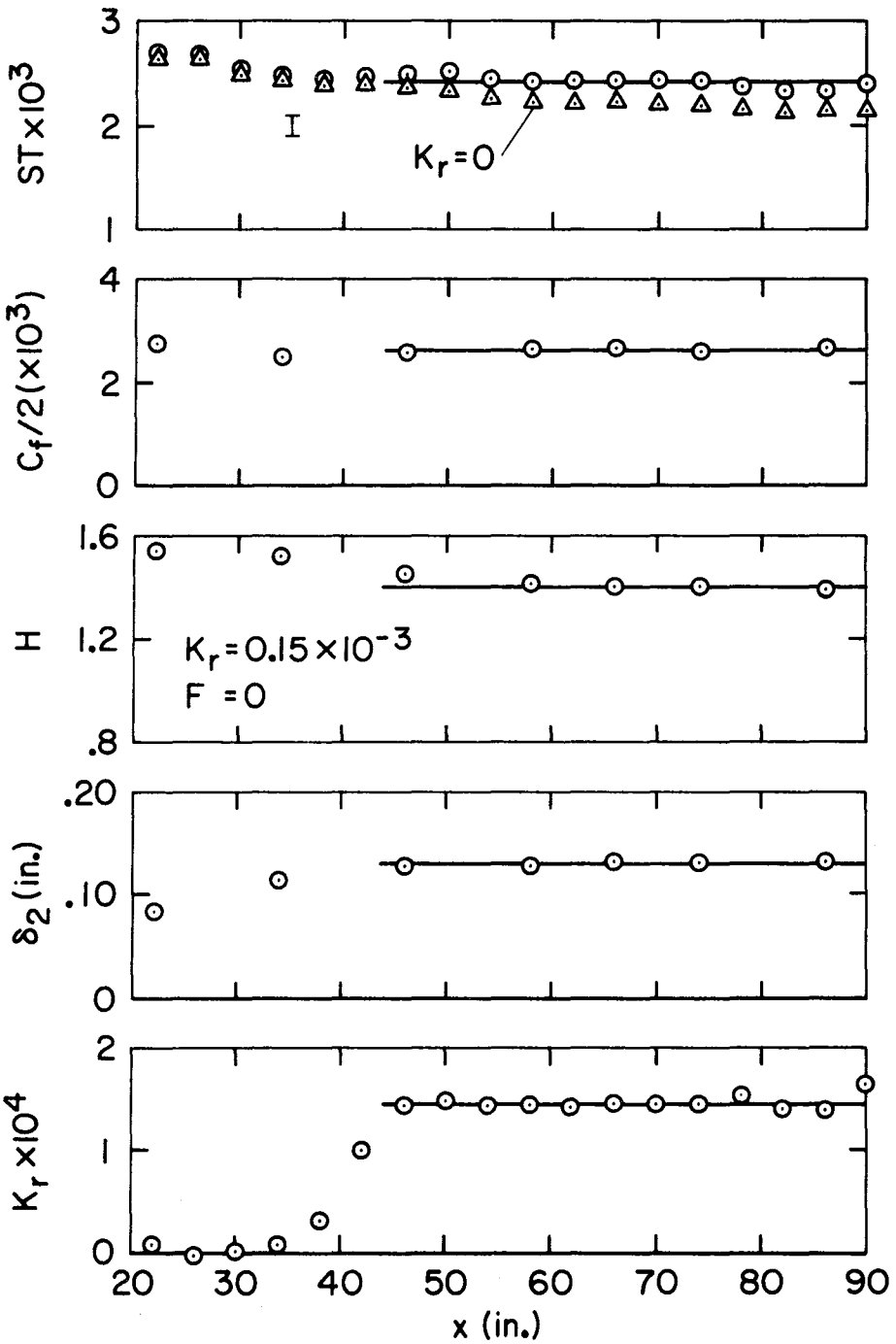

Figure 3-5. Summary Data for $K_r = 0.15 \times 10^{-3}$
F = 0 Equilibrium Acceleration Case

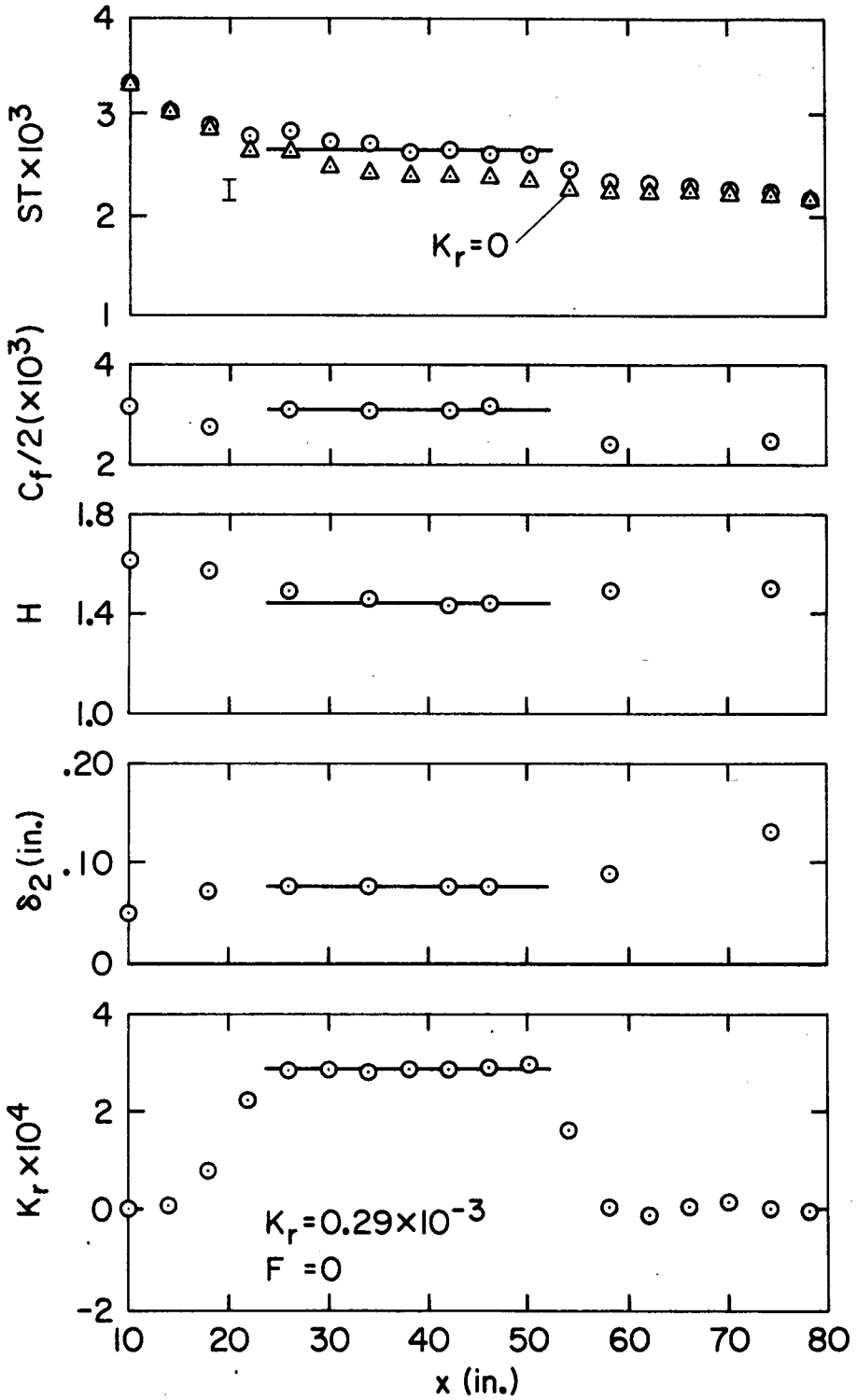

Figure 3-6. Summary Data for $K_r = 0.29 \times 10^{-3}$, F = 0 Equilibrium Acceleration Case

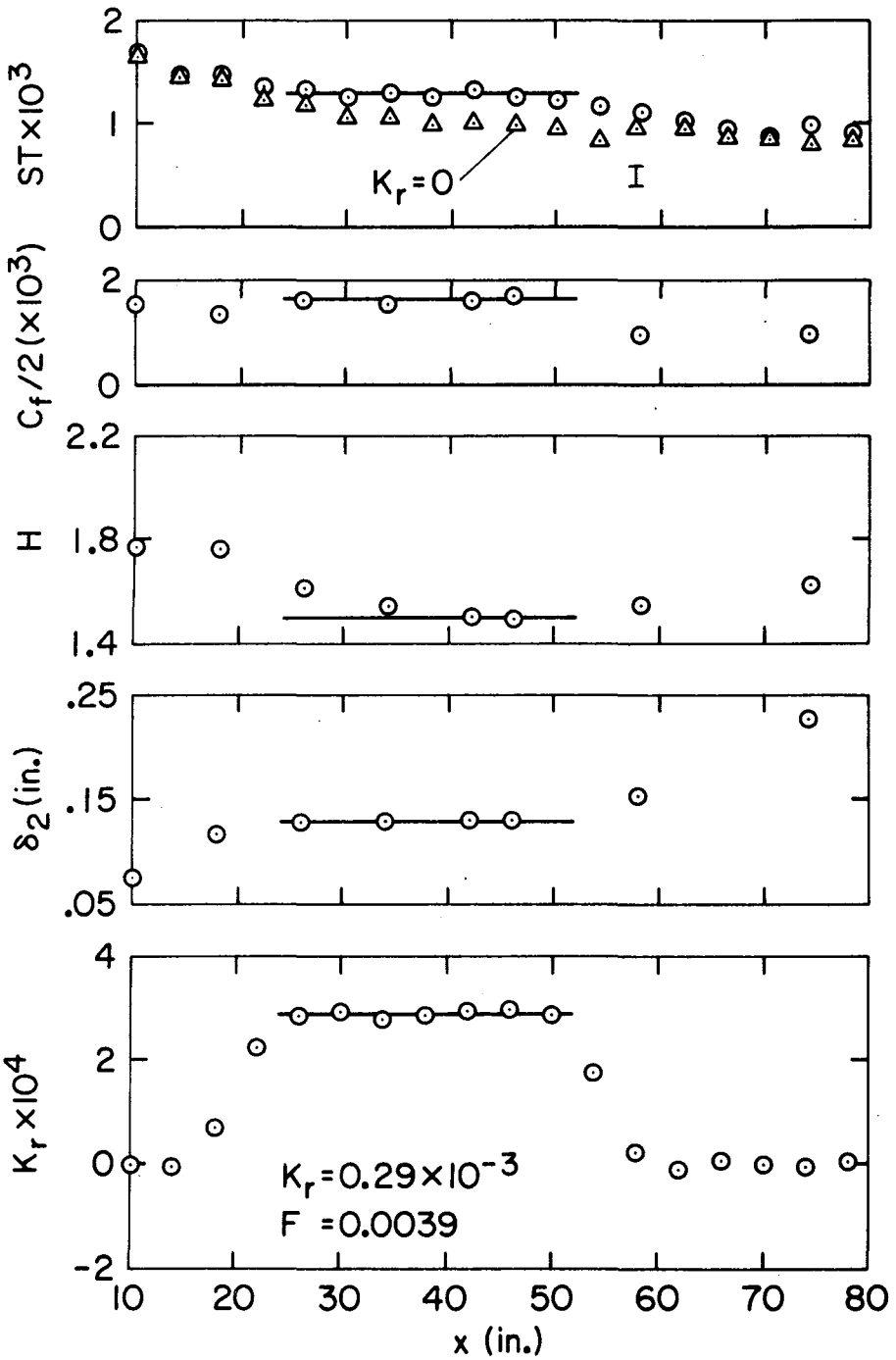

Figure 3-7. Summary Data for $K_r = 0.29 \times 10^{-3}$, F = 0.0039 Equilibrium Acceleration Case

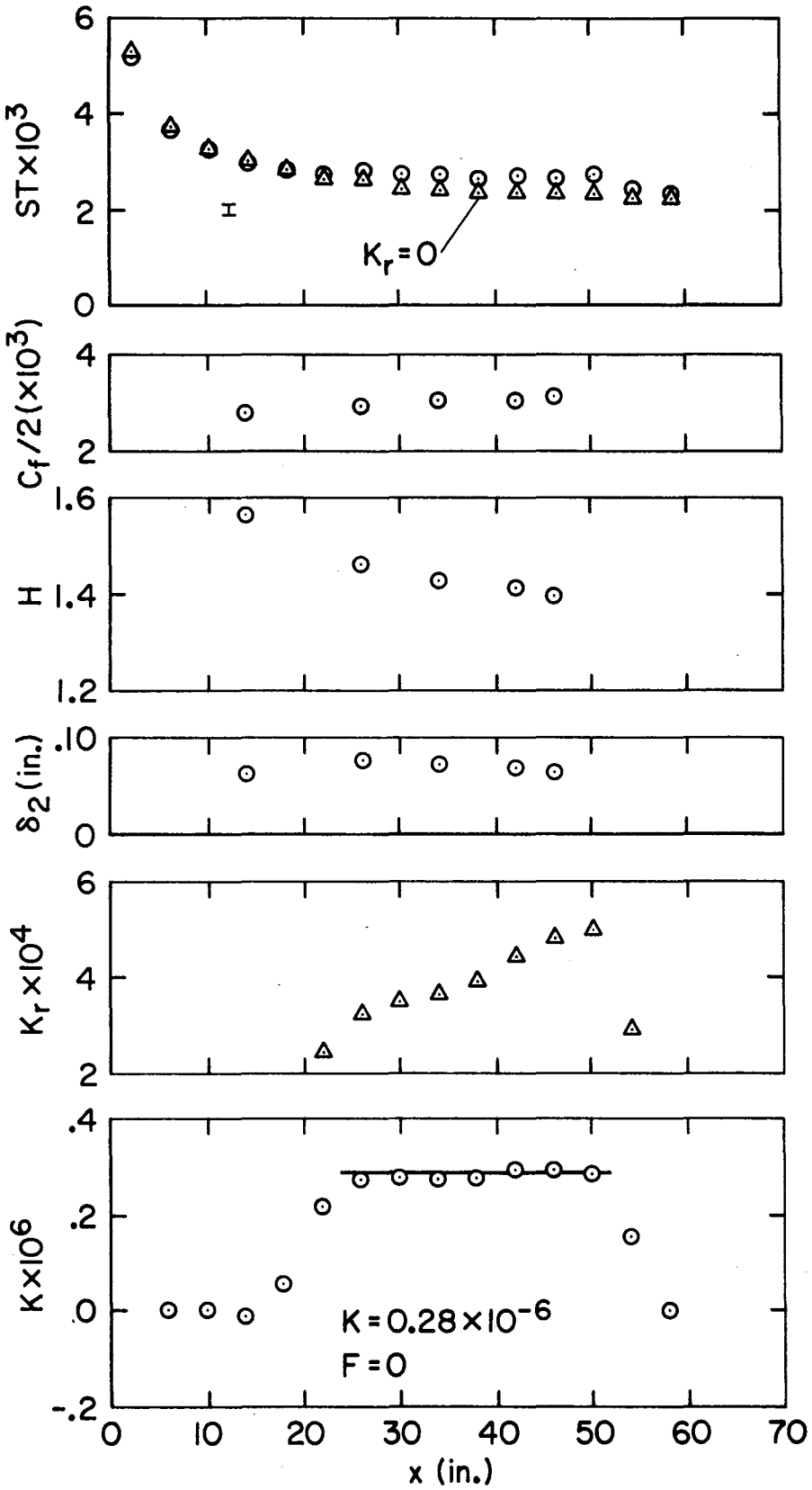

Figure 3-8. Summary Data for $K = 0.28 \times 10^{-6}$, $F = 0$ Nonequilibrium Acceleration Case

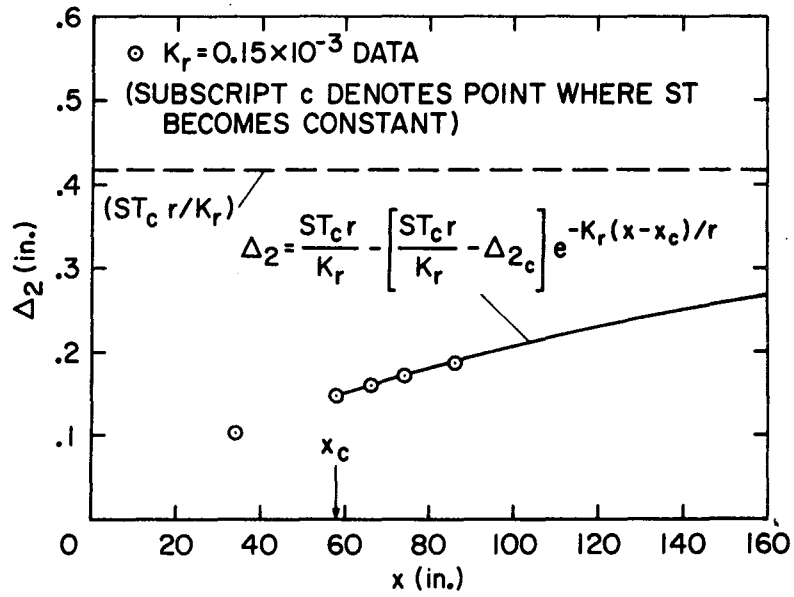

Figure 3-9. Comparison of Enthalpy Thickness Data and Solution for Equilibrium Enthalpy Thickness Behavior

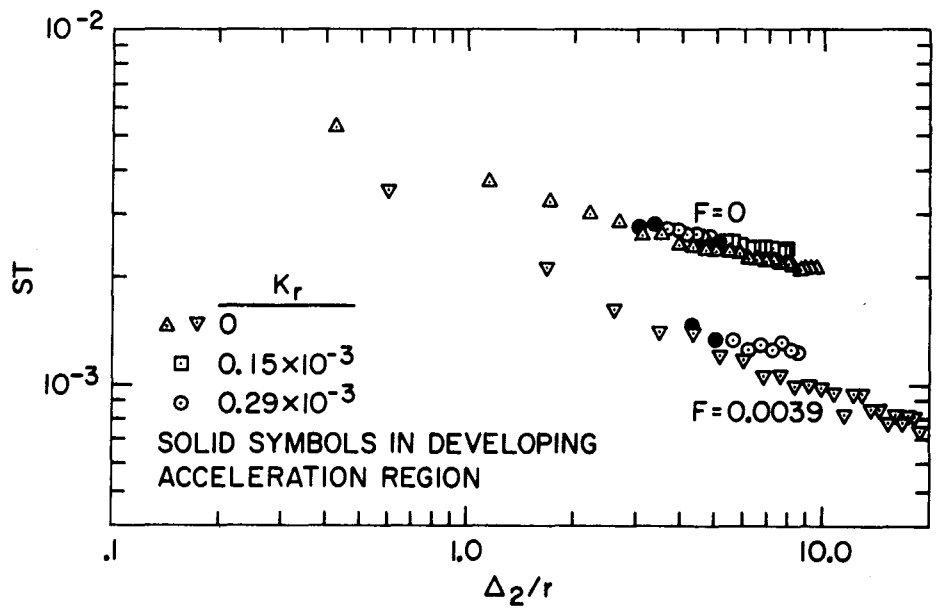

Figure 3-10. Equilibrium Acceleration Stanton Number Data vs (Enthalpy Thickness/Sphere Radius)

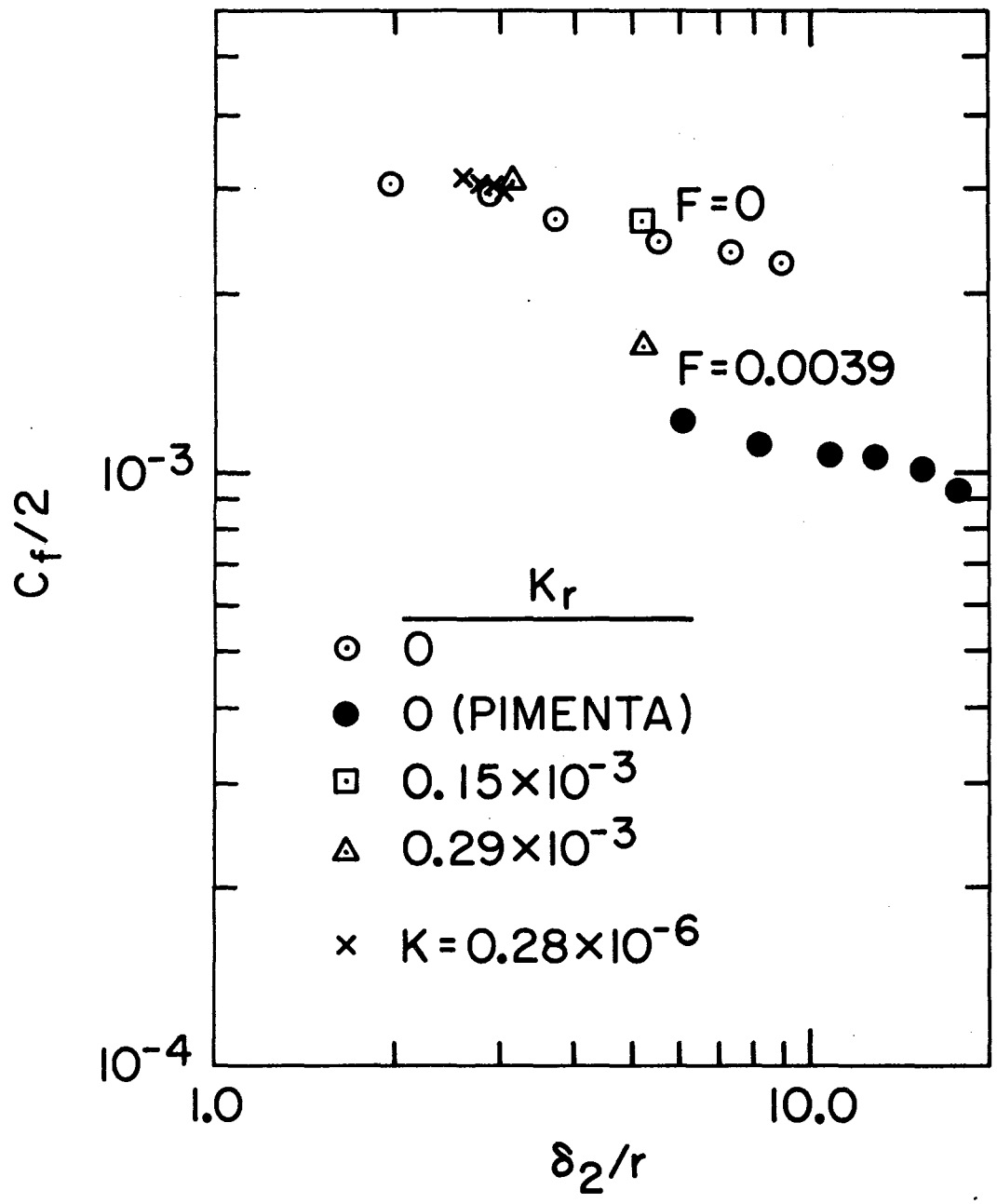

Figure 3-11. Skin Friction Coefficient Data vs (Momentum Thickness/Sphere Radius)

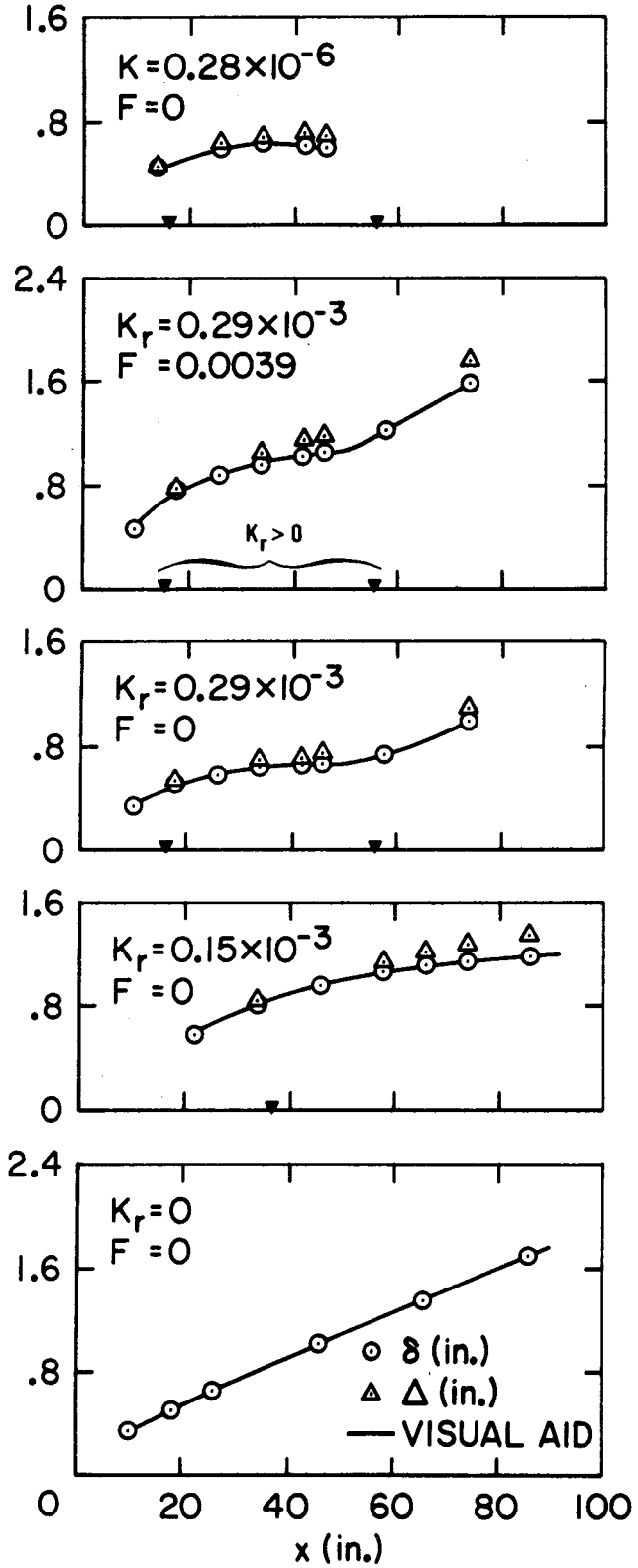

Figure 3-12. Thermal and Velocity Boundary Layer Thicknesses Variation with Axial Distance

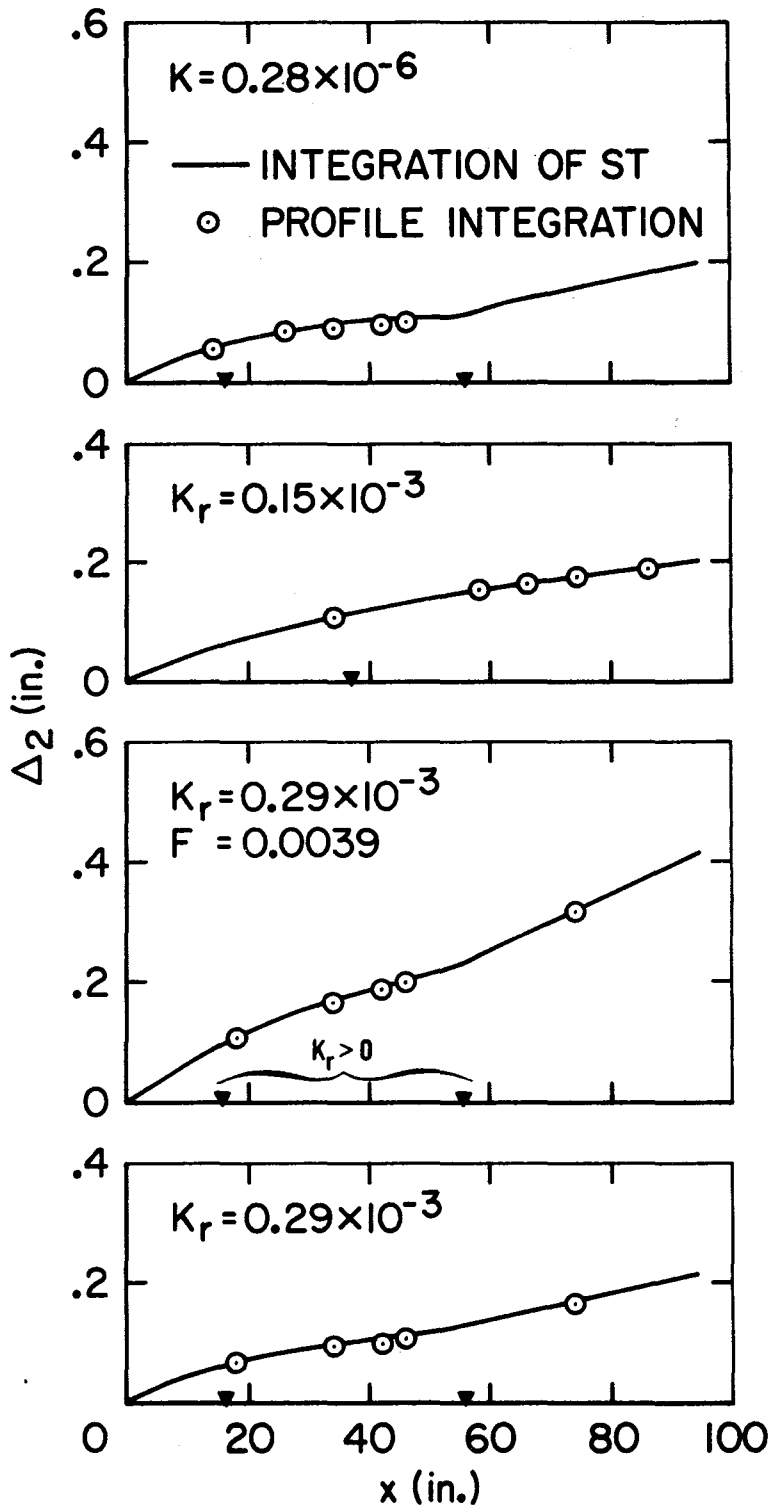

Figure 3-13. Enthalpy Thickness Variation with Axial Distance

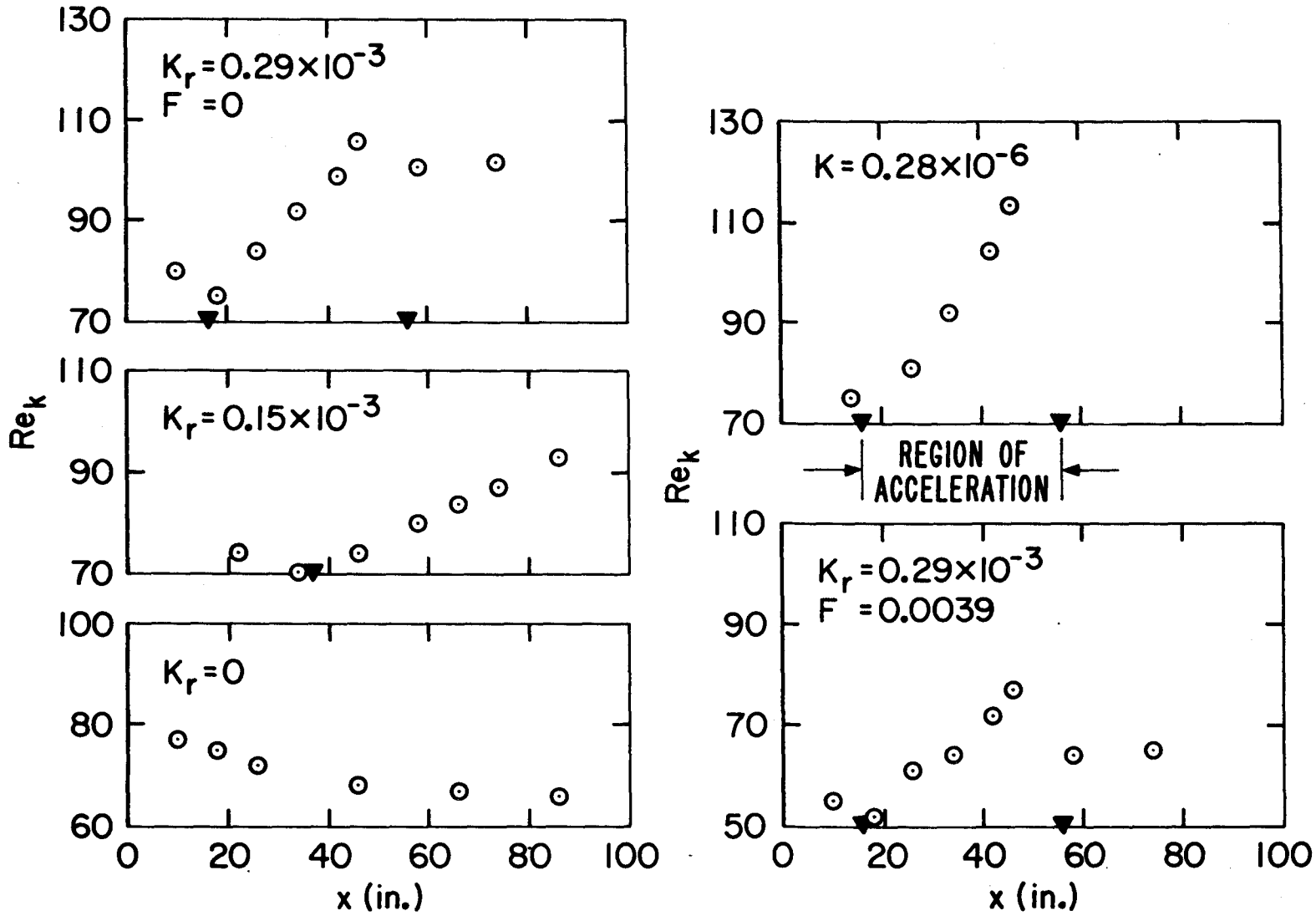

Figure 3-14. Roughness Reynolds Number Variation with Axial Distance

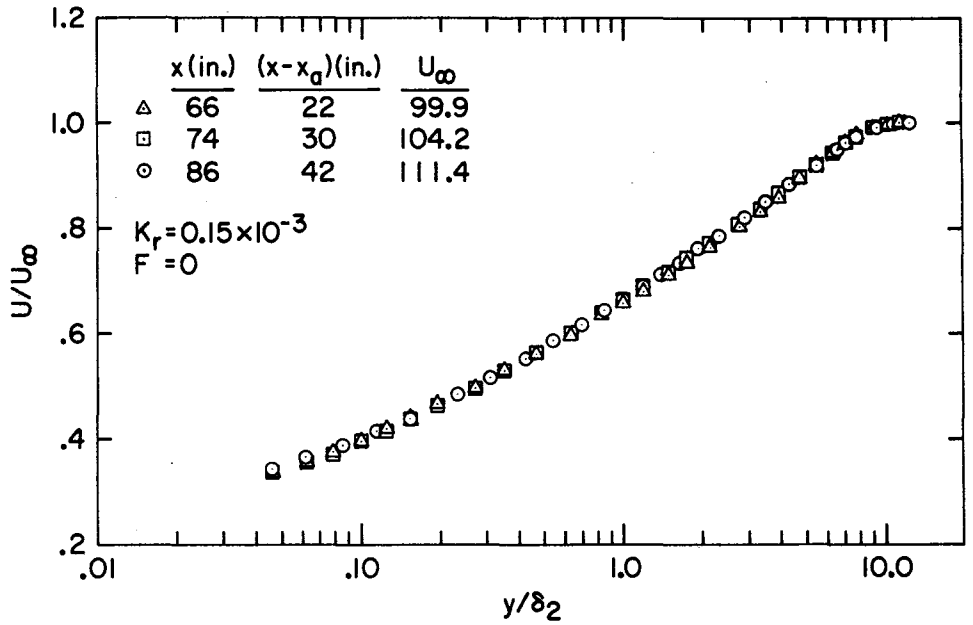

Figure 3-15. Mean Velocity Profiles Illustrating Similarity in Flow Direction (K_r = 0.15 x 10^{-3})

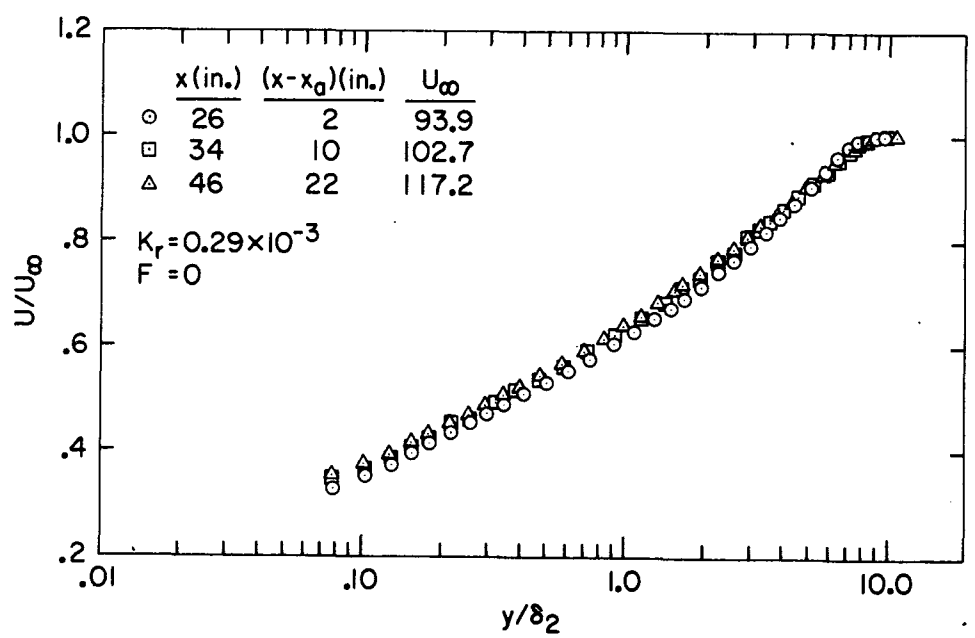

Figure 3-16. Mean Velocity Profiles Illustrating Similarity in Flow Direction (K_r = 0.29 x 10^{-3}, F = 0)

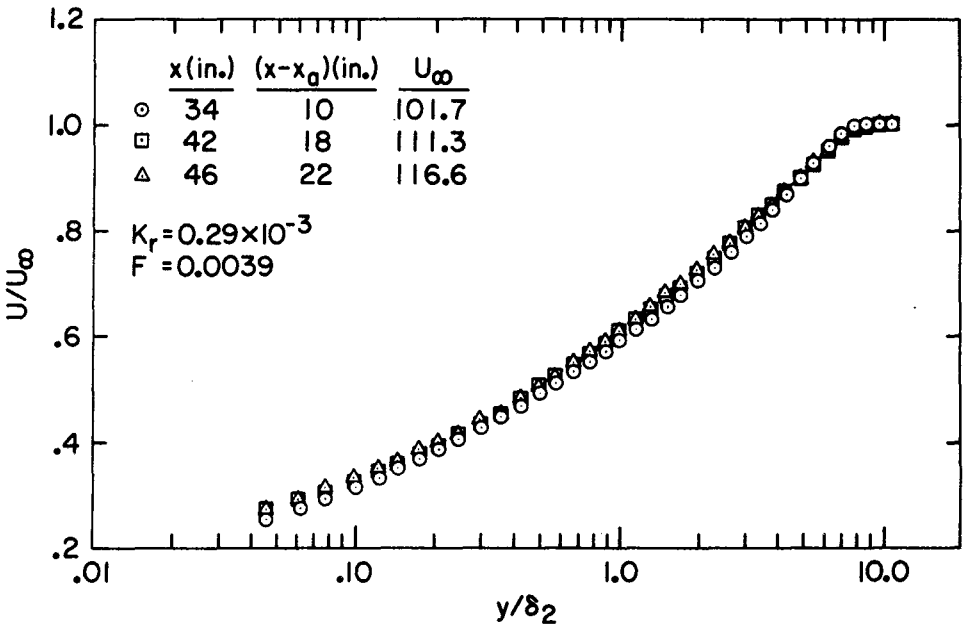

Figure 3-17. Mean Velocity Profiles Illustrating Similarity in Flow Direction (K_r = 0.29 x 10^{-3}, F = 0.0039)

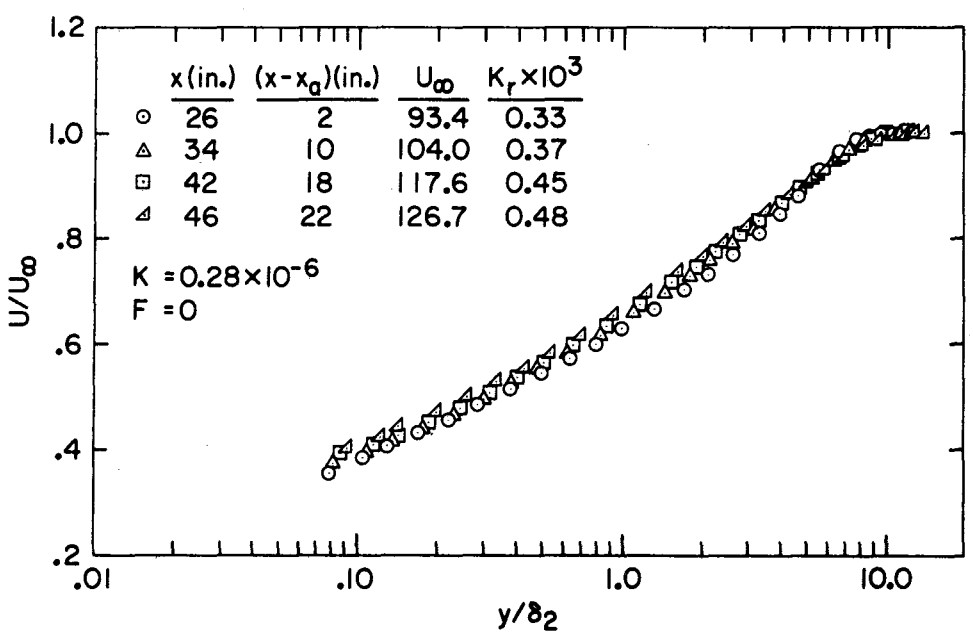

Figure 3-18. Mean Velocity Profiles Illustrating Lack of Similarity in Flow Direction (K = 0.28 x 10^{-6})

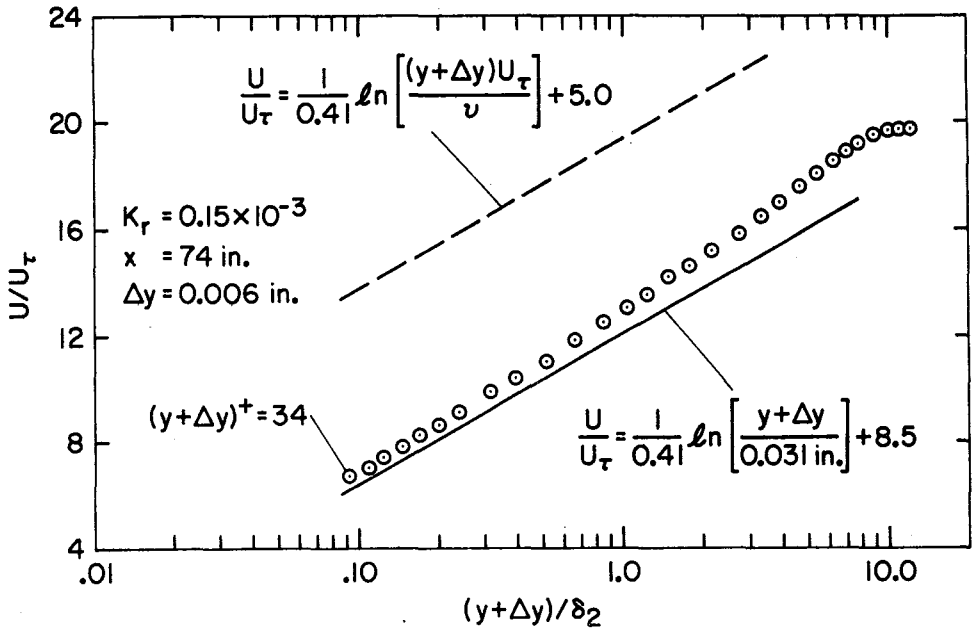

Figure 3-19. Mean Velocity Profile Plotted Using Shifted Wall Position (K_r = 0.15 x 10^{-3})

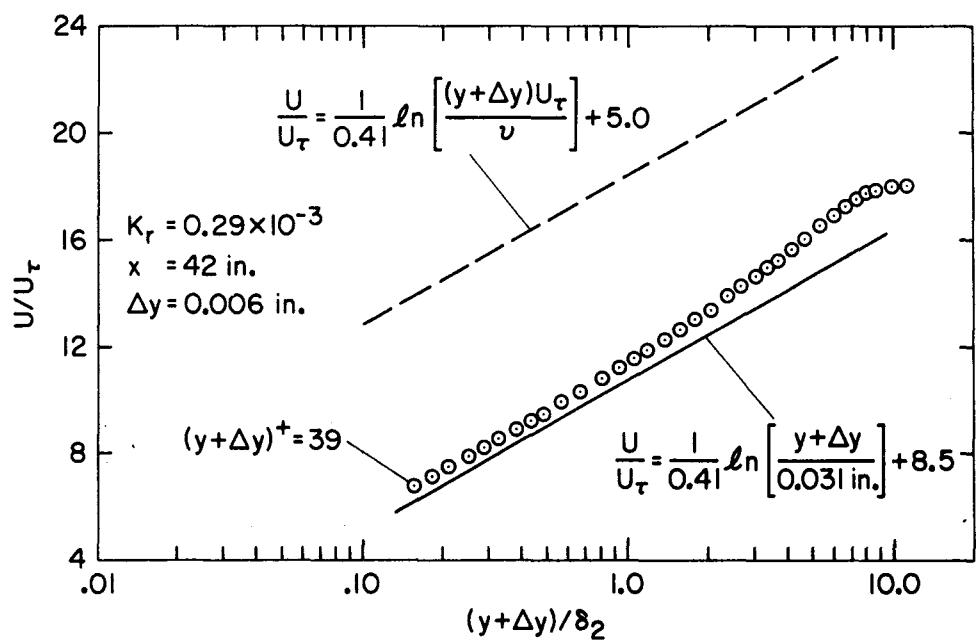

Figure 3-20. Mean Velocity Profile Plotted Using Shifted Wall Position (K_r = 0.29 x 10^{-3}, F = 0)

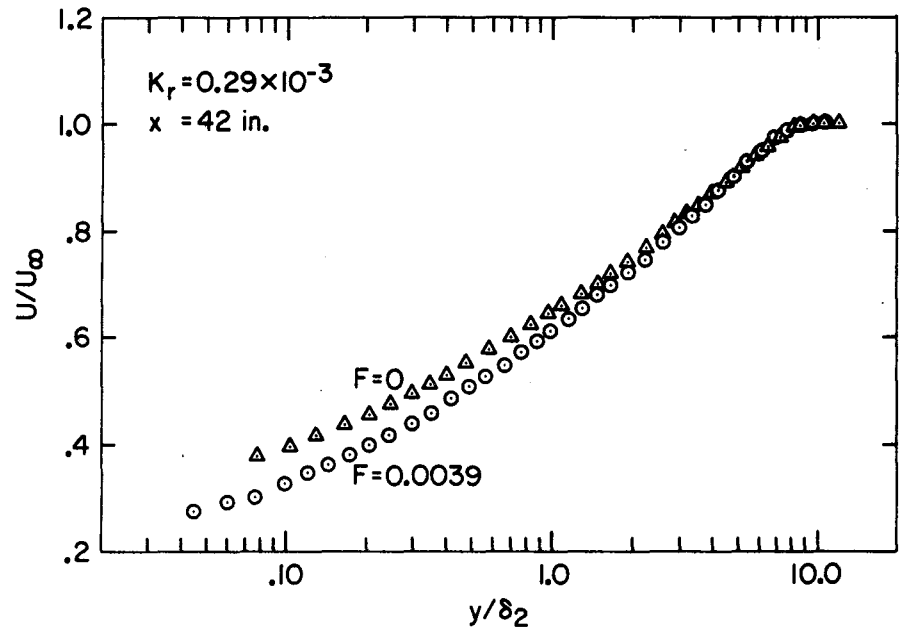

Figure 3-21. Comparison of Blown and Unblown Mean Velocity Profiles at Same Axial Position ($K_r = 0.29 \times 10^{-3}$)

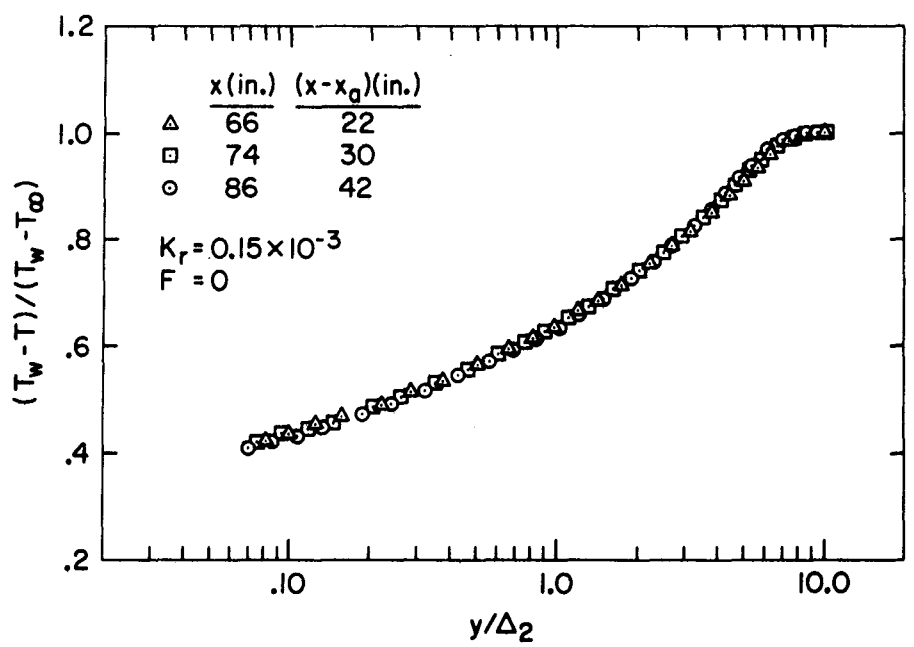

Figure 3-22. Nondimensional Mean Temperature Profiles Illustrating Similarity in Flow Direction ($K_r = 0.15 \times 10^{-3}$)

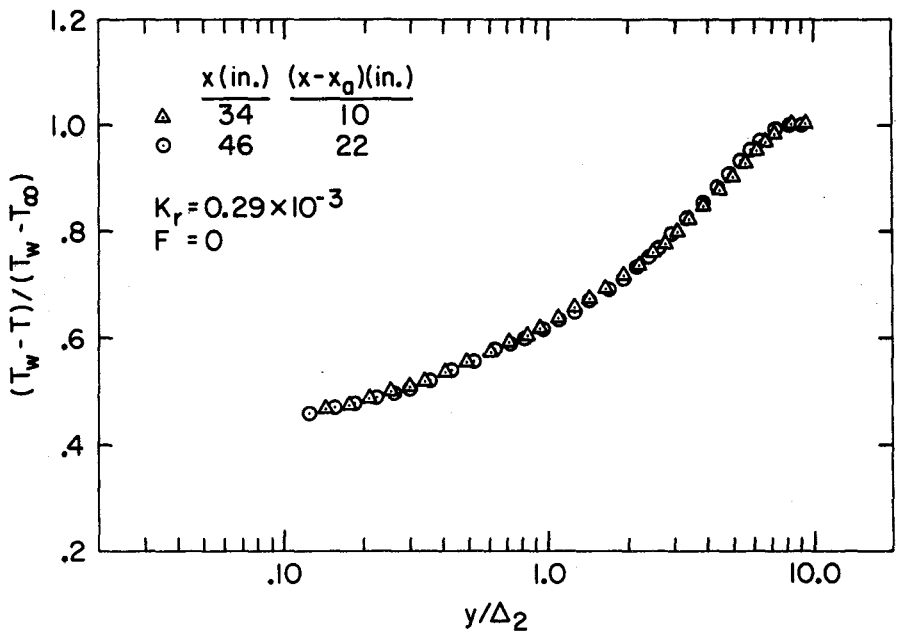

Figure 3-23. Nondimensional Mean Temperature Profiles Illustrating Similarity in Flow Direction (K_r = 0.29 x 10^{-3}, F = 0)

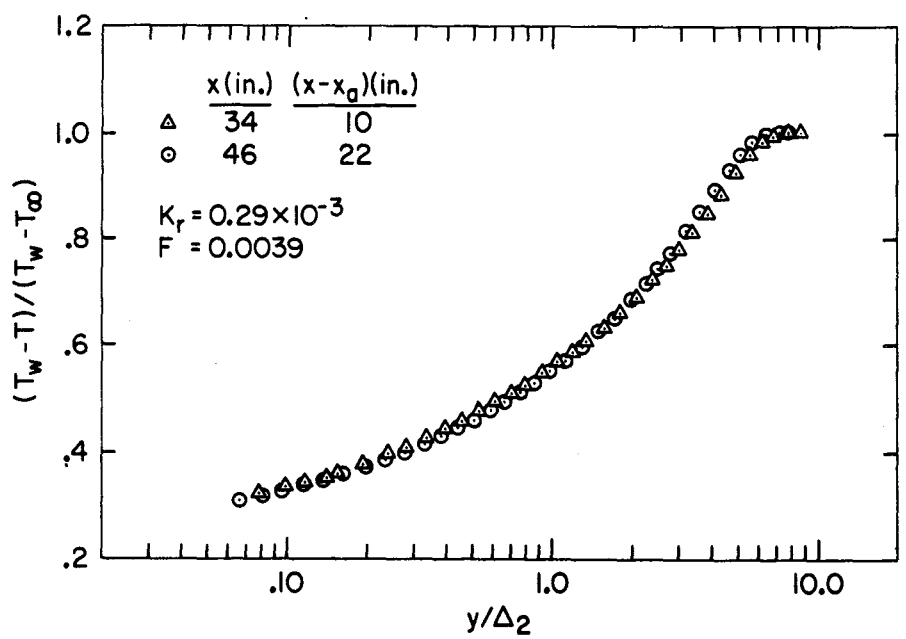

Figure 3-24. Nondimensional Mean Temperature Profiles Illustrating Similarity in Flow Direction (K_r = 0.29 x 10^{-3}, F = 0.0039)

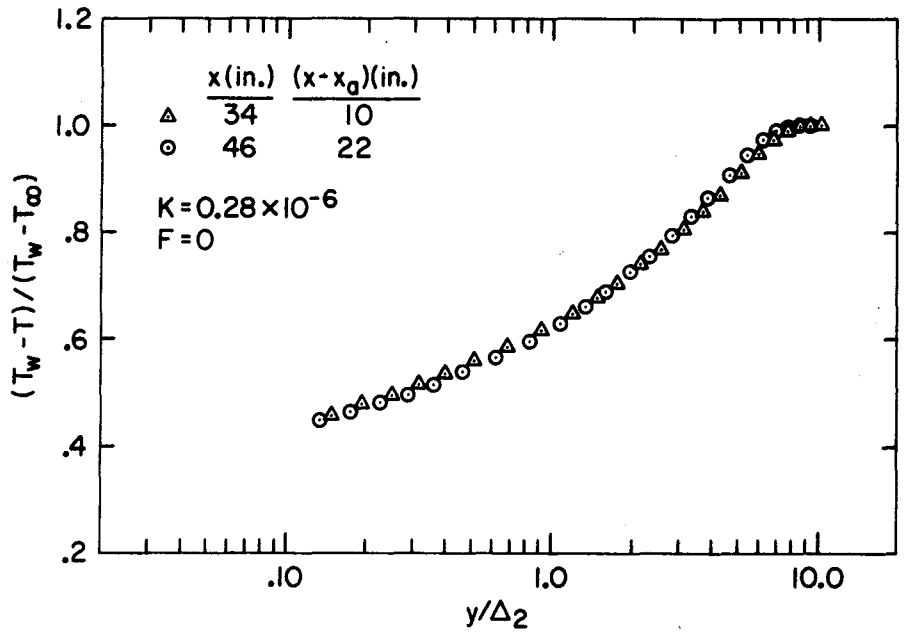

Figure 3-25. Nondimensional Mean Temperature Profiles for Nonequilibrium Acceleration Run ($K = 0.28 \times 10^{-6}$)

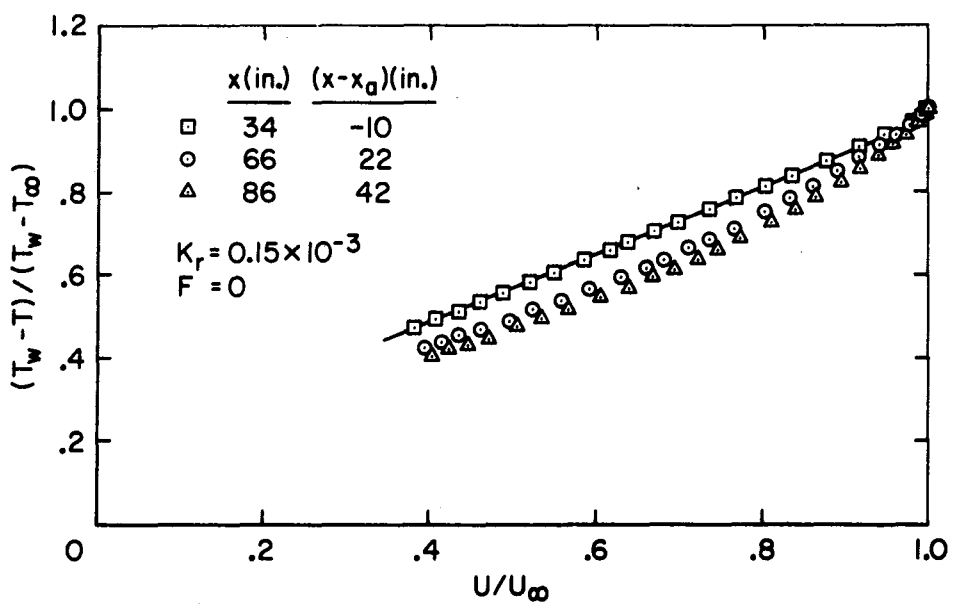

Figure 3-26. Nondimensional Mean Temperature Plotted versus Nondimensional Mean Velocity ($K_r = 0.15 \times 10^{-3}$)

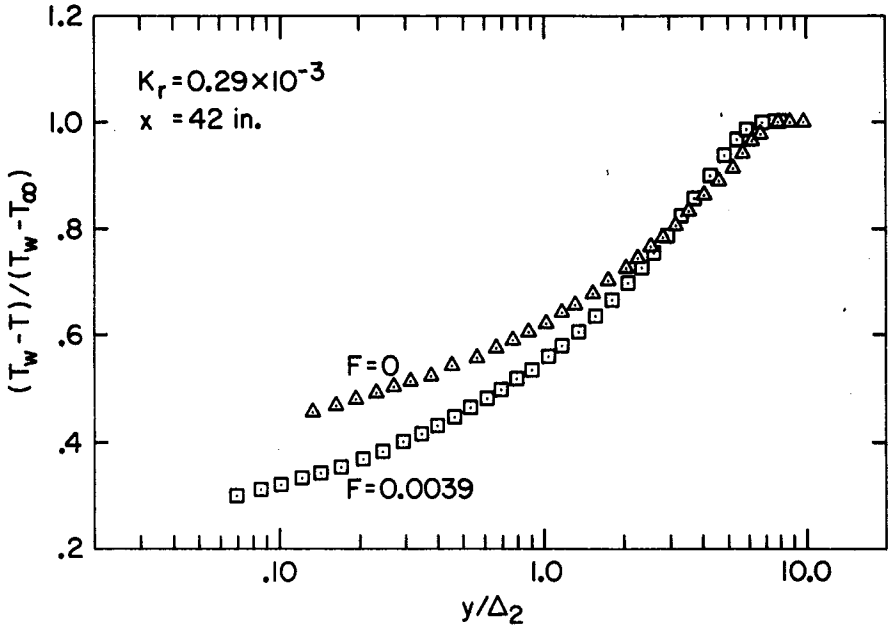

Figure 3-27. Comparison of Blown and Unblown Nondimensional Mean Temperature Profiles at Same Axial Position (K_r = 0.29 x 10^{-3})

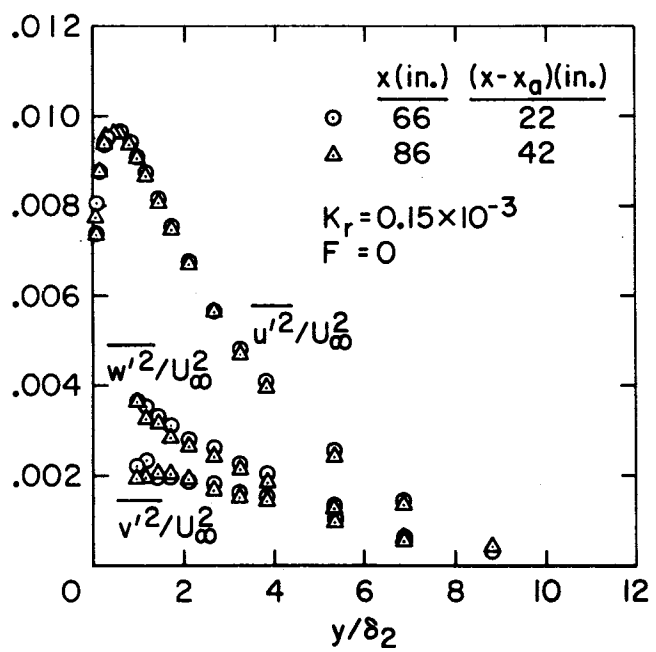

Figure 3-28. Profiles of Turbulent Kinetic Energy Components Illustrating Similarity in Flow Direction (K_r = 0.15 x 10^{-3})

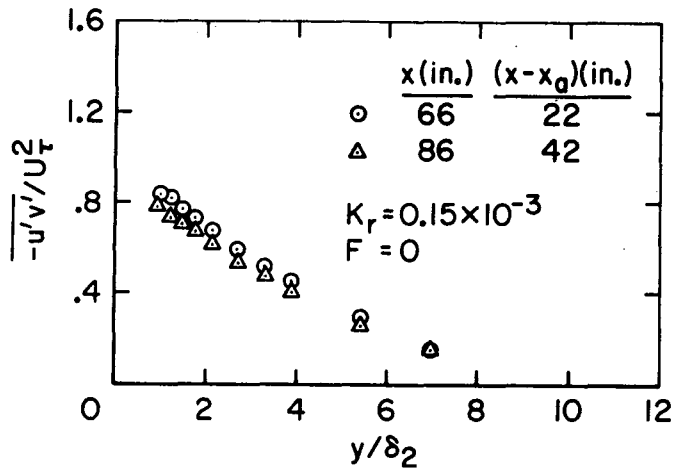

Figure 3-29. Profiles of Reynolds Shear Stress Compared at Two Axial Positions (K_r = 0.15 x 10^{-3})

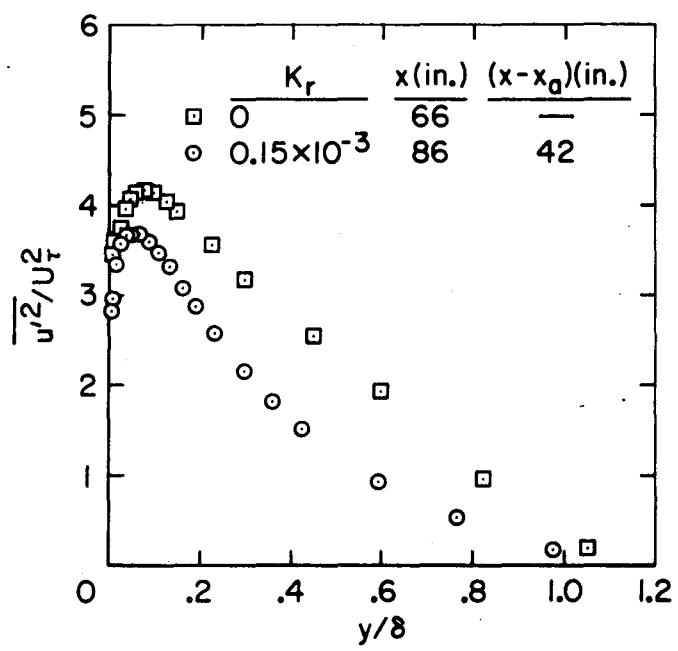

Figure 3-30. $\overline{u'^2}/U_\tau^2$ Profiles Compared for K_r = 0 and K_r = 0.15 x 10^{-3}

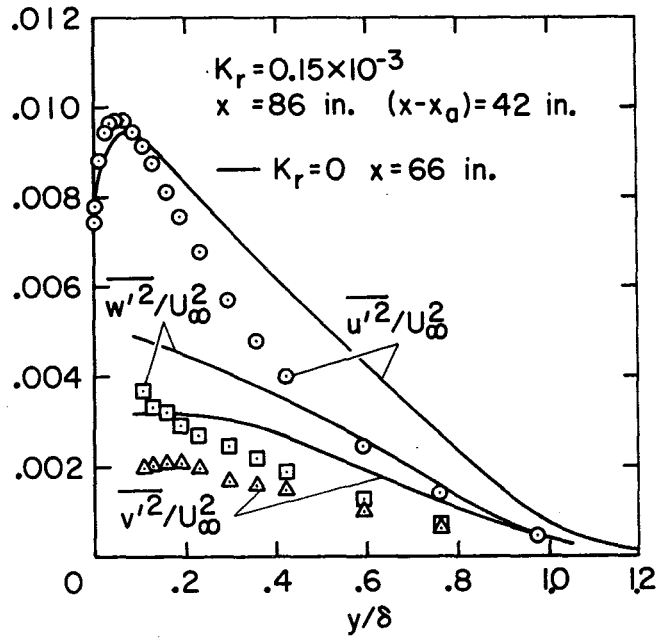

Figure 3-31. Profiles of Components of Turbulent Kinetic Energy Compared for $K_r = 0$ and $K_r = 0.15 \times 10^{-3}$

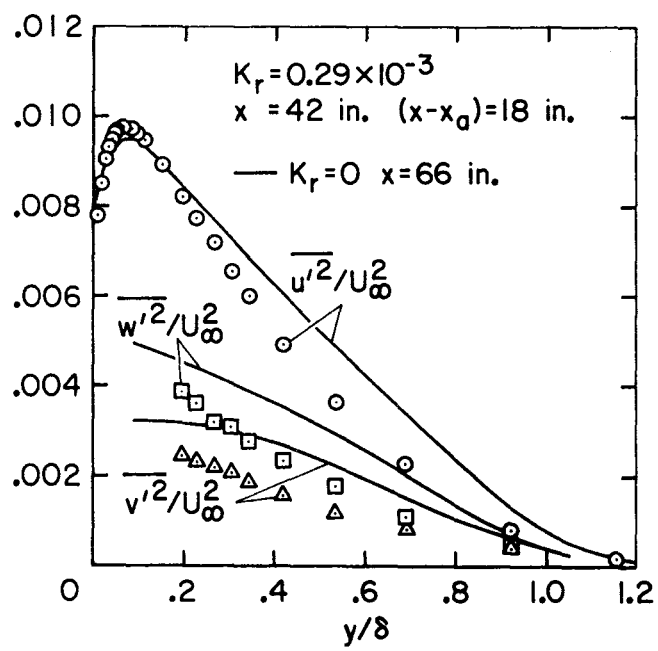

Figure 3-32. Profiles of Components of Turbulent Kinetic Energy Compared for $K_r = 0$ and $K_r = 0.29 \times 10^{-3}$, F = 0

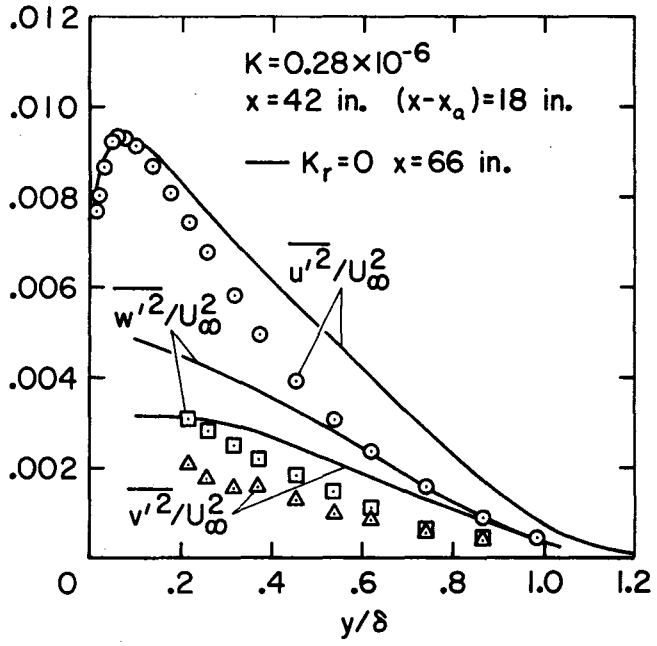

Figure 3-33. Profiles of Components of Turbulent Kinetic Energy Compared for $K_r = 0$ and $K = 0.28 \times 10^{-6}$

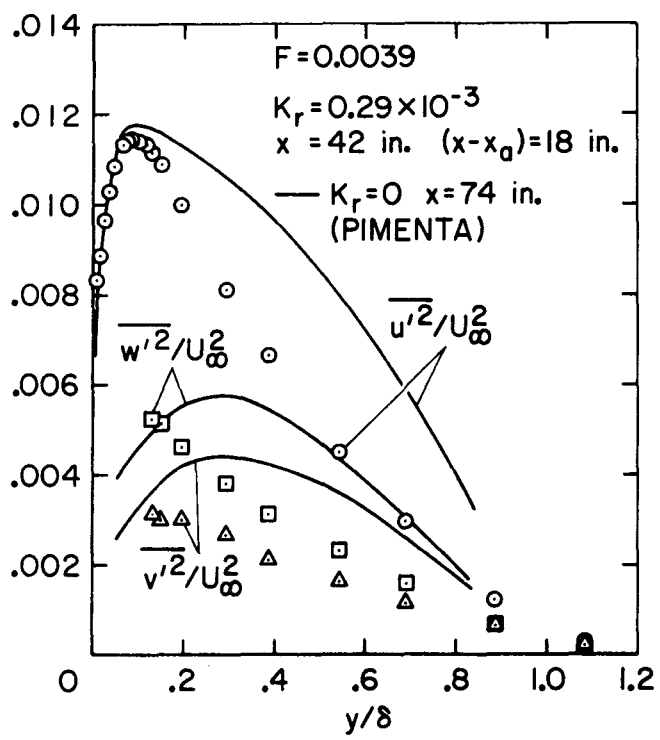

Figure 3-34. Profiles of Components of Turbulent Kinetic Energy Compared for $K_r = 0$, $F = 0.0039$ and $K_r = 0.29 \times 10^{-3}$, $F = 0.0039$

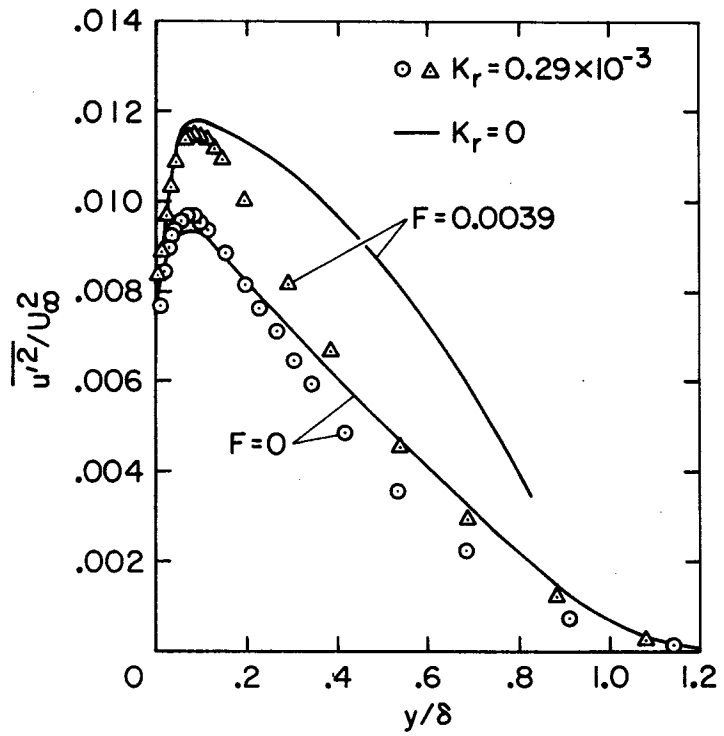

Figure 3-35. Comparison of Blown and Unblown Profiles of $\overline{u'^2}/U_\infty^2$ for Unaccelerated (K_r = 0) and Accelerated (K_r = 0.29 x 10^{-3}) Cases

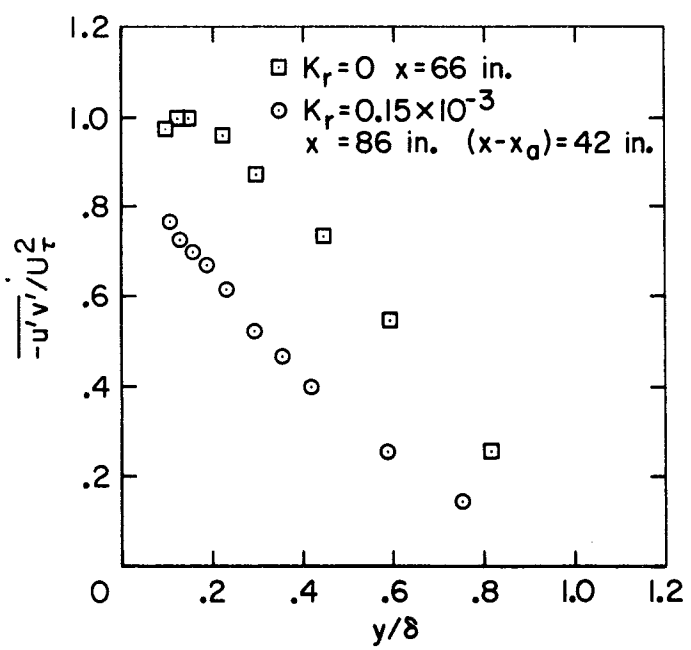

Figure 3-36. Comparison of Reynolds Shear Stress Profiles for K_r = 0 and K_r = 0.15 x 10^{-3}

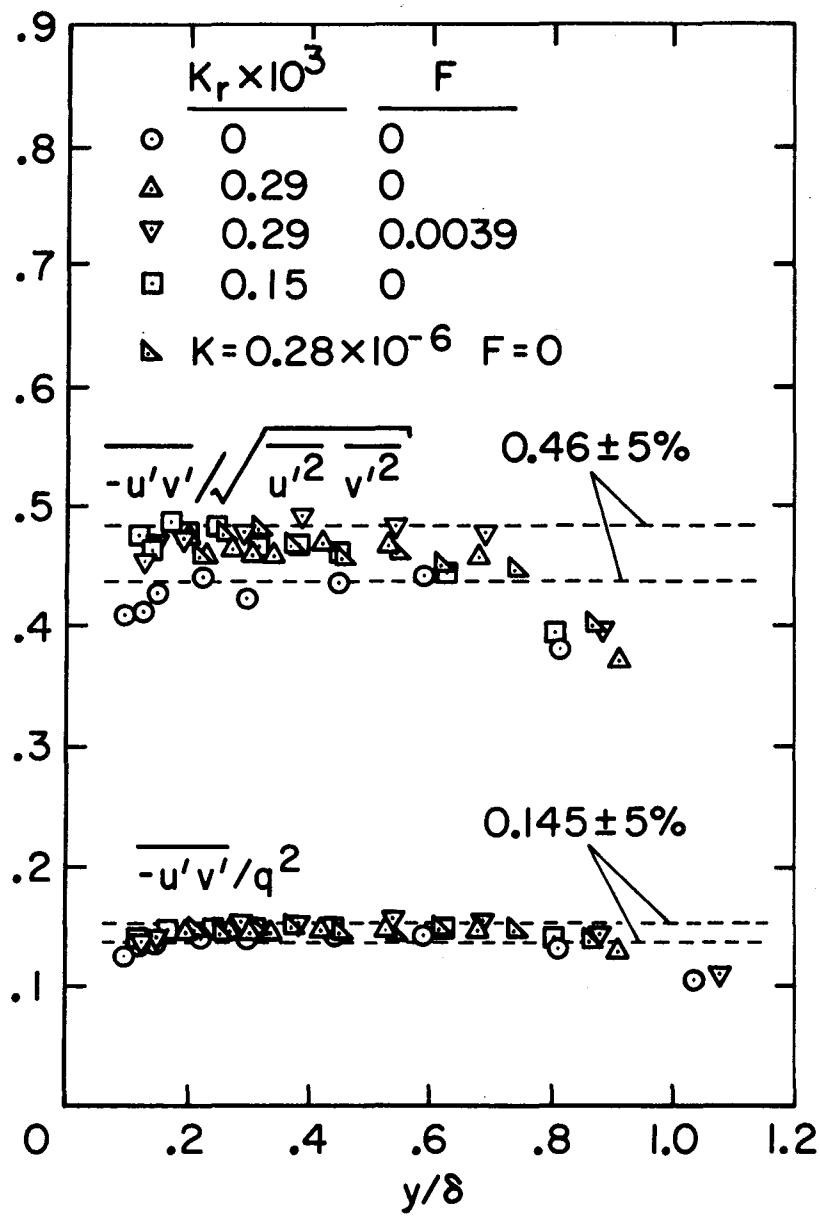

Figure 3-37. Distribution of Reynolds Shear Stress Correlation Coefficients through the Boundary Layer

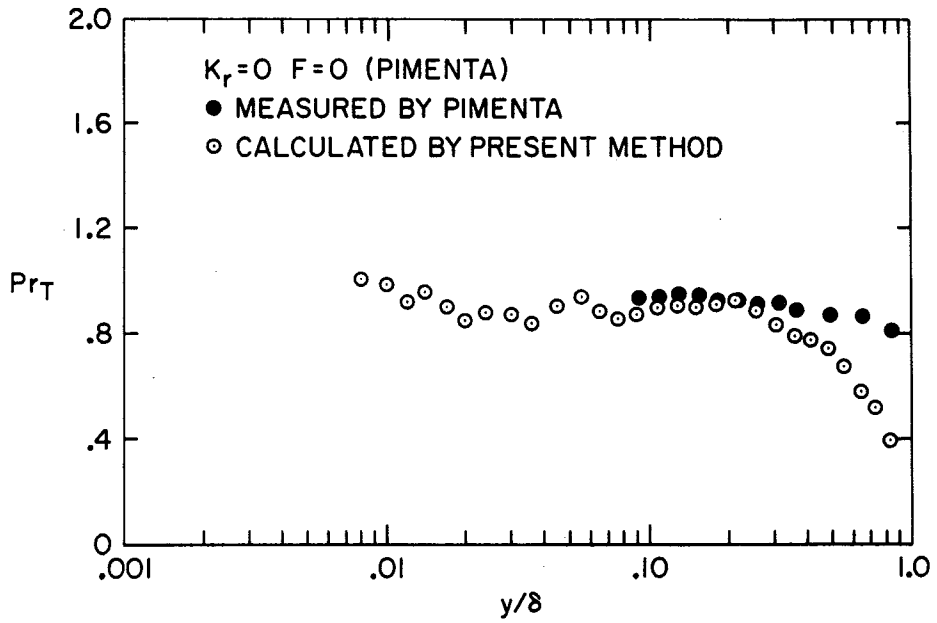

Figure 3-38. Comparison of Turbulent Prandtl Numbers Measured by Pimenta[2] and Calculated by Present Method for $K_r = 0$

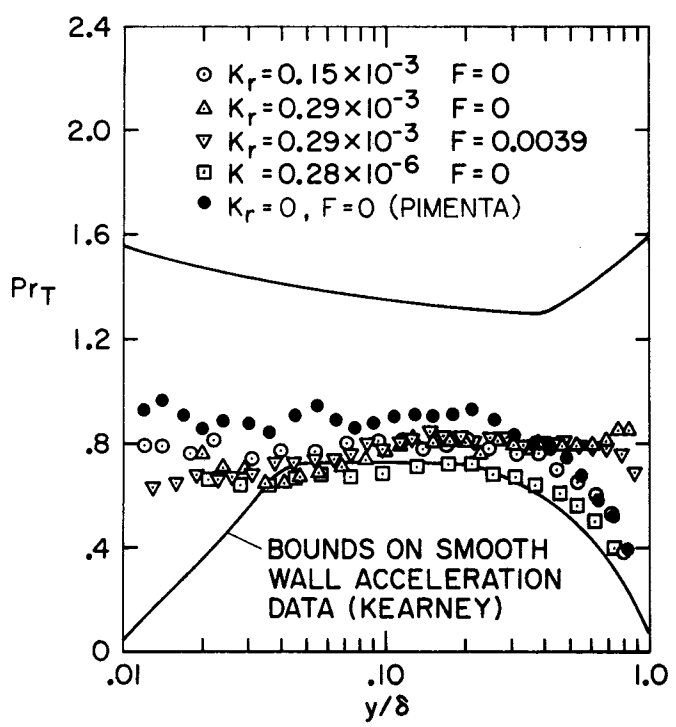

Figure 3-39. Turbulent Prandtl Number Distributions for the Acceleration Cases of the Present Study

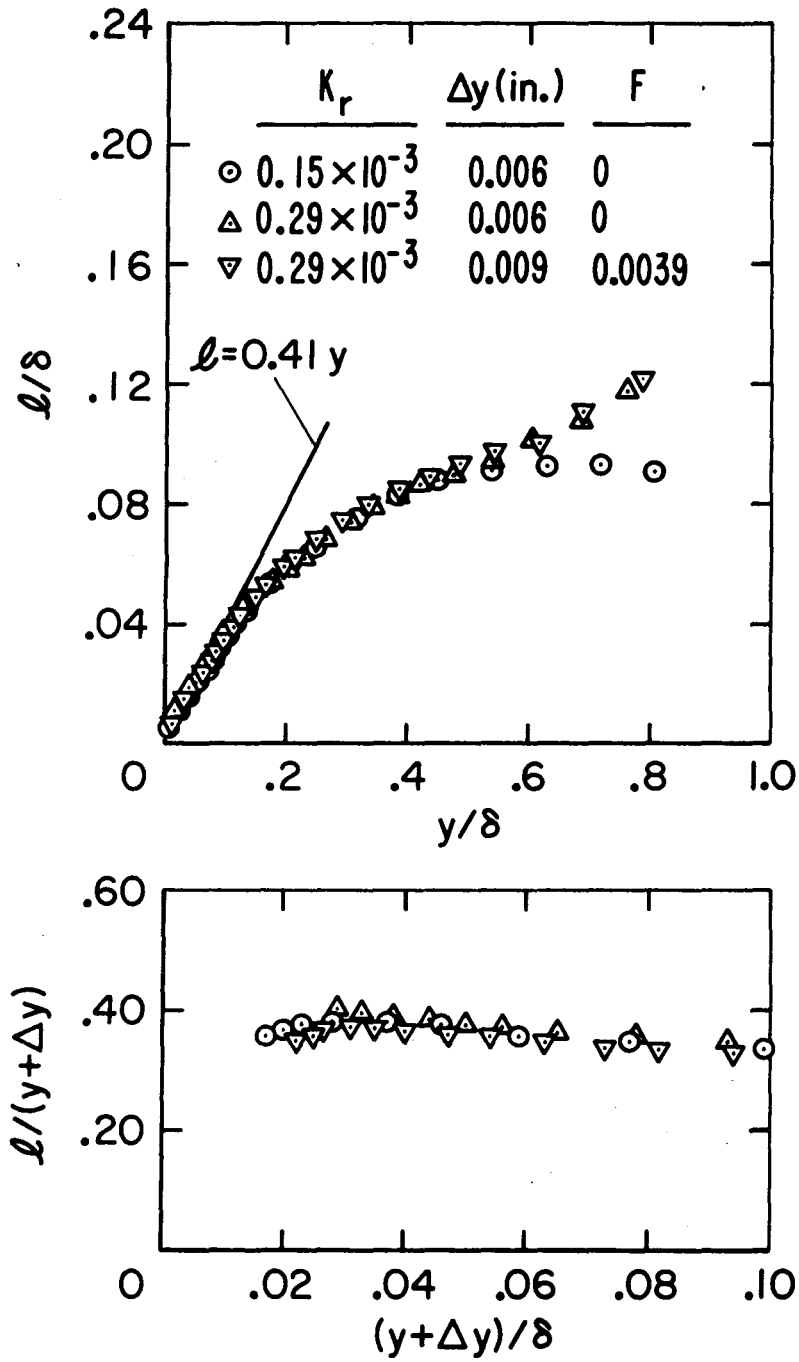

Figure 3-40. Mixing Length Distributions for the Equilibrium Acceleration Cases of the Present Study

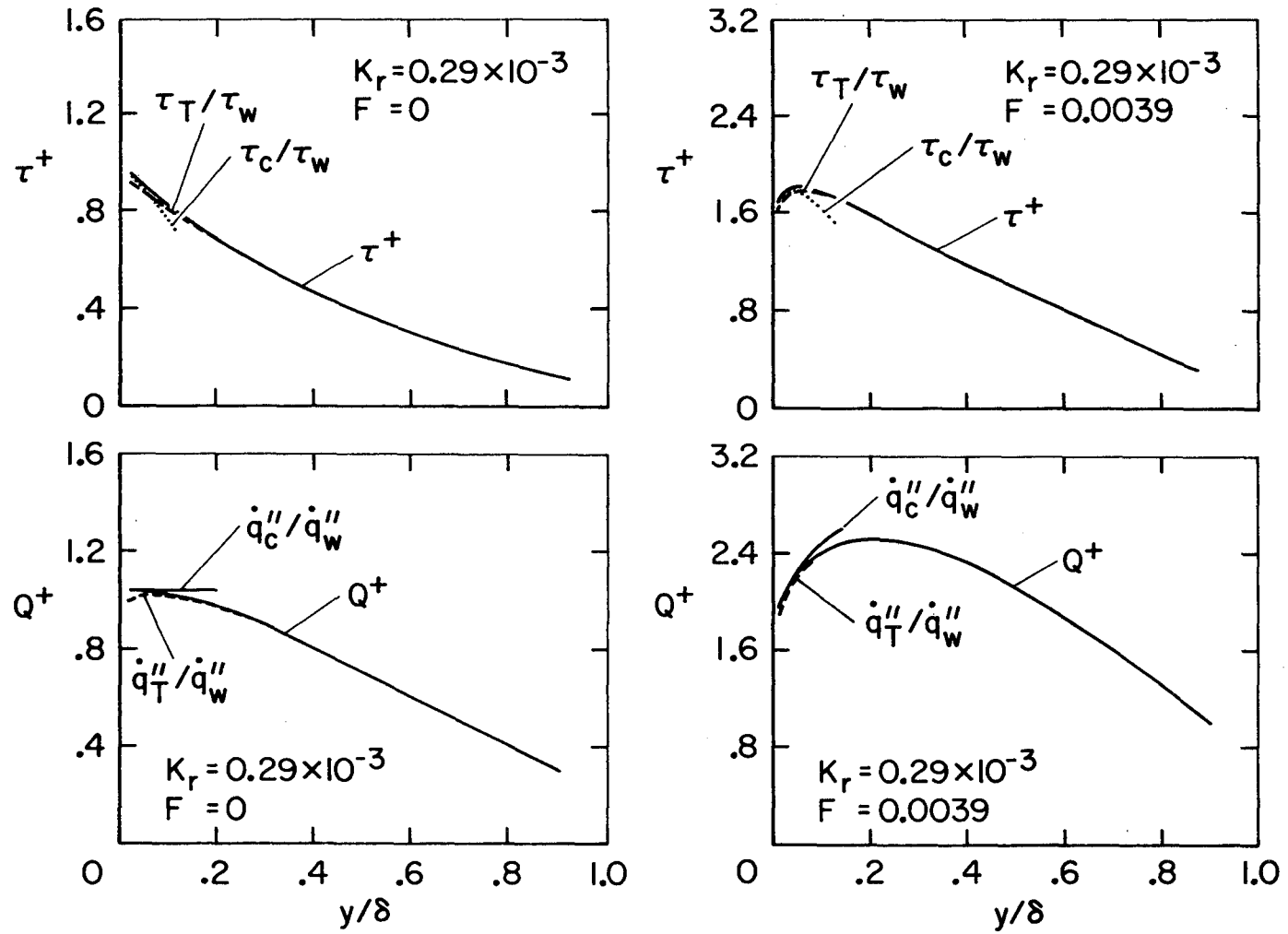

Figure 3-41. τ^+ and Q^+ Distributions for the $K_r = 0.29 \times 10^{-3}$, F = 0 and F = 0.0039 Runs

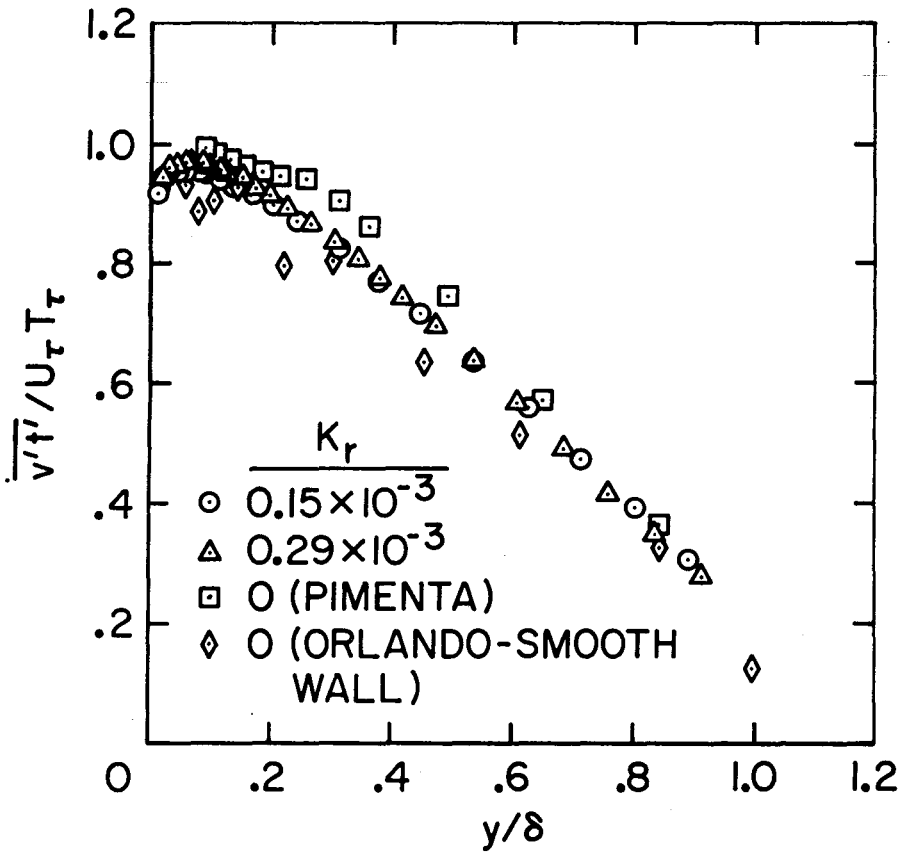

Figure 3-42. Comparison of the Unblown $\overline{v't'}/U_\tau T_\tau$ Profiles for the Equilibrium Accelerations of the Present Study with the Unaccelerated Profiles for Smooth and Rough Wall Layers

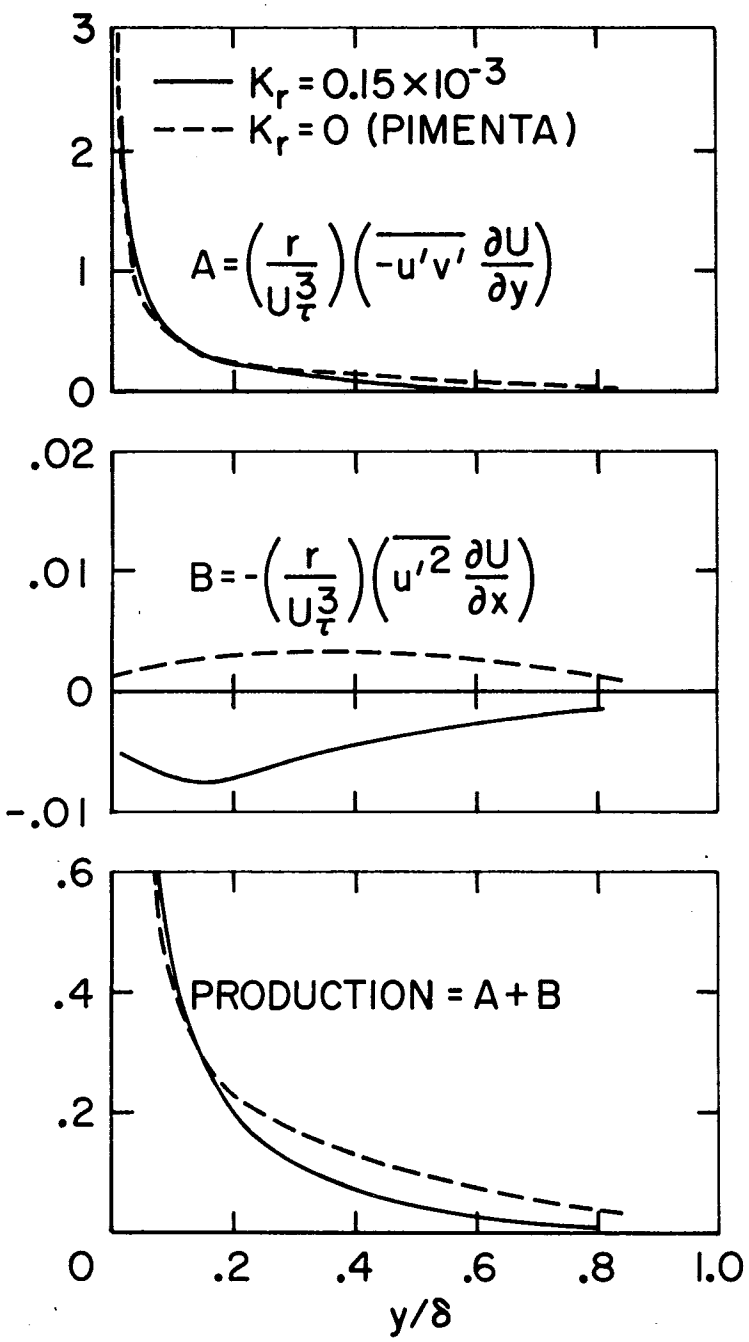

Figure 3-43. Calculated Distribution of the Nondimensional Turbulent Kinetic Energy Production for $K_r = 0$ and $K_r = 0.15 \times 10^{-3}$

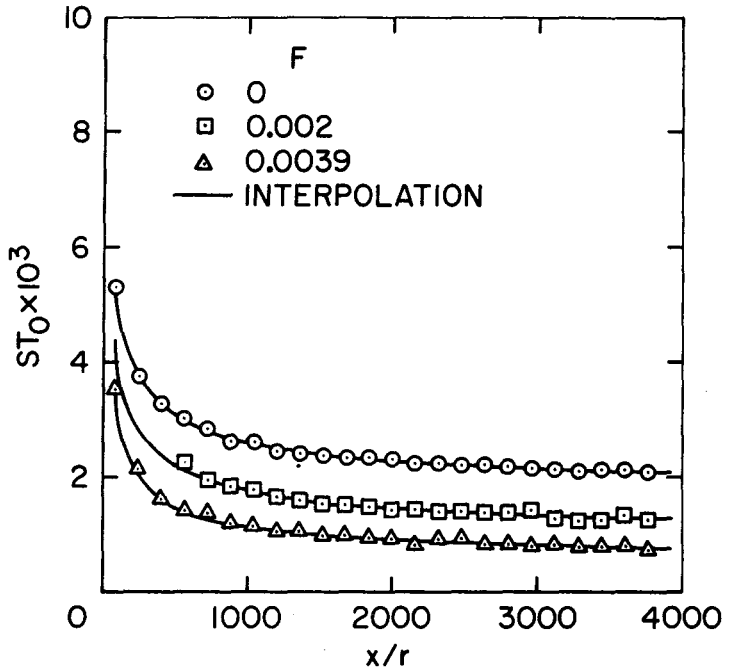

Figure 3-44. Comparison of St Data and Interpolation Expression for U_∞, T_W and F Constant

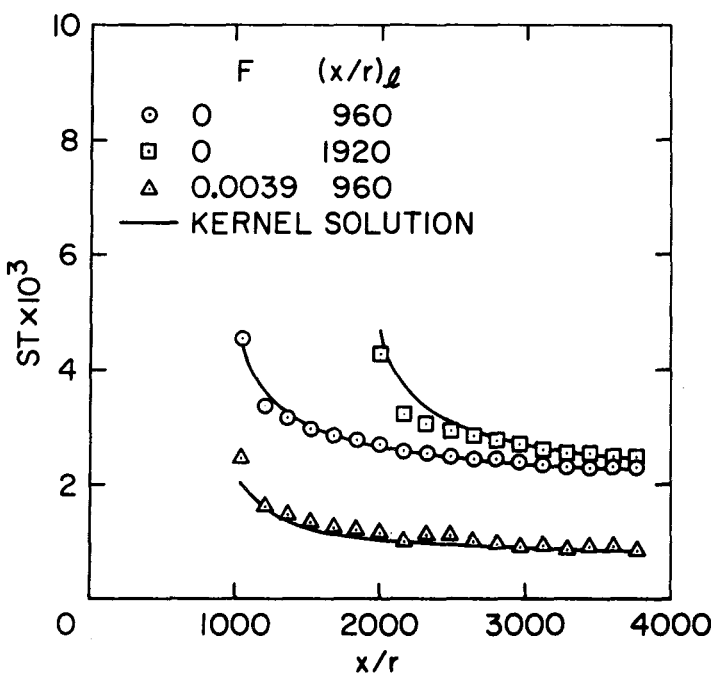

Figure 3-45. Comparison of Unheated Starting Length St Data with Results of Kernel Solution for U_∞ and F Constant

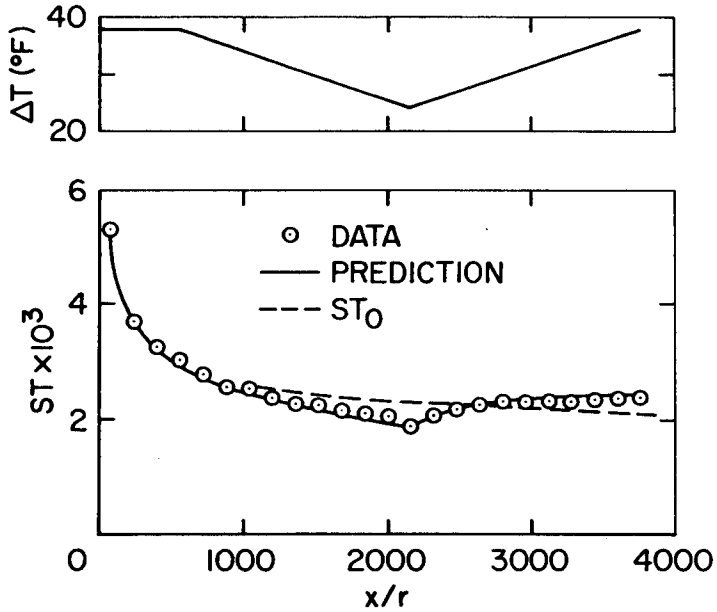

Figure 3-46. Comparison of St Data and Prediction for a Bilinear Variation of T_w with U_∞ Constant, F = 0

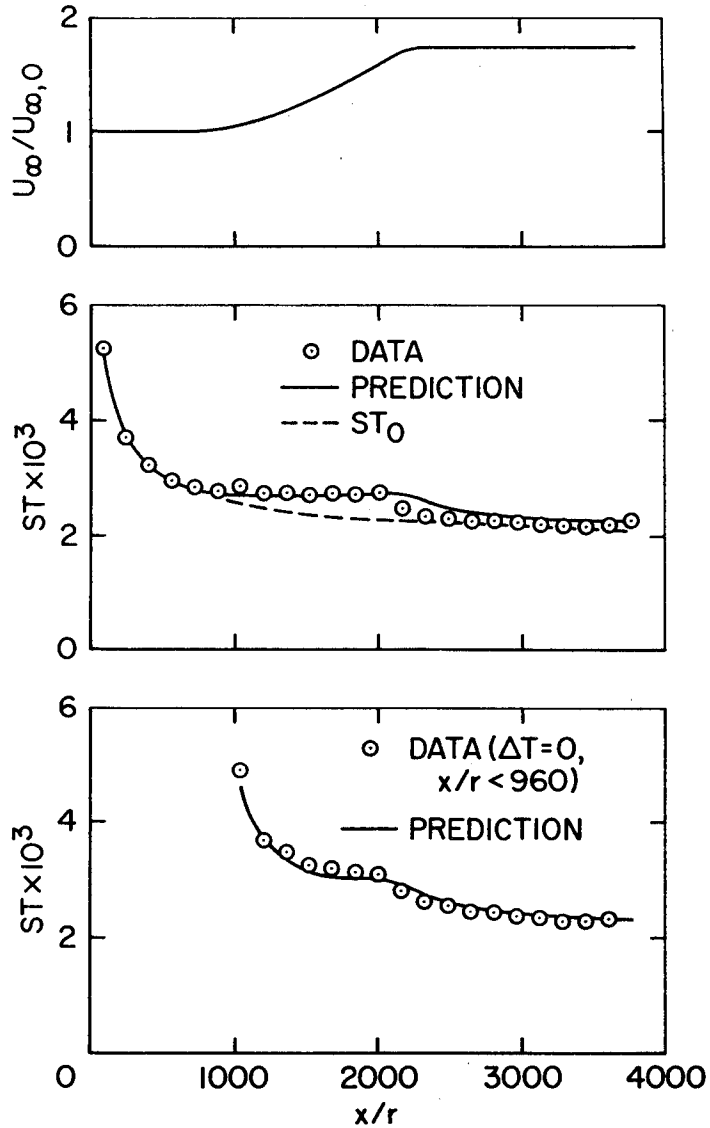

Figure 3-47. Comparison of St Data and Predictions for $K = 0.28 \times 10^{-6}$, F = 0 Run Both with and Without an Unheated Starting Length

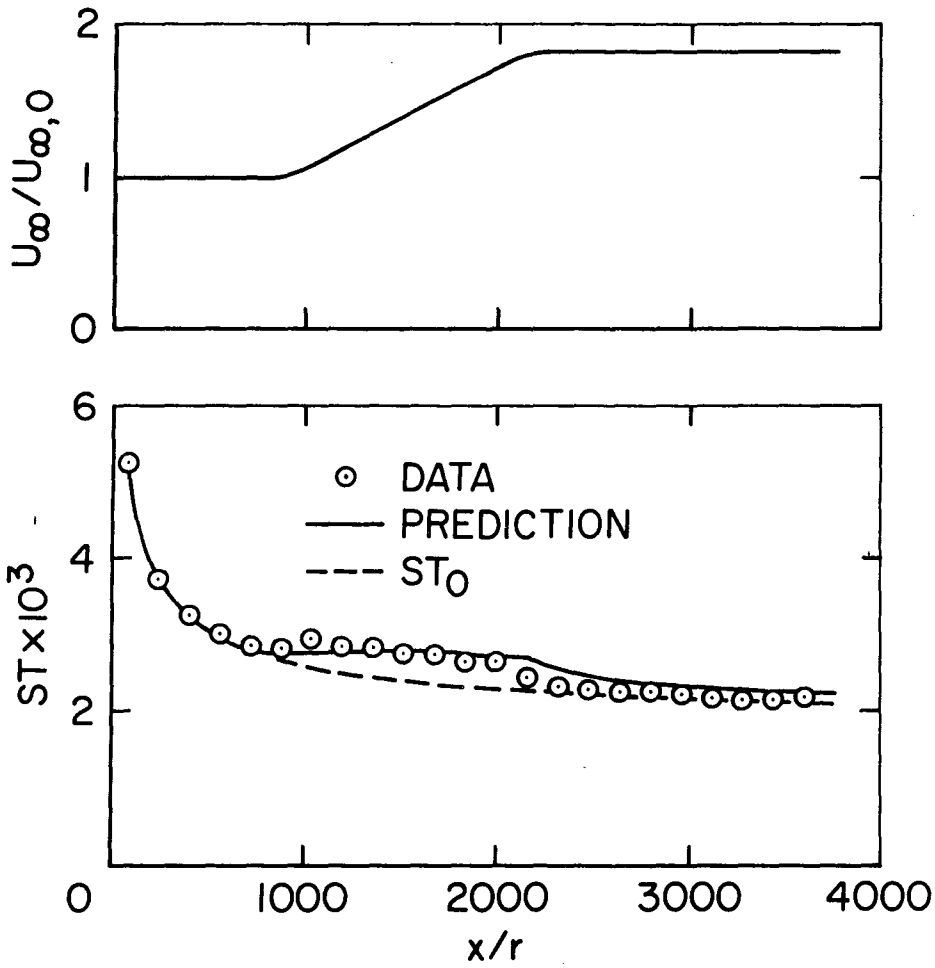

Figure 3-48. Comparison of St Data and Prediction for $K_r = 0.50 \times 10^{-3}$, F = 0 Run with T_w Constant

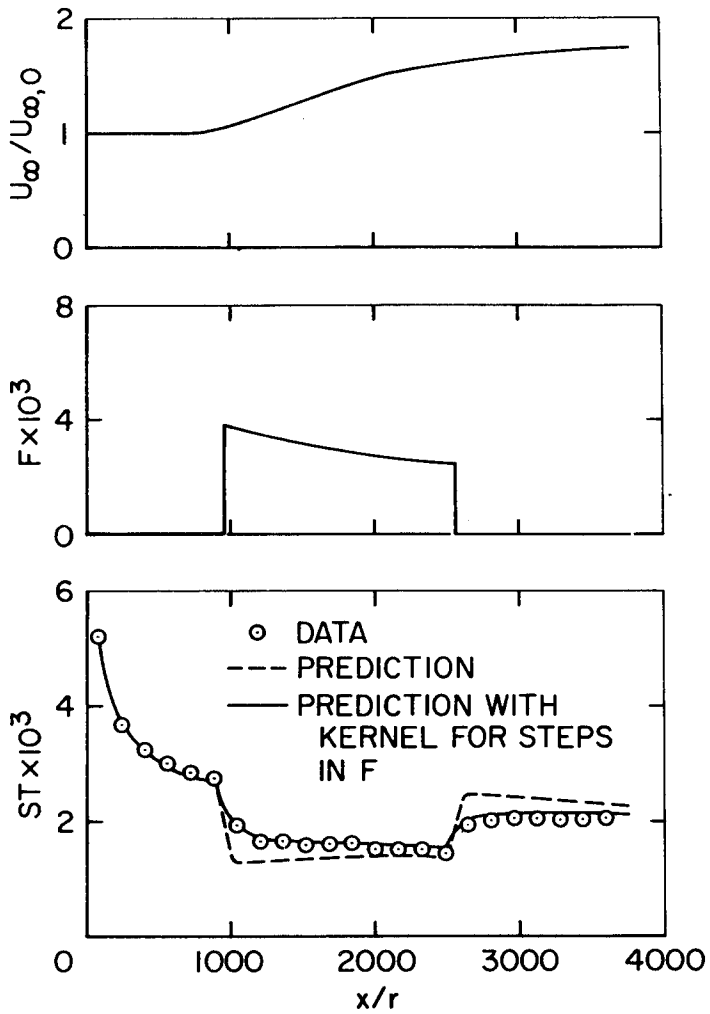

Figure 3-49. Comparison of St Data and Predictions for Arbitrary U_∞ Variation with Steps in F, F Variable and T_w Constant

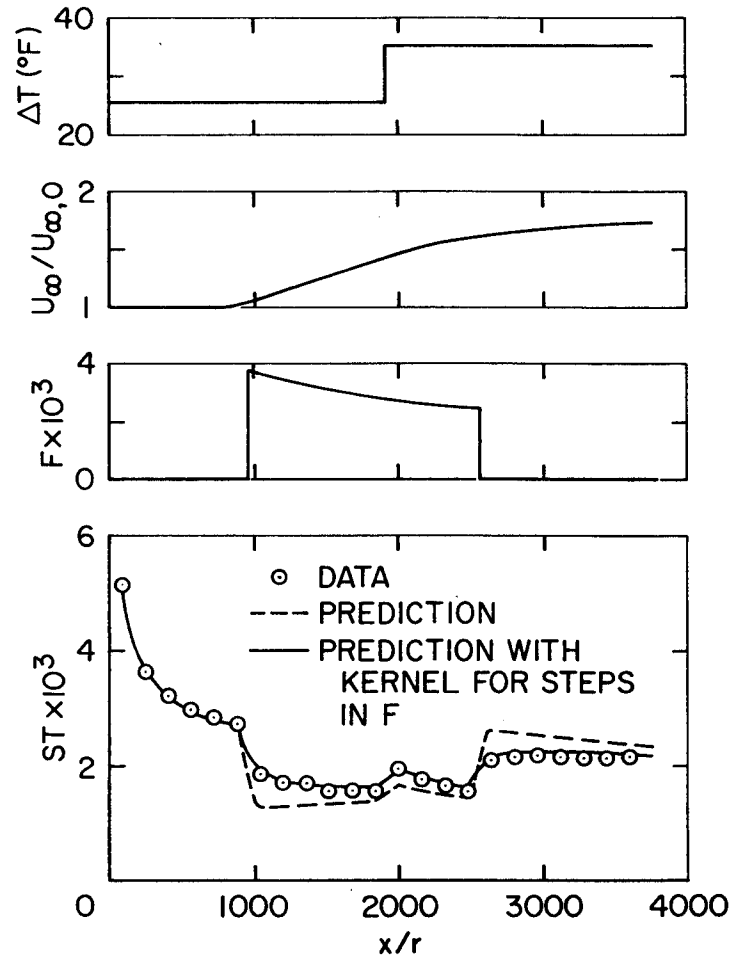

Figure 3-50. Comparison of St Data and Predictions for Arbitrary U_∞ Variation with Steps in F, F Variable and a Step in T_w in the Blowing Region

CHAPTER 4

EFFECTS OF ACCELERATION ON THE FULLY ROUGH TURBULENT BOUNDARY LAYER

In the previous chapter the various sets of data taken in this study were presented and some details of the boundary layer behavior indicated by the data were discussed. A more general, integrated discussion of the effects of acceleration on the fully rough turbulent boundary layer is presented in this chapter.

In smooth wall turbulent boundary layers, a viscous sublayer develops which, in a sense, provides a "buffer" between the surface and the more energetic turbulent fluid in the outer portion of the layer. For flow on a rough surface, once the boundary layer is in the fully rough state the viscous sublayer has been effectively destroyed, at least above the crests of the roughness elements. The outer flow, therefore, interacts with near-wall fluid of higher momentum, energy and vorticity than in the smooth wall case. Thus, the fully rough flow near the wall is characterized by shorter time scales and larger velocity scales than for a smooth wall flow and is unaffected by molecular viscosity down to the tops of the roughness elements. Among the elements, the pressure fluctuations are thought to be more important than the viscous forces [2]. Blake [21] found that pressure fluctuation intensity near the wall increased with roughness and scaled with the wall shear stress when compared to smooth wall values.

In view of these characteristics, it is not surprising that the proper acceleration parameter for fully rough flow $\left(K_r = \frac{r}{U_\infty}\frac{dU_\infty}{dx}\right)$ is independent

of molecular viscosity and contains a length scale dependent on the wall roughness elements. As shown in Chapter 3, imposition of a K_r = constant acceleration on a fully rough flow with F constant and ≥ 0 results in a boundary layer which approaches an asymptotic condition for which $C_f/2$, δ_2, H, β, and G are all constant with x. This type of boundary layer satisfies the conditions found by Rotta [16] for an exactly equilibrium flow, i.e.,

$$C_f/2 = \text{constant}$$

$$d\delta_1/dx = \text{constant } (=0)$$

and

$$\beta = \frac{\delta_1}{\tau_w} \frac{dP}{dx} = \text{constant}$$

In the equilibrium accelerated fully rough layer, the mean velocity profiles become similar, and the profiles of the Reynolds stress tensor components also approach a similar behavior. The roughness Reynolds number, Re_k, increases throughout the acceleration region, indicating an evolution toward a "rougher" layer rather than a transitionally rough or smooth behavior. This is opposite to the behavior of the accelerated smooth wall turbulent boundary layer, which evolves toward a state resembling laminar flow. These differences in behavior are consistent with the Stanton number trends observed with acceleration. In the fully rough layer, Stanton numbers are increased with acceleration compared to unaccelerated values at the same x, Δ_2, or Re_{Δ_2}. In the smooth wall layer, however, Stanton numbers are either unchanged or are decreased (depending on the strength of the acceleration) compared with unaccelerated values at the same position or Reynolds number.

The virtual position of the wall, found using the method suggested by Monin and Yaglom [30] and based on the mean velocity profiles, is unaffected by either acceleration or axial position x. The wall shift, Δy, reported by Pimenta [2] for the present surface with $K_r = 0$ remained valid under all conditions investigated in this study.

Although the accelerated $(T_w-T)/(T_w-T_\infty)$ vs U/U_∞ data do not exhibit the linearity observed in $K_r = 0$ data [2], a temperature "jump" at the extrapolated $U/U_\infty = 0$ point is still indicated. Therefore, there are different apparent wall positions for the mean velocity and mean temperature profiles in both zero pressure gradient and accelerated fully rough flows, with the virtual wall indicated by the mean temperature profiles being further below the crests of the roughness elements than the apparent wall determined from the mean velocity profiles.

The turbulence field is dramatically affected when a fully rough turbulent boundary layer is accelerated. The nondimensionalized turbulent kinetic energy (q^2/U_∞^2 or q^2/U_τ^2) is substantially reduced over the entire layer compared to the unaccelerated case. This is the same trend that can be inferred from the data for accelerated smooth wall layers. Although no measurements of $\overline{v'^2}$ and $\overline{w'^2}$ in accelerated smooth wall layers are known to the author, $\overline{u'^2}/U_\infty^2$ profiles are decreased by acceleration [5], and a decrease in bursting has been noted with acceleration [36]. The present data also show that an accelerated fully rough layer is much more anisotropic in the inner region than is a $K_r = 0$ fully rough layer. This is probably due to the influence of acceleration on the pressure field-velocity field interaction terms $\left(\overline{p' \frac{\partial v'}{\partial y}}, \overline{p' \frac{\partial w'}{\partial z}}\right)$ which transfer energy from the u' to the v' and w' components of q^2.

In the accelerated layer with blowing investigated in this study, the decrease in q^2/U_∞^2 in the outer region observed in the unblown cases was noted, but the increased anisotropy in the inner region observed for F = 0 was not seen for F = 0.0039. This trend was also noted in the $K_r = 0$ fully rough data of Pimenta [2], who found that blowing produced a more isotropic turbulence field than that of an unblown layer. It thus appears that, in the present data, the effects of acceleration and blowing on the turbulence field in the inner region of the layer are approximately equal and opposite.

The values of the Reynolds shear stress correlation coefficients found in this study are in agreement with the values ($R_{uv} \approx 0.45$, $R_q^2 \approx 0.15$) previously reported for smooth wall [32,33,34] and $K_r = 0$ rough wall [2] turbulent boundary layers. This observation indicates a universal mechanism in the bursting and decay process. Although the magnitudes of the components of the Reynolds stress tensor are dependent on surface condition, blowing and pressure gradient, the constancy of the correlation coefficients indicates a universal and constant relationship among these components.

There are indications from the present data that in a fully rough turbulent boundary layer with K_r, F, and T_w constant, the layer approaches an equilibrium state in the thermal sense also. Unfortunately, the range of the present thermal data is not large enough to allow a definitive conclusion in this regard. It is proposed that in such an equilibrium state Stanton number would become constant, enthalpy thickness would approach an asymptote, and nondimensional temperature profiles would be similar in the flow direction. In the present data the fluid dynamic field (which is a major influence on the development of the thermal field) is in an equilibrium state described previously, and the mean temperature profiles are similar in the flow direction. However, due to the relatively small range of Δ_2

covered in the accelerating regions, it is not possible to show that the present Stanton number data are constant rather than weak functions of enthalpy thickness.

As in the case of the Reynolds shear stress correlation coefficients, the distribution of the turbulent heat flux correlation coefficient $\overline{v't'}/U_\tau T_\tau$ calculated from the data of the present study is identical with the profiles reported for zero pressure gradient rough wall [2] and smooth wall layers [34].

Results of turbulent Prandtl number calculations based on data of the present experiment indicate an approximately constant value of 0.7 - 0.8 across the layer. This value is lower than turbulent Prandtl numbers reported for the unaccelerated fully rough case [2], which vary from ~ 1.0 in the near wall region to ~ 0.7 - 0.8 in the outer region. The present values of Pr_T are in the lower range of the data reported by Kearney [25] for smooth wall accelerated layers.

As shown in Section 3.4, the response of Stanton number in fully rough flow to either acceleration or variable wall temperature can be represented using the same kernel function, $\left(1 - \frac{\ell}{x}\right)^{-0.22}$. This behavior is related to the absence of a viscous sublayer, which leads to greater turbulent mixing and more vigorous interaction between the wall region and outer flow [38,2]. By contrast, in a smooth wall layer the viscous sublayer damps or buffers the interaction between the wall and the fully turbulent layer, and the response of Stanton number is different for variations in velocity and wall temperature.

The fact that variations in velocity and temperature have equivalent effects on Stanton number and that the process can be modeled in the manner described above indicates that turbulent Prandtl number should be unity.

This information complements the results of the Pr_T calculations described above, since the calculated values are of order one.

CHAPTER 5. CONCLUSIONS

All statements in this chapter, unless otherwise indicated, refer to the flow of a fully rough turbulent boundary layer over a three-dimensional, densely packed, uniformly rough test surface such as that used in this study. Based on the discussion in the previous chapters, the important results and conclusions of the study are:

1. The proper acceleration parameter for use with fully rough flow is $K_r = \frac{r}{U_\infty}\frac{dU_\infty}{dx}$, where r is a characteristic roughness length.

2. In a constant K_r acceleration with $F \geq 0$ and constant, the fully rough layer develops toward an equilibrium state where $C_f/2$, δ_2, H, β and G are all constant. Both mean velocity profiles and the components of the Reynolds stress tensor approach similarity in the flow direction.

3. Although inherent uncertainty in the Stanton number data and the restricted length of the acceleration region prevent a definite conclusion, the present thermal data indicate the possibility that a layer with K_r, T_w and $F(\geq 0)$ constant approaches an equilibrium state in the thermal sense, also. Such a state would be characterized by Stanton number becoming constant, enthalpy thickness approaching an asymptote, and temperature profiles being similar in the flow direction.

4. Stanton numbers increase with acceleration compared to zero pressure gradient values at the same position or enthalpy thickness. This behavior is quite different from that of a smooth wall layer, where Stanton numbers are unchanged for small values of K and decrease with increasing K compared to zero pressure gradient data at the same position or Reynolds number.
5. Roughness Reynolds number increases in a region of acceleration, indicating that the fully rough layer does not tend toward the transitionally rough or smooth wall state when accelerated.
6. For F = 0, acceleration decreases the turbulent kinetic energy throughout the boundary layer, and in the inner region the turbulence is much more anisotropic than in the $K_r = 0$ layer.
7. In the blown layer, acceleration decreases the turbulent kinetic energy in the outer region of the layer and substantially alters the shape of the profiles of $\overline{u'^2}$, $\overline{v'^2}$, $\overline{w'^2}$ compared with the blown, unaccelerated boundary layer (Figure 3-34).
8. The values of the Reynolds shear stress coefficients obtained in this study are the same as those reported for smooth wall flows and $K_r = 0$ fully rough flows, indicating that these values are truly universal.
9. The profiles of $\overline{v't'}/U_\tau T_\tau$ calculated from the present accelerated data are in good agreement with those reported for smooth and rough wall zero pressure gradient layers. It thus appears that the turbulent heat flux profile, nondimensionalized in this manner, is independent of surface condition and favorable pressure gradient.
10. In a fully rough flow, the response of Stanton number to either variable wall temperature or acceleration can be represented using the same kernel function, $\left(1 - \frac{\ell}{x}\right)^{-0.22}$.

11. From (10) above one would expect a turbulent Prandtl number of approximately unity. The values of Pr_T calculated from the present data support this, having an approximately constant value of 0.7 - 0.8 across the boundary layer.

12. The virtual origin of the wall (based on mean velocity profiles) is independent of acceleration and position in the flow direction.

REFERENCES

1. Healzer, J. M., Moffat, R. J., and Kays, W. M., "The Turbulent Boundary Layer on a Rough, Porous Plate: Experimental Heat Transfer with Uniform Blowing," Report HMT-18, Thermosciences Division, Dept. of Mech. Eng., Stanford University, 1974.

2. Pimenta, M. M., Moffat, R. J., and Kays, W. M., "The Turbulent Boundary Layer: An Experimental Study of the Transport of Momentum and Heat with the Effect of Roughness," Report HMT-21, Thermosciences Division, Dept. of Mech. Eng., Stanford University, 1975.

3. Nikuradse, J., "Stromugsgestze in rauhen Rohren," VDI Forschungsheft, No. 361, 1933, English Translation, NACA TM 1292.

4. Kays, W. M., and Moffat, R. J., "The Behavior of Transpired Turbulent Boundary Layers," Report HMT-20, Thermosciences Division, Dept. of Mech. Eng., Stanford University, 1975.

5. Badri Narayanan, M. A., and Ramjee, V., "On the Criteria for Reverse Transition in a Two-Dimensional Boundary Layer Flow," Jn. Fluid Mech., Vol. 35, pp. 225-241, 1969.

6. Reshotko, M. Boldman, D. R., and Ehlers, R. C., "Heat Transfer in a 60° Half-Angle of Convergence Nozzle with Various Degrees of Roughness," NASA TN D-5887, 1970.

7. Banerian, G., and McKillop, A. A., "The Effects of Surface Roughness in Nozzles on Heat Transfer," Proc. of the Fifth International Heat Transfer Conference, V. II, pp. 234-238, 1974.

8. Chen, K. K., "Compressible Turbulent Boundary-Layer Heat Transfer to Rough Surfaces in Pressure Gradient," AIAA J., 10, pp. 623-629, 1972.

9. Blackwell, B. F., Kays, W. M., and Moffat, R. J., "The Turbulent Boundary Layer on a Porous Plate: An Experimental Study of the Heat Transfer Behavior with Adverse Pressure Gradients," Report No. HMT-16, Thermosciences Division, Dept. of Mech. Eng., Stanford University, 1972.

10. Rotta, J., "Uber die Theorie der turbulenten Grenzschichten," Mitteilungen aus dem Max-Planck-Institut fur Stromungsforschung (Gottingen), No. 1, 1950. English translation NACA TM 1344, 1953.

11. Clauser, F. H., "Turbulent Boundary Layers in Adverse Pressure Gradients," Jn. Aero. Sci., Vol. 21, pp. 91-108, 1954.

12. Clauser, F. H., "The Turbulent Boundary Layer," Advances in Applied Mechanics, Vol. IV, pp. 1-51, Academic Press, New York, 1956.

13. Rotta, J. C., "Similar Solutions of Turbulent Boundary Layers," Jn. Aero. Sci., Vol. 22, pp. 215-216, 1955.

14. Townsend, A. A., "The Properties of Equilibrium Boundary Layers," Jn. Fluid Mech., Vol. 1, pp. 561-573, 1956.

15. Coles, D., "Remarks on the Equilibrium Turbulent Boundary Layer," Jn. Aero. Sci., Vol. 24, pp. 495-506, 1957

16. Rotta, J. C., "Turbulent Boundary Layers in Incompressible Flow," Prog. in Aero. Sci., Vol. 2, pp. 1-219, Pergamon Press, 1962.

17. Perry, A. E., Schofield, W. H., and Joubert, P. H., "Rough Wall Turbulent Boundary Layers," Jn. Fluid Mech., Vol. 37, pp. 383-413, 1969.

18. Schlichting, H., Boundary Layer Theory, 6th Edition, McGraw-Hill Book Co., Inc., New York, 1968.

19. Andersen, P. S., Kays, W. M., and Moffat, R. J., "The Turbulent Boundary Layer on a Porous Plate: An Experimental Study of the Fluid Mechanics for Adverse Free-Stream Pressure Gradients," Report No. HMT-15, Thermosciences Division, Dept. of Mech. Eng., Stanford University, 1972.

20. Klebanoff, P. S. "Characteristics of Turbulence in a Boundary Layer with Zero Pressure Gradient," NACA Report 1247, 1955.

21. Blake, W. K., "Turbulent Boundary-Layer Wall-Pressure Fluctuations on Smooth and Rough Walls," Jn. Fluid Mech., Vol. 44, pp. 637-660, 1970.

22. Hinze, J. O., Turbulence - An Introduction to its Mechanism and Theory, McGraw-Hill Book Co., 1959.

23. Corrsin, S., and Kistler, A. L., "The Free Stream Boundaries of Turbulent Flows," NACA Tech. Note 3133, January 1954.

24. Thielbahr, W. H., Kays, W. M., and Moffat, R. J., "The Turbulent Boundary Layer: Experimental Heat Transfer with Blowing, Suction and Favorable Pressure Gradient," Report No. HMT-5, Thermosciences Division, Dept. of Mech. Eng., Stanford University, 1969.

25. Kearney, D. W., Moffat, R. J., and Kays, W. M., "The Turbulent Boundary Layer: Experimental Heat Transfer with Strong Favorable Pressure Gradients and Blowing," Report No. HMT-12, Thermosciences Division, Dept. of Mech. Eng., Stanford University, 1970.

26. Moretti, P. M., and Kays, W. M., "Heat Transfer to a Turbulent Boundary Layer with Varying Free-Stream Velocity and Varying Surface Temperature - An Experimental Study," Int. J. Heat Mass Transfer, Vol. 8, pp. 1187-1202, 1965.

27. Julien, H. L., Kays, W. M., and Moffat, R. J., "The Turbulent Layer on a Porous Plate: Experimental Study of the Effects of a Favorable Pressure Gradient," Report No. HMT-4, Thermosciences Division, Dept. of Mech. Eng., Stanford University, 1969.

28. Loyd, R. J., Moffat, R. J., and Kays, W. M., "The Turbulent Boundary Layer on a Porous Plate: An Experimental Study of the Fluid Dynamics with Strong Favorable Pressure Gradients and Blowing," Report No. HMT-13, Thermosciences Division, Dept. of Mech. Eng., Stanford University, 1970.

29. Kays, W. M., Convective Heat and Mass Transfer, McGraw-Hill Book Co., New York, 1966.

30. Monin, A. S., and Yaglom, A. M., Statistical Fluid Mechanics, Vol. 1, The MIT Press, 1971.

31. Tennekes, H., and Lumley, J. L., A First Course in Turbulence, The MIT Press, 1972.

32. Townsend, A. A., The Structure of Turbulent Shear Flow, Cambridge University Press, 1956.

33. Bradshaw, P., "The Turbulence Structure of Equilibrium Boundary Layers," NPL Aero Report 1184, 1966.

34. Orlando, A. F., Moffat, R. J., and Kays, W. M., "Turbulent Transport of Heat and Momentum in a Boundary Layer Subject to Deceleration, Suction and Variable Wall Temperature," Report No. HMT-17, Thermosciences Division, Dept. of Mech. Eng., Stanford University, 1974.

35. Kim, H. T., Kline, S. J., and Reynolds, W. C., "The Production of Turbulence Near a Smooth Wall in a Turbulent Boundary Layer," Jn. Fluid Mech., Vol. 50, pp. 133-160, 1971.

36. Kline, S. J., Reynolds, W. C., Schraub, F. A., and Runstadler, P. W., "The Structure of Turbulent Boundary Layers," Jn. Fluid Mech., Vol. 30, pp. 741-773, 1967.

37. Offen, G. R., and Kline, S. J., "Combined Dye-Streak and Hydrogen-Bubble Visual Observations of a Turbulent Boundary Layer," Jn. Fluid Mech., Vol. 62, pp. 223-239, 1974.

38. Grass, A. J., "Structural Features of Turbulent Flow over Smooth and Rough Boundaries," Jn. Fluid Mech., Vol. 50, pp. 233-256, 1971.

39. Reynolds, W. C., Kays, W. M., and Kline, S. J., "Heat Transfer in the Turbulent Incompressible Boundary Layer with Arbitrary Wall Temperature and Heat Flux," Final Report - Part III, Dept. of Mech. Eng., Stanford University, 1957.

40. Whitten, D. G., Kays, W. M., and Moffat, R. J., "The Turbulent Boundary Layer on a Porous Plate: Experimental Heat Transfer with Variable Suction, Blowing, and Surface Temperature," Report No. HMT-3, Thermosciences Division, Dept. of Mech. Eng., Stanford University, 1967.

41. Hottel, H. C., and Kalitinsky, A., "Temperature Measurements in High-Velocity Air Streams," Jn. Appl. Mech., Vol. 12, pp. A25-A32, 1945.

42. Jorgensen, F. E., "Directional Sensitivity of Wire and Hot-Film Probes," DISA Information No. 11, 1971.

43. Repik, Y. E. U., and Ponomareva, V. S., "The Effect of Proximity of Walls on the Readings of a Hot-Wire Anemometer in Turbulent Boundary Layers," Heat Transfer - Soviet Research, Vol. 2, No. 4, 1970.

44. Ligrani, P., private communication, Dept. of Mech. Eng., Stanford University, 1975.

APPENDICES

APPENDIX I

DESCRIPTION OF EXPERIMENTAL APPARATUS AND MEASUREMENT TECHNIQUES

The experimental apparatus and measurement techniques used in this investigation are discussed below. Since comprehensive descriptions of the design, construction, and basic qualification of the Roughness Rig have been reported by Healzer [1] and Pimenta [2], these details will not be repeated here. The interested reader is referred to the cited reports. Since some differences exist between the hot wire techniques used by Pimenta [2] and the present author, a more detailed discussion of this area is presented.

I.1 Experimental Apparatus

A schematic diagram of the Roughness Rig was presented previously in Figure 1-1 and a brief description was given in Chapter 1. Details of a typical plate and casting assembly are shown in Figure I-1 for reference. Each of the 24 plates which make up the rough test surface has its own plate power control, transpiration air control, and five thermocouples which are averaged to give an effective plate temperature.

Stanton numbers were determined from an energy balance on each plate. The energy gained by the transpired air while passing through the plate and the plate losses were subtracted from the measured plate power input to determine the wall heat flux, $\dot{q}''_w$. Stanton number was then calculated from the definition

$$St \equiv \frac{\dot{q}''_w}{\rho_\infty U_\infty C_p \ (T_w - T_{\infty,0})} \qquad (I.1)$$

The plate losses considered were the radiative losses from the upper and lower surfaces of the plate, the conduction losses from the plate to the casting, and the conduction loss through the stagnant air below the test plate when there was no transpiration. The same models for these losses were used in this investigation as were used by Healzer [1] and Pimenta [2]. (See Appendix II for a discussion of qualification tests).

Based on the results of the qualification tests, the uncertainty of the Stanton number data is within ± 0.0001 Stanton number units for the conditions of this investigation.

Two modifications were made to the Rig after completion of Pimenta's [2] zero pressure gradient study and prior to the present work. First, a 1/2" wide, 1/32" thick phenolic trip was installed with the front edge three inches inside the nozzle exit. This was done to insure stable conditions at the beginning of the acceleration region from run to run.

The second modification was to the top of the test section. The single-section plexiglass top wall was replaced by a top wall of 1/2" thick plexiglass constructed in five sections joined with plexiglass inserts. This wall allowed more precise control of the pressure gradient which was set along the tunnel length. The new top wall was actually a reworked version of the one used by Julien [28] and Thielbahr [24] in their smooth wall investigations.

I.2 Measurement Techniques

I.2.1 Pressure Measurements

Two Statham unbonded strain gauge differential pressure transducers were used - a model PM-5 with a 0 to 0.5 psi range and a model PM-97 with a 0 to 0.05 psi range. Each unit had a zeroing circuit and was

calibrated at the beginning of this investigation using a 30" Meriam Micromanometer (Model 34FB2) as a standard. The calibrations were linear for 10% to 80% of full scale for both units and were stable to within 0.001 inches of water. Signals from the transducers were integrated for ten seconds using a Hewlett-Packard Model 2401C integrating digital voltmeter (IDVM) with an external quartz crystal oscillator clock which provided 1, 10, and 100 second integrating period options.

The transducers were used to read the tunnel static pressures from the 0.040" diameter taps located 2" apart in the flow direction on the tunnel side wall. This gave a pressure reading at the front, middle, and rear of each 4" plate length. The value of the pressure gradient was calculated from a quadratic fit to the pressures measured at three adjacent taps.

Total pressures in the freestream were measured with a Kiel probe located in the potential flow region using the pressure transducers.

I.2.2 Temperature Measurements

Mean temperature profiles were measured with a 0.003" diameter, butt-welded Chromel-constantan thermocouple probe mounted in a traversing probe holder similar to that used with the horizontal hot wire (see Section I.2.3). The probe was designed with a length of approximately 0.625" to minimize conduction errors (see Blackwell's [9] analysis), and was calibrated in an oil bath using a Hewlett-Packard Model 2801A Quartz Thermometer as a standard. Recovery factor for this probe was assumed to be 0.66 based on the work of Hottel and Kalitinsky [41].

The freestream temperature (for use in Stanton number runs and monitoring during hot wire data acquisition) was measured with a probe made of 0.004 inch iron-constantan wire welded into a bead. This probe was also calibrated against the quartz thermometer and a recovery factor of 0.86 was used.

Estimated accuracy of temperature measurements: $\pm$ 0.15 °F.

I.2.3 Hot Wire Measurements

Two hot wire probes were used in this investigation: (1) a DISA 55P05 horizontal, boundary-layer-type probe of 5 micron tungsten wire with gold plated ends, and (2) a DISA 55F02 45° slant probe of 5 micron tungsten wire with gold plated ends. The wires were mounted in the same probe traversing mechanisms described by Pimenta [2] and which are shown in Figures I-2 and I-3 for reference. The slant wire could be rotated about the probe axis with stops positioned 45° apart ($\theta = n\pi/4$, where $n = 0,\ldots,7$).

Two DISA 55M01 anemometers with CTA Standard Bridges were operated in the constant-temperature mode. Each of the two hot wires was paired with an anemometer. The anemometer output voltages were linearized using two TSI Model 1072 fourth order linearizers.

A DISA Model 55D15 true rms meter was used to determine the mean square values of the fluctuating voltages. The rms meter was calibrated against standard sine waves with known rms values. Resulting accuracy of the rms meter output was 1% of the measured value.

Mean velocities were determined by integrating the linearizer output for 10 seconds with the IDVM, while mean square values were determined by integrating the true rms meter output for 100 seconds with the IDVM. The rms meter was used with a 10 second time constant setting, and four time constants (40 seconds) were allowed to elapse before the 100 second integration was begun.

The hot wire probes were calibrated using the calibrator described by Pimenta. This consists of a length of 3" diameter PVC pipe with flow straighteners and screens at its inlet and is followed by a 20:1 contraction

ASME nozzle. The probes were placed in the free jet at the exit of the nozzle where the velocity is uniform across the central region of the jet. The air temperature was maintained constant and at the same temperature at which the data were taken in the tunnel (~ 68°F).

The directional sensitivity of a hot wire and the resulting equations have been widely reported in the literature and will be only briefly covered here. According to Jorgensen [42], the directional sensitivity of a hot wire can be written as

$$u_{eff}^2 = u_2^2 + k_1^2 v_2^2 + k_2^2 w_2^2 \tag{I.2}$$

where u_2, v_2, and w_2 are the velocity components in the wire coordinate system (Figure I-4) and k_1 and k_2 are constants which depend on wire and prong construction characteristics. For the DISA 55F02, the values are taken as $k_1 = 0.20$ and $k_2 = 1.02$.

Equation (I.2) can be rewritten in terms of u_1, v_1, w_1, the velocity components in the laboratory coordinate system, as

$$u_{eff}^2 = Au_1^2 + Bv_1^2 + Cw_1^2 + Du_1v_1 + Ev_1w_1 + Fu_1w_1 \tag{I.3}$$

where

$$A = \cos^2\phi + k_1^2 \sin^2\phi$$

$$B = (\sin^2\phi + k_1^2 \cos^2\phi) \cos^2\theta + k_2^2 \sin^2\theta$$

$$C = (\sin^2\phi + k_1^2 \cos^2\phi) \sin^2\theta + k_2^2 \cos^2\theta$$

$$D = (1 - k_1^2) \sin 2\phi \cos\theta$$

$$E = (\sin^2\phi + k_1^2 \cos^2\theta - k_2^2) \sin 2\theta$$

$$F = (1 - k_1^2) \sin 2\phi \sin\theta$$

For a boundary layer flow where

$$u_1 = U + u'$$

$$v_1 = v'$$

$$w_1 = w'$$

it can be shown [2,34] that

$$\overline{u'^2_{eff}} = A\,\overline{u'^2} + \frac{D^2}{4A}\,\overline{v'^2} + \frac{F^2}{4A}\,\overline{w'^2} + D\,\overline{u'v'} + \frac{DF}{2A}\,\overline{v'w'} + F\,\overline{u'w'} + 0(3) \quad (I.4)$$

and

$$U_{eff} = \sqrt{A}\,U + 0(2) \quad (I.5)$$

In a two-dimensional boundary layer, the $\overline{v'w'}$ and $\overline{u'w'}$ terms can be assumed zero by symmetry. In the present tests, it was verified that both these terms were essentially zero to within the accuracy of the rms meter (see Appendix II). With this information, U and $\overline{u'^2}$ can be measured with the horizontal wire, and measurements at three rotations of the slant wire allow determination of $\overline{v'^2}$, $\overline{w'^2}$, and $\overline{u'v'}$. In this investigation, slant wire measurements were taken at θ = 45°, 90°, and 135°. These angles were chosen after an initial investigation to determine typical values of $\overline{e'^2}$ at different θ's. Solution for $\overline{v'^2}$, $\overline{w'^2}$, and $\overline{u'v'}$ involves finding small differences between large numbers. The choice of θ = 45°, 90°, and 135° was an attempt to maximize this difference and thus minimize the error involved. In addition, these values of θ minimize the effect of the velocity gradient in the 0° - 180° plane.

Estimated uncertainties in the indicated quantities are:

$$U: \pm 2\%$$

$$\overline{u'^2}: \pm 5\%$$

$$\overline{v'^2}, \overline{w'^2}, \overline{u'v'}: \pm 10\%$$

No wall proximity corrections were applied to the hot wire measurements, since by the criteria of Repik and Ponomareva [43] none were required for the conditions under which the measurements were made.

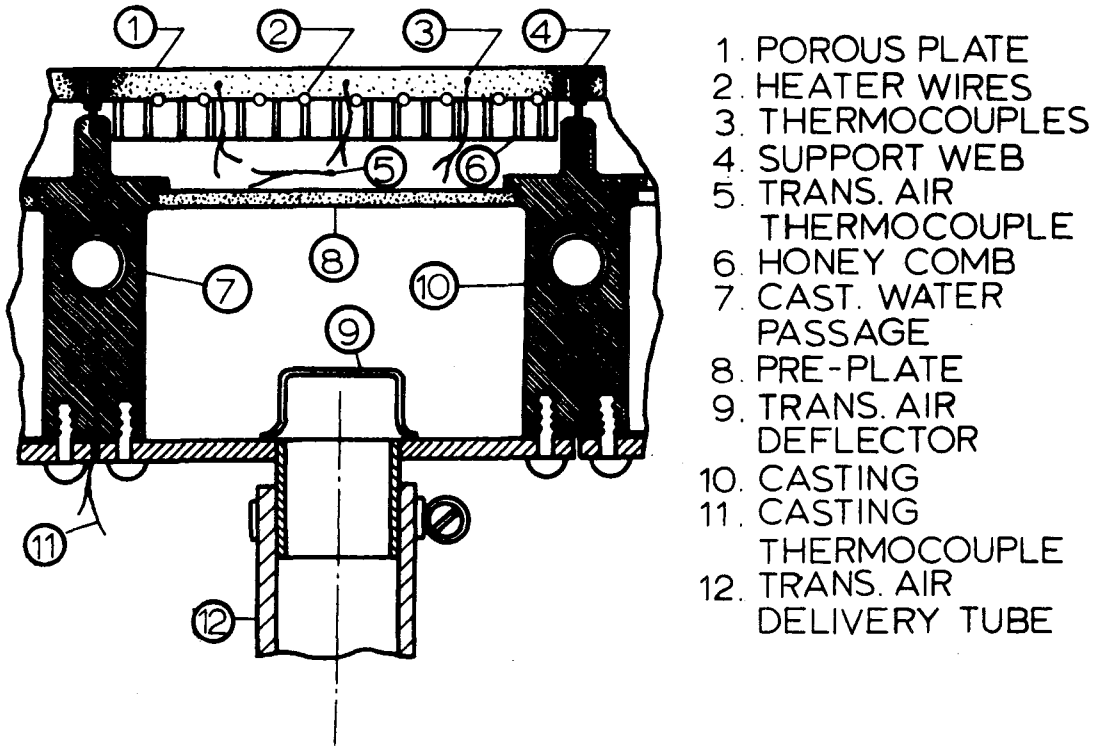

Figure I-1. Cross-Section of Typical Test Plate--Casting Configuration

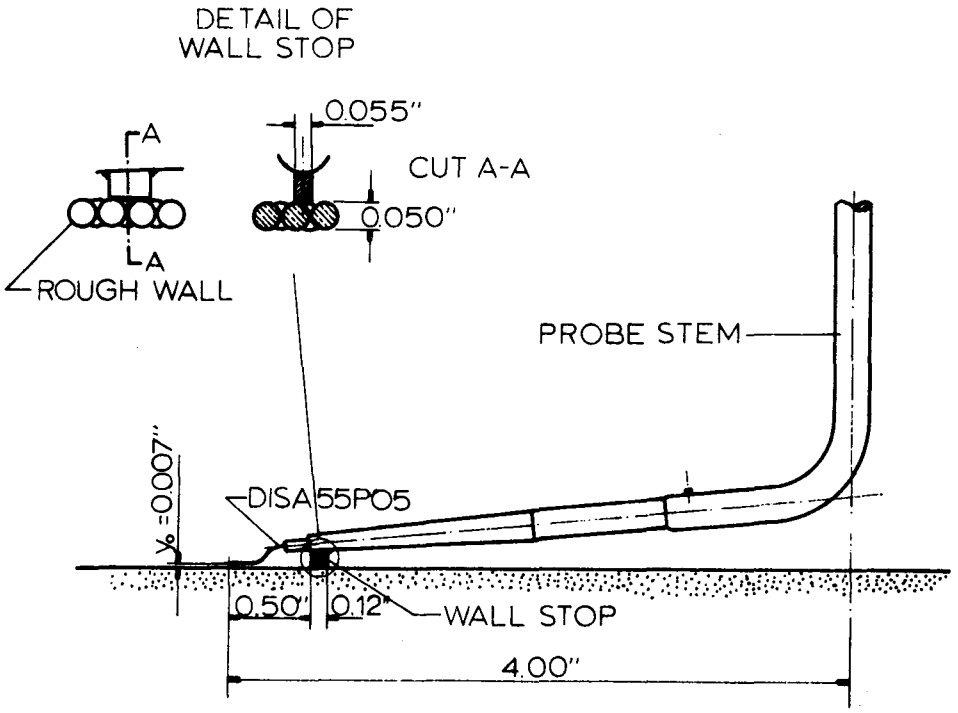

Figure I-2. Schematic of the Horizontal Hot-Wire Probe Configuration

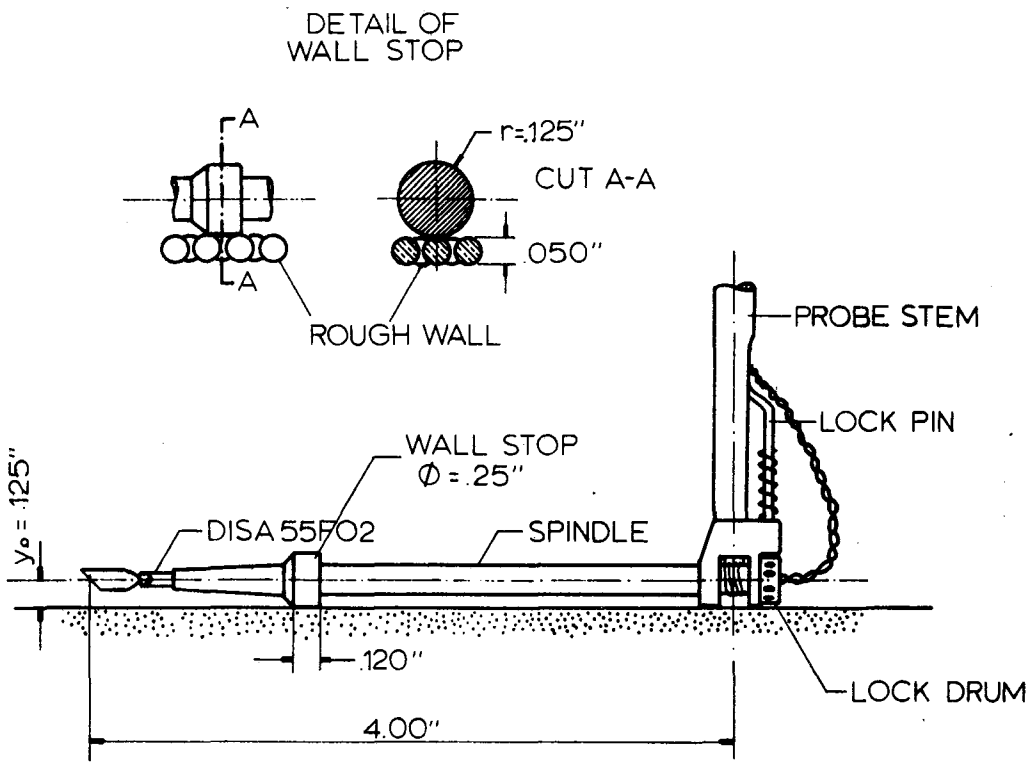

Figure I-3. Schematic of the Rotatable Slant Hot-Wire Probe Configuration

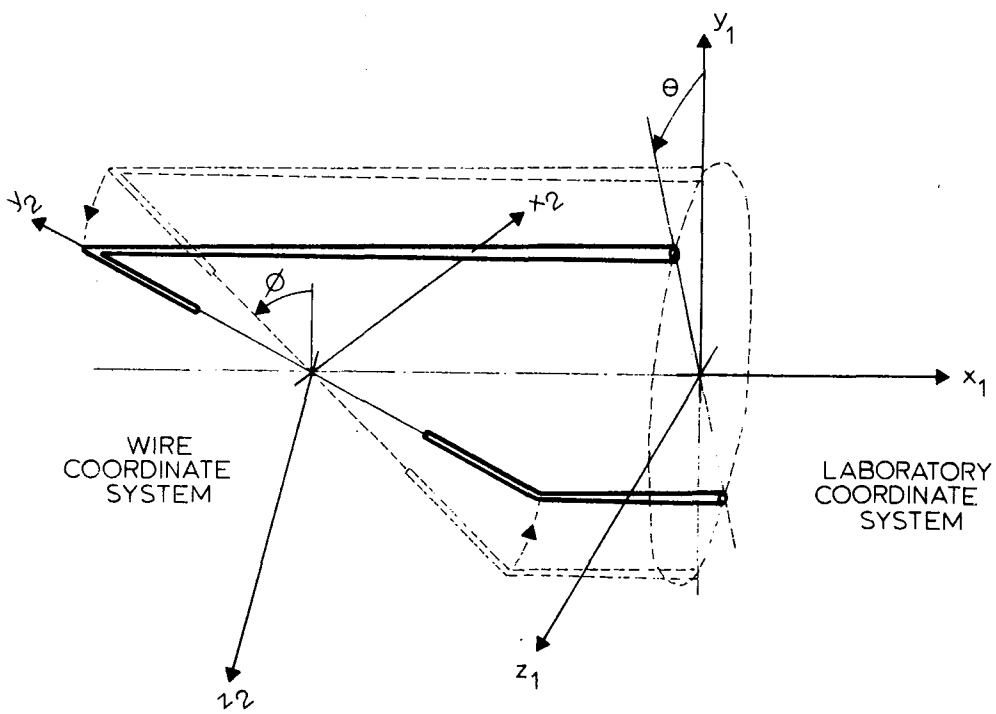

Figure I-4. Coordinate Systems for Analysis of Slant Wire Directional Characteristics

APPENDIX II

QUALIFICATION TESTS

II.1 Stanton Number Data

The original energy balance tests on the Roughness Rig were performed by Healzer [1], and the St data of Pimenta [2] were taken shortly after these tests. Since the present St data for $K_r = 0$, F = 0 and 0.0039 are in excellent agreement with those of Pimenta (see Figure 3-1) for large values of enthalpy thickness, it was concluded that the models for the energy losses were still valid.

This conclusion was confirmed when both blown and unblown energy balance tests were conducted several months after this investigation was completed. Results of these tests [44] were in excellent agreement with the original tests of Healzer.

II.2 Two Dimensionality Check

After installation of the boundary layer trip, a zero pressure gradient flow was established in the test section and velocity profiles were taken at x = 24" both on the centerline and 3 inches on either side (z = 0, ± 3 inches). Across this center 6" section of the tunnel, the variation of U_∞ was less than 1% and the variation of momentum thickness was less than 2%.

When a favorable pressure gradient (acceleration) is imposed on a flow in a test section of finite size, a divergence of the streamlines is expected due to the thinning of the boundary layers on the smooth side and

top walls. Since the accelerations applied in this investigation were milder (lower values of K) than those studied in the smooth wall layer investigations of Julien [27], Thielbahr [24], Loyd [28], and Kearney [25], the three-dimensionality induced by acceleration was anticipated to be negligible in this study. To check this effect on the turbulence measurements, the values of $\overline{v'w'}$ and $\overline{u'w'}$ were determined for each acceleration condition at the x-position where turbulence profiles were taken. In every case, $\overline{v'w'}$ and $\overline{u'w'}$ were essentially zero within the accuracy of the rms meter, and in no case were they greater than 2% of $\overline{u'v'}$. It was concluded that the accelerated boundary layers of this investigation could be considered two-dimensional with negligible loss of accuracy.

II.3 Sensitivity of Calculated Data to Origin of Wall

The sensitivity to the assumed origin of the wall of all accelerated data calculated by integration of profiles outward from the wall was considered. All calculated quantities reported in this thesis were determined assuming y = 0 at the crests of the spherical roughness elements.

Additional calculations were made considering the origin of the wall to be 0.006 inches below the crests of the roughness elements. Typical results, presented as the percentage change due to the 0.006" wall shift, were:

$$\delta \rightarrow 1\%$$
$$\delta_1 \rightarrow 4\%$$
$$\delta_2 \rightarrow 1\%$$
$$H \rightarrow 4\%$$
$$\Delta \rightarrow 1\%$$
$$\Delta_2 \rightarrow 1\%$$
$$Pr_T \rightarrow 3\%$$
$$C_f/2 \rightarrow 2\% \ .$$

II.4 Hot Wire Measurements

Great care was taken when hot wire measurements were being made to insure that the wire calibration and instrument calibrations were maintained. Periodic checks of wire calibration were made in the freestream by comparison with measurements of U_∞ obtained with a Pitot probe and the calibrated pressure transducers. The calibration settings of the linearizers, rms meter, and IDVM were checked after every one or two profiles to insure that these instruments had a minimum of drift. The temperature of the flow was maintained constant within $\pm$ 0.5°F during measurement periods by monitoring the output of a thermocouple in the freestream on an auxiliary digital voltmeter.

APPENDIX III

INDUCED TRANSPIRATION EFFECTS ON ACCELERATION DATA

Imposition of a pressure gradient, dP/dx, along the test section results in an induced flow through the porous plates for a nominal F = 0 condition. When there is blowing through the plates, the nominal distribution of F along the test section is altered by the flow induced by the pressure gradient. This section presents an analysis which quantifies these effects.

A cross-section diagram of a typical plate and casting assembly was shown in Figure I-1. In the following analysis it will be assumed that, for F = 0, the preplate is impermeable since its porosity is much less than that of the test plate. Static pressures on the front edge, center, and rear edge of the test plate will be denoted by P_1, P_2, and P_3, respectively. For a linear variation of pressure along the plate, the pressure in the plenum between the preplate and test plate is assumed to be $(P_1 + P_3)/2$ for F = 0. Under the favorable pressure gradients of this study, for a nominal F = 0 condition there is suction on the front half of the plate and blowing on the rear half.

The pressure drop versus flow rate characteristics of a typical plate were determined experimentally. The pressure differential across a test plate was measured for 11 different settings of the transpiration control valve (while there was no mainstream flow). It was found that the data follow the relationship

$$\dot{m} = 25.58\ \Delta P^{0.942} \qquad \text{(III.1)}$$

where $\dot{m}$ is the flow rate (ft^3/min) through the 0.5 ft^2 plate area and ΔP is the pressure drop across the test plate (inches H_2O). This expression is valid for ΔP from 0.019 to 0.56" H_2O and $\dot{m}$ from 0.58 to 14.68 ft^3/min.

Calculations were made using Equation (III.1), the assumptions stated above, and assuming negligible induced flow axially in the test plate due to the longer flow path in that direction than in the direction normal to the plate surface. Results are shown below, where F_{min} and F_{max} are the blowing fractions at the leading and trailing edges of the plate, respectively. Maximum induced suction occurred at the leading edge, maximum induced blowing at the trailing edge, and the value of F induced at the middle of the plate was zero.

Run	$(x-x_a)$	$F_{nominal}$	F_{max}	F_{min}
$K_r = 0.15 \times 10^{-3}$	22 42	0.0 0.0	0.0005 0.0006	-0.0006 -0.0006
$K_r = 0.29 \times 10^{-3}$	10 22	0.0 0.0	0.0010 0.0011	-0.0010 -0.0012
$K_r = 0.29 \times 10^{-3}$	10 22	0.0039 0.0039	0.0046 0.0049	-0.0031 -0.0030
$K = 0.28 \times 10^{-6}$	10 22	0.0 0.0	0.0013 0.0019	-0.0014 -0.0021

APPENDIX IV

Tabulation of Experimental Data

This appendix provides tabular listings of the experimental data of this investigation. Data are presented in the following order: (1) Stanton numbers, (2) mean temperature profiles, (3) mean velocity profiles, and (4) Reynolds stress tensor component profiles.

Abbreviations used in the listings are:

RUN	Date (month, day, year)	--
TINFO	Freestream total temperature	(°F)
TDB	Dry bulb temperature	(°F)
TWB	Wet bulb temperature	(°F)
PL	Plate number	--
X	Axial position from nozzle exit	(In.)
ST	Stanton number	--
DEH2	Enthalpy thickness, Δ_2	(In.)
REDEH2	Enthalpy thickness Reynolds number, Re_{Δ_2}	--
F	Blowing fraction	--
UINF	Freestream velocity	(ft/sec)
TW	Wall temperature	(°F)
TINF	Freestream static temperature	(°F)
KR	Fully rough acceleration parameter, K_r	--
K	Smooth wall acceleration parameter, K	--

DEH	Thermal boundary layer thickness, Δ	(In.)
DE	Velocity boundary layer thickness, δ	(In.)
DE2	Momentum thickness, δ_2	(In.)
PT	Point number in profile	--
Y	Distance normal to test surface	(In.)
T	Mean static temperature	(°F)
TBAR	$(T_w - T)/(T_w - T_\infty)$	--
CF/2	Skin friction coefficient, $C_f/2$	--
UTAU	Friction velocity, U_τ	(ft/sec)
DE1	Displacement thickness, δ_1	(In.)
H	Shape factor, δ_1/δ_2	--
G	Clauser shape factor	--
BETA	Pressure gradient parameter, $\beta = (\delta_1/\tau_w)(dP/dx)$	--
REDE2	Momentum thickness Reynolds number, Re_{δ_2}	--
REK	Roughness Reynolds number, Re_k	--
U	Mean velocity	(ft/sec)
UP2/UI2	$\overline{u'^2}/U_\infty^2$	--
VP2/UI2	$\overline{v'^2}/U_\infty^2$	--
WP2/UI2	$\overline{w'^2}/U_\infty^2$	--
-UV/UI2	$-\overline{u'v'}/U_\infty^2$	--
Q2/UI2	q^2/U_∞^2	--
RUV	$-\overline{u'v'}/\sqrt{\overline{u'^2}\ \overline{v'^2}}$	--
RQ2	$-\overline{u'v'}/q^2$	--

STANTON NO. RUN - KR=0, F=0
RUN = 040975 TDB = 70.00
TINFC = 66.60 TWB = 57.00

PL	X	ST	DEH2	REDEH2	F	UINF	TW	TINF	KR
1	2	.00531	.011	484.	0.0000	88.08	92.2	66.0	0.
2	6	.00372	.029	1308.	0.0000	88.08	92.3	66.0	0.
3	10	.00327	.043	1945.	0.0000	88.08	92.4	66.0	0.
4	14	.00301	.055	2517.	0.0000	88.08	92.4	66.0	0.
5	18	.00285	.067	3052.	0.0000	88.08	92.3	66.0	0.
6	22	.00263	.078	3552.	0.0000	88.08	92.3	66.0	0.
7	26	.00263	.088	4032.	0.0000	88.08	92.3	66.0	0.
8	30	.00248	.099	4498.	0.0000	88.08	92.4	66.0	0.
9	34	.00242	.109	4945.	0.0000	88.08	92.3	66.0	0.
10	38	.00238	.118	5384.	0.0000	88.08	92.4	66.0	0.
11	42	.00238	.128	5818.	0.0000	88.08	92.3	66.0	0.
12	46	.00236	.137	6249.	0.0000	88.08	92.2	66.0	0.
13	50	.00233	.147	6677.	0.0000	88.08	92.3	66.0	0.
14	54	.00225	.156	7095.	0.0000	88.08	92.4	66.0	0.
15	58	.00222	.165	7502.	0.0000	88.08	92.5	66.0	0.
16	62	.00221	.173	7907.	0.0000	88.08	92.4	66.0	0.
17	66	.00222	.182	8311.	0.0000	88.08	92.5	66.0	0.
18	70	.00219	.191	8713.	0.0000	88.08	92.5	66.0	0.
19	74	.00218	.200	9112.	0.0000	88.08	92.4	66.0	0.
20	78	.00214	.209	9506.	0.0000	88.08	92.5	66.0	0.
21	82	.00210	.217	9893.	0.0000	88.08	92.4	66.0	0.
22	86	.00212	.225	10277.	0.0000	88.08	92.5	66.0	0.
23	90	.00212	.234	10663.	0.0000	88.08	92.4	66.0	0.

STANTON NO. RUN - KR=0, F=0 - FIRST 6 PLATES UNHEATED
RUN = 040975 TDB = 70.00
TINFO = 67.50 TWB = 57.00

PL	X	ST	DEH2	REDEH2	F	UINF	TW	TINF	KR
1	2	0.00000	0.000	0.	0.0000	88.16	67.9	66.9	0.
2	6	0.00000	0.000	0.	0.0000	88.16	67.7	66.9	0.
3	10	0.00000	0.000	0.	0.0000	88.16	67.5	66.9	0.
4	14	0.00000	0.000	0.	0.0000	88.16	67.3	66.9	0.
5	18	0.00000	0.000	0.	0.0000	88.16	67.5	66.9	0.
6	22	0.00000	0.000	0.	0.0000	88.16	68.4	66.9	0.
7	26	.00455	.009	414.	0.0000	88.16	93.3	66.9	0.
8	30	.00335	.025	1133.	0.0000	88.16	93.3	66.9	0.
9	34	.00314	.038	1724.	0.0000	88.16	93.2	66.9	0.
10	38	.00297	.050	2280.	0.0000	88.16	93.4	66.9	0.
11	42	.00284	.062	2808.	0.0000	88.16	93.0	66.9	0.
12	46	.00278	.073	3319.	0.0000	88.16	93.1	66.9	0.
13	50	.00270	.084	3818.	0.0000	88.16	93.0	66.9	0.
14	54	.00259	.095	4299.	0.0000	88.16	93.1	66.9	0.
15	58	.00253	.105	4765.	0.0000	88.16	93.2	66.9	0.
16	62	.00250	.115	5223.	0.0000	88.16	93.1	66.9	0.
17	66	.00247	.125	5675.	0.0000	88.16	93.2	66.9	0.
18	70	.00244	.135	6121.	0.0000	88.16	93.2	66.9	0.
19	74	.00240	.144	6561.	0.0000	88.16	93.2	66.9	0.
20	78	.00235	.154	6993.	0.0000	88.16	93.3	66.9	0.
21	82	.00229	.163	7416.	0.0000	88.16	93.4	66.9	0.
22	86	.00230	.172	7834.	0.0000	88.16	93.4	66.9	0.
23	90	.00230	.181	8253.	0.0000	88.16	93.4	66.9	0.

STANTON NO. RUN - KR=0, F=0 - FIRST 12 PLATES UNHEATED
RUN = 040975 TDB = 70.00
TINFO = 67.20 TWB = 57.00

PL	X	ST	DEH2	REDEH2	F	UINF	TW	TINF	KR
1	2	0.00000	0.000	0.	0.0000	88.13	67.9	66.6	0.
2	6	0.00000	0.000	0.	0.0000	88.13	67.6	66.6	0.
3	10	0.00000	0.000	0.	0.0000	88.13	67.3	66.6	0.
4	14	0.00000	0.000	0.	0.0000	88.13	67.2	66.6	0.
5	18	0.00000	0.000	0.	0.0000	88.13	67.4	66.6	0.
6	22	0.00000	0.000	0.	0.0000	88.13	67.3	66.6	0.
7	26	0.00000	0.000	0.	0.0000	88.13	67.3	66.6	0.
8	30	0.00000	0.000	0.	0.0000	88.13	67.2	66.6	0.
9	34	0.00000	0.000	0.	0.0000	88.13	67.2	66.6	0.
10	38	0.00000	0.000	0.	0.0000	88.13	67.1	66.6	0.
11	42	0.00000	0.000	0.	0.0000	88.13	67.3	66.6	0.
12	46	0.00000	0.000	0.	0.0000	88.13	68.1	66.6	0.
13	50	.00427	.009	389.	0.0000	88.13	93.4	66.6	0.
14	54	.00320	.024	1069.	0.0000	88.13	93.4	66.6	0.
15	58	.00304	.036	1638.	0.0000	88.13	93.5	66.6	0.
16	62	.00292	.048	2181.	0.0000	88.13	93.3	66.6	0.
17	66	.00283	.059	2704.	0.0000	88.13	93.4	66.6	0.
18	70	.00276	.071	3212.	0.0000	88.13	93.3	66.6	0.
19	74	.00269	.081	3708.	0.0000	88.13	93.5	66.6	0.
20	78	.00260	.092	4189.	0.0000	88.13	93.5	66.6	0.
21	82	.00252	.102	4655.	0.0000	88.13	93.5	66.6	0.
22	86	.00251	.112	5113.	0.0000	88.13	93.5	66.6	0.
23	90	.00250	.122	5569.	0.0000	88.13	93.4	66.6	0.

STANTON NO. RUN - KR=0, F=0 - LINEAR TWALL VARIATION
RUN = 041075 TDB = 70.00
TINFO = 64.20 TWB = 56.00

PL	X	ST	DEH2	REDEH2	F	UINF	TW	TINF	KR
1	2	.00529	.011	485.	0.0000	88.05	102.0	63.9	0.
2	6	.00371	.029	1308.	0.0000	88.05	102.1	63.9	0.
3	10	.00327	.043	1947.	0.0000	88.05	102.1	63.9	0.
4	14	.00301	.055	2538.	0.0000	88.05	101.8	63.9	0.
5	18	.00281	.068	3114.	0.0000	88.05	101.2	63.9	0.
6	22	.00260	.080	3669.	0.0000	88.05	100.5	63.9	0.
7	26	.00259	.092	4212.	0.0000	88.05	99.9	63.9	0.
8	30	.00243	.104	4746.	0.0000	88.05	99.2	63.9	0.
9	34	.00237	.116	5292.	0.0000	88.05	98.5	63.9	0.
10	38	.00231	.127	5819.	0.0000	88.05	97.9	63.9	0.
11	42	.00228	.139	6374.	0.0000	88.05	97.1	63.9	0.
12	46	.00225	.151	6906.	0.0000	88.05	96.5	63.9	0.
13	50	.00223	.163	7475.	0.0000	88.05	95.8	63.9	0.
14	54	.00211	.175	8032.	0.0000	88.05	95.1	63.9	0.
15	58	.00209	.188	8621.	0.0000	88.05	94.4	63.9	0.
16	62	.00207	.201	9196.	0.0000	88.05	93.7	63.9	0.
17	66	.00205	.214	9785.	0.0000	88.05	93.1	63.9	0.
18	70	.00202	.227	10414.	0.0000	88.05	92.3	63.9	0.
19	74	.00200	.241	11020.	0.0000	88.05	91.7	63.9	0.
20	78	.00194	.255	11682.	0.0000	88.05	91.0	63.9	0.
21	82	.00190	.270	12361.	0.0000	88.05	90.3	63.9	0.
22	86	.00189	.284	13013.	0.0000	88.05	89.7	63.9	0.
23	90	.00189	.300	13727.	0.0000	88.05	89.0	63.9	0.

STANTON NO. RUN - KR=0, F=0 - BILINEAR TWALL VARIATION
RUN = 041075 TDB = 70.00
TINFO = 64.30 TWB = 56.00

PL	X	ST	DEH2	REDEH2	F	UINF	TW	TINF	KR
1	2	.00529	.011	485.	0.0000	88.06	102.2	64.0	0.
2	6	.00371	.029	1309.	0.0000	88.06	102.2	64.0	0.
3	10	.00327	.043	1949.	0.0000	88.06	102.2	64.0	0.
4	14	.00303	.055	2525.	0.0000	88.06	102.2	64.0	0.
5	18	.00278	.069	3146.	0.0000	88.06	100.9	64.0	0.
6	22	.00257	.083	3779.	0.0000	88.06	99.4	64.0	0.
7	26	.00253	.096	4393.	0.0000	88.06	98.0	64.0	0.
8	30	.00237	.110	5011.	0.0000	88.06	96.8	64.0	0.
9	34	.00228	.124	5677.	0.0000	88.06	95.3	64.0	0.
10	38	.00223	.139	6343.	0.0000	88.06	94.0	64.0	0.
11	42	.00214	.155	7089.	0.0000	88.06	92.5	64.0	0.
12	46	.00209	.171	7836.	0.0000	88.06	91.1	64.0	0.
13	50	.00205	.189	8668.	0.0000	88.06	89.7	64.0	0.
14	54	.00187	.207	9454.	0.0000	88.06	88.5	64.0	0.
15	58	.00208	.205	9372.	0.0000	88.06	89.7	64.0	0.
16	62	.00217	.202	9261.	0.0000	88.06	91.1	64.0	0.
17	66	.00223	.200	9161.	0.0000	88.06	92.6	64.0	0.
18	70	.00228	.200	9132.	0.0000	88.06	94.0	64.0	0.
19	74	.00228	.200	9130.	0.0000	88.06	95.5	64.0	0.
20	78	.00228	.200	9166.	0.0000	88.06	96.8	64.0	0.
21	82	.00227	.201	9198.	0.0000	88.06	98.2	64.0	0.
22	86	.00231	.202	9263.	0.0000	88.06	99.6	64.0	0.
23	90	.00233	.204	9328.	0.0000	88.06	101.0	64.0	0.

STANTON NO. RUN - KR=0, F=0.0039
RUN = 041775 TDB = 71.50
TINFO = 67.30 TWB = 57.00

PL	X	ST	DEH2	REDEH2	F	UINF	TW	TINF	KR
1	2	.00353	.015	677.	.0039	87.98	97.7	66.9	0.
2	6	.00213	.042	1899.	.0039	87.98	97.7	66.9	0.
3	10	.00162	.065	2948.	.0040	87.98	97.8	66.9	0.
4	14	.00142	.087	3949.	.0040	87.98	97.7	66.9	0.
5	18	.00139	.108	4918.	.0040	87.98	97.8	66.9	0.
6	22	.00121	.130	5875.	.0039	87.98	97.7	66.9	0.
7	26	.00117	.150	6796.	.0039	87.98	97.8	66.9	0.
8	30	.00105	.170	7701.	.0039	87.98	97.8	66.9	0.
9	34	.00105	.190	8614.	.0040	87.98	97.8	66.9	0.
10	38	.00099	.210	9534.	.0039	87.98	97.7	66.9	0.
11	42	.00100	.230	10420.	.0040	87.98	97.7	66.9	0.
12	46	.00098	.249	11293.	.0039	87.98	97.8	66.9	0.
13	50	.00095	.269	12183.	.0039	87.98	97.8	66.9	0.
14	54	.00082	.288	13047.	.0040	87.98	97.8	66.9	0.
15	58	.00094	.307	13936.	.0039	87.98	97.8	66.9	0.
16	62	.00094	.326	14802.	.0039	87.98	97.8	66.9	0.
17	66	.00085	.345	15663.	.0040	87.98	97.9	66.9	0.
18	70	.00085	.366	16586.	.0039	87.98	97.8	66.9	0.
19	74	.00078	.385	17466.	.0039	87.98	97.7	66.9	0.
20	78	.00082	.405	18365.	.0039	87.98	97.7	66.9	0.
21	82	.00078	.423	19182.	.0040	87.98	97.7	66.9	0.
22	86	.00081	.441	20022.	.0040	87.98	97.8	66.9	0.
23	90	.00081	.460	20841.	.0039	87.98	97.8	66.9	0.

STANTON NO. RUN - KR=0, F=0.0039 - FIRST 6 PLATES UNHEATED
RUN = 041775 TDB = 71.50
TINFO = 66.90 TWB = 57.00

PL	X	ST	DEH2	REDEH2	F	UINF	TW	TINF	KR
1	2	0.00000	.008	356.	.0039	87.95	68.2	66.5	0.
2	6	0.00000	.025	1141.	.0039	87.95	68.0	66.5	0.
3	10	0.00000	.048	2156.	.0040	87.95	67.8	66.5	0.
4	14	0.00000	.080	3648.	.0040	87.95	67.7	66.5	0.
5	18	0.00000	.063	2842.	.0040	87.95	68.0	66.5	0.
6	22	0.00000	.049	2230.	.0039	87.95	68.8	66.5	0.
7	26	.00245	.023	1049.	.0039	87.95	97.7	66.5	0.
8	30	.00160	.047	2121.	.0039	87.95	97.9	66.5	0.
9	34	.00148	.069	3114.	.0040	87.95	97.9	66.5	0.
10	38	.00133	.090	4085.	.0039	87.95	97.9	66.5	0.
11	42	.00127	.111	5055.	.0040	87.95	97.7	66.5	0.
12	46	.00121	.132	5987.	.0039	87.95	97.8	66.5	0.
13	50	.00116	.153	6931.	.0039	87.95	97.7	66.5	0.
14	54	.00102	.173	7848.	.0040	87.95	97.7	66.5	0.
15	58	.00112	.193	8739.	.0039	87.95	97.8	66.5	0.
16	62	.00110	.213	9663.	.0039	87.95	97.8	66.5	0.
17	66	.00101	.232	10538.	.0039	87.95	97.9	66.5	0.
18	70	.00098	.252	11422.	.0039	87.95	97.9	66.5	0.
19	74	.00092	.272	12333.	.0039	87.95	97.8	66.5	0.
20	78	.00094	.290	13174.	.0039	87.95	97.9	66.5	0.
21	82	.00089	.310	14070.	.0040	87.95	97.9	66.5	0.
22	86	.00091	.329	14952.	.0040	87.95	97.9	66.5	0.
23	90	.00091	.349	15850.	.0039	87.95	97.9	66.5	0.

STANTON NO. RUN - KR=0, F=0.0039 - BILINEAR TWALL VARIATION
RUN = 041775 TDB = 71.50
TINFO = 67.30 TWB = 57.00

PL	X	ST	DEH2	REDEH2	F	UINF	TW	TINF	KR
1	2	.00355	.015	678.	.0039	87.98	97.6	66.9	0.
2	6	.00215	.042	1905.	.0039	87.98	97.7	66.9	0.
3	10	.00165	.065	2957.	.0040	87.98	97.8	66.9	0.
4	14	.00145	.088	3967.	.0040	87.98	97.7	66.9	0.
5	18	.00136	.113	5101.	.0040	87.98	96.5	66.9	0.
6	22	.00116	.138	6280.	.0039	87.98	95.2	66.9	0.
7	26	.00111	.166	7544.	.0039	87.98	93.8	66.9	0.
8	30	.00095	.195	8862.	.0039	87.98	92.4	66.9	0.
9	34	.00095	.226	10243.	.0040	87.98	91.1	66.9	0.
10	38	.00086	.261	11846.	.0039	87.98	89.5	66.9	0.
11	42	.00085	.295	13366.	.0040	87.98	88.4	66.9	0.
12	46	.00076	.337	15303.	.0039	87.98	86.8	66.9	0.
13	50	.00082	.383	17375.	.0039	87.98	85.4	66.9	0.
14	54	.00047	.427	19352.	.0040	87.98	84.3	66.9	0.
15	58	.00086	.417	18924.	.0039	87.98	85.5	66.9	0.
16	62	.00092	.408	18506.	.0039	87.98	86.8	66.9	0.
17	66	.00088	.401	18179.	.0040	87.98	88.1	66.9	0.
18	70	.00095	.396	17942.	.0039	87.98	89.5	66.9	0.
19	74	.00085	.391	17733.	.0039	87.98	90.9	66.9	0.
20	78	.00099	.389	17648.	.0039	87.98	92.2	66.9	0.
21	82	.00093	.386	17512.	.0040	87.98	93.8	66.9	0.
22	86	.00086	.388	17619.	.0040	87.98	95.0	66.9	0.
23	90	.00084	.388	17607.	.0039	87.98	96.4	66.9	0.

STANTON NO. RUN - KR=0.15E-3, F=0
RUN = 040175 TDB = 73.00
TINFO = 67.20 TWB = 56.00

PL	X	ST	DEH2	REDEH2	F	UINF	TW	TINF	KR
1	2	.00527	.011	482.	0.0000	88.46	93.6	66.7	0.
2	6	.00372	.029	1302.	0.0000	88.10	93.6	66.7	-.123E-04
3	10	.00329	.043	1940.	0.0000	88.00	93.5	66.7	-.600E-05
4	14	.00304	.055	2516.	0.0000	88.00	93.5	66.7	.179E-05
5	18	.00287	.067	3055.	0.0000	88.03	93.6	66.7	.538E-05
6	22	.00268	.078	3560.	0.0000	88.12	93.6	66.7	.335E-05
7	26	.00267	.089	4047.	0.0000	88.17	93.5	66.7	-.140E-06
8	30	.00252	.099	4520.	0.0000	88.11	93.6	66.7	-.112E-05
9	34	.00247	.109	4975.	0.0000	88.09	93.5	66.7	.532E-05
10	38	.00244	.119	5422.	0.0000	88.31	93.5	66.7	.332E-04
11	42	.00247	.128	5872.	0.0000	89.13	93.5	66.7	.101E-03
12	46	.00250	.135	6335.	0.0000	91.05	93.5	66.7	.144E-03
13	50	.00251	.141	6813.	0.0000	93.32	93.5	66.7	.151E-03
14	54	.00245	.148	7297.	0.0000	95.53	93.5	66.6	.143E-03
15	58	.00242	.154	7783.	0.0000	97.76	93.5	66.6	.147E-03
16	62	.00242	.160	8277.	0.0000	100.02	93.4	66.6	.142E-03
17	66	.00242	.166	8783.	0.0000	102.47	93.4	66.5	.153E-03
18	70	.00243	.172	9303.	0.0000	104.87	93.5	66.5	.143E-03
19	74	.00242	.178	9833.	0.0000	107.31	93.6	66.5	.141E-03
20	78	.00236	.183	10368.	0.0000	109.98	93.6	66.4	.156E-03
21	82	.00232	.188	10905.	0.0000	112.68	93.6	66.4	.147E-03
22	86	.00232	.193	11450.	0.0000	115.18	93.6	66.4	.139E-03
23	90	.00237	.198	12013.	0.0000	117.86	93.5	66.3	.165E-03

STANTON NO. RUN - KR=0.15E-3, F=0 - FIRST 6 PLATES UNHEATED
RUN = 032575 TDB = 71.08
TINFO = 66.10 TWB = 58.00

PL	X	ST	DEH2	REDEH2	F	UINF	TW	TINF	KR
1	2	0.00000	0.000	0.	0.0000	88.28	66.7	65.7	-.241E-04
2	6	0.00000	0.000	0.	0.0000	87.94	66.4	65.8	-.143E-04
3	10	0.00000	0.000	0.	0.0000	87.79	66.3	65.8	-.583E-05
4	14	0.00000	0.000	0.	0.0000	87.75	66.1	65.8	.163E-05
5	18	0.00000	0.000	0.	0.0000	87.84	66.2	65.8	.591E-05
6	22	0.00000	0.000	0.	0.0000	87.90	67.3	65.8	.246E-05
7	26	.00461	.009	417.	0.0000	88.00	92.7	65.7	-.277E-05
8	30	.00340	.025	1140.	0.0000	87.82	92.7	65.8	-.330E-05
9	34	.00319	.039	1735.	0.0000	87.88	92.6	65.8	.935E-05
10	38	.00303	.051	2297.	0.0000	88.08	92.8	65.7	.320E-04
11	42	.00297	.062	2843.	0.0000	88.87	92.7	65.7	.103E-03
12	46	.00296	.073	3389.	0.0000	90.88	92.7	65.7	.142E-03
13	50	.00292	.083	3944.	0.0000	92.99	92.7	65.7	.149E-03
14	54	.00282	.092	4499.	0.0000	95.28	92.8	65.7	.145E-03
15	58	.00275	.101	5050.	0.0000	97.45	92.8	65.6	.147E-03
16	62	.00273	.110	5605.	0.0000	99.73	92.6	65.6	.143E-03
17	66	.00269	.118	6167.	0.0000	102.13	92.7	65.6	.152E-03
18	70	.00268	.126	6737.	0.0000	104.62	92.7	65.5	.146E-03
19	74	.00264	.133	7315.	0.0000	107.08	92.7	65.5	.145E-03
20	78	.00258	.140	7895.	0.0000	109.77	92.7	65.4	.155E-03
21	82	.00253	.147	8476.	0.0000	112.37	92.8	65.4	.143E-03
22	86	.00252	.154	9063.	0.0000	114.91	92.7	65.4	.137E-03
23	90	.00254	.161	9665.	0.0000	117.55	92.8	65.3	.161E-03

STANTON NO. RUN - KR=0.29E-3, F=0
RUN = 022575 TDB = 73.00
TINFO = 66.10 TWB = 60.00

PL	X	ST	DEH2	REDEH2	F	UINF	TW	TINF	KR
1	2	.00523	.011	472.	0.0000	87.24	93.4	65.7	0.
2	6	.00370	.028	1277.	0.0000	86.99	93.4	65.7	-.549E-05
3	10	.00327	.042	1906.	0.0000	87.08	93.3	65.7	.312E-05
4	14	.00302	.055	2473.	0.0000	87.08	93.3	65.7	-.631E-06
5	18	.00287	.067	3005.	0.0000	87.35	93.5	65.7	.722E-04
6	22	.00278	.076	3523.	0.0000	89.51	93.4	65.7	.238E-03
7	26	.00284	.084	4055.	0.0000	93.53	93.4	65.6	.282E-03
8	30	.00272	.091	4606.	0.0000	97.94	93.4	65.6	.285E-03
9	34	.00271	.098	5168.	0.0000	102.30	93.2	65.5	.279E-03
10	38	.00263	.104	5746.	0.0000	106.93	93.2	65.4	.280E-03
11	42	.00265	.110	6343.	0.0000	111.97	93.4	65.3	.280E-03
12	46	.00261	.115	6966.	0.0000	117.32	93.3	65.3	.289E-03
13	50	.00260	.120	7612.	0.0000	122.79	93.4	65.2	.301E-03
14	54	.00244	.125	8264.	0.0000	128.44	93.3	65.1	.166E-03
15	58	.00233	.134	8897.	0.0000	129.19	93.2	65.0	-.184E-05
16	62	.00231	.143	9515.	0.0000	128.80	93.2	65.1	-.170E-04
17	66	.00225	.152	10121.	0.0000	129.02	93.3	65.1	.210E-04
18	70	.00224	.161	10721.	0.0000	129.34	93.3	65.0	.179E-04
19	74	.00221	.169	11315.	0.0000	129.52	93.4	65.0	-.107E-04
20	78	.00215	.178	11898.	0.0000	129.52	93.4	65.0	.415E-05
21	82	.00212	.187	12468.	0.0000	129.42	93.2	65.0	-.924E-05
22	86	.00210	.196	13031.	0.0000	129.22	93.3	65.0	-.176E-04
23	90	.00214	.205	13594.	0.0000	128.49	93.3	65.1	-.358E-04

STANTON NO. RUN - KR=0.29E-3, F=0.0039
RUN = 030875 TDB = 71.00
TINFO = 66.90 TWB = 59.00

PL	X	ST	DEH2	REDEH2	F	UINF	TW	TINF	KR
1	2	.00356	.015	667.	.0039	87.00	98.0	66.5	0.
2	6	.00212	.042	1871.	.0039	86.87	98.1	66.5	-.244E-05
3	10	.00167	.065	2906.	.0039	86.80	98.2	66.5	-.240E-05
4	14	.00145	.087	3882.	.0039	86.80	98.2	66.5	-.124E-04
5	18	.00145	.108	4840.	.0039	86.82	98.0	66.5	.552E-04
6	22	.00134	.126	5800.	.0039	88.82	98.1	66.5	.239E-03
7	26	.00133	.141	6777.	.0039	92.98	98.2	66.4	.296E-03
8	30	.00125	.155	7789.	.0039	97.49	98.1	66.3	.294E-03
9	34	.00129	.168	8848.	.0039	102.09	98.1	66.3	.284E-03
10	38	.00125	.181	9958.	.0039	106.83	98.1	66.2	.279E-03
11	42	.00132	.193	11125.	.0039	111.71	98.0	66.1	.300E-03
12	46	.00125	.204	12347.	.0039	117.42	98.0	66.0	.295E-03
13	50	.00122	.215	13613.	.0039	122.96	97.9	65.9	.299E-03
14	54	.00116	.225	14923.	.0039	128.72	98.0	65.8	.195E-03
15	58	.00110	.243	16252.	.0039	130.10	98.0	65.8	.669E-05
16	62	.00103	.263	17571.	.0039	129.95	98.1	65.8	-.158E-04
17	66	.00096	.282	18876.	.0039	129.83	98.0	65.8	.854E-05
18	70	.00086	.301	20158.	.0039	129.92	98.0	65.8	-.197E-05
19	74	.00098	.321	21442.	.0039	129.84	98.1	65.8	-.863E-05
20	78	.00086	.340	22731.	.0039	129.81	98.1	65.8	-.291E-05
21	82	.00080	.359	23994.	.0039	129.89	98.1	65.8	.628E-05
22	86	.00071	.378	25236.	.0039	129.74	98.2	65.8	-.526E-05
23	90	.00079	.396	26476.	.0039	129.76	98.2	65.8	.789E-05

STANTON NO. RUN - K=0.28E-6, F=0
RUN = 042975 TDB = 74.00
TINFO = 67.30 TWB = 58.00

PL	X	ST	DEH2	REDEH2	F	UINF	TW	TINF	K
1	2	.00523	.011	470.	0.0000	87.09	95.1	66.9	-.121E-07
2	6	.00369	.028	1270.	0.0000	86.90	95.1	66.9	-.549E-08
3	10	.00326	.042	1890.	0.0000	86.92	95.2	66.9	-.389E-08
4	14	.00301	.055	2451.	0.0000	86.82	95.2	66.9	-.154E-07
5	18	.00287	.067	2967.	0.0000	86.56	95.3	66.9	.540E-07
6	22	.00279	.076	3482.	0.0000	88.76	95.3	66.8	.216E-06
7	26	.00288	.084	4015.	0.0000	93.36	95.3	66.8	.272E-06
8	30	.00277	.090	4590.	0.0000	98.65	95.1	66.7	.278E-06
9	34	.00277	.096	5171.	0.0000	104.41	95.1	66.6	.272E-06
10	38	.00270	.101	5779.	0.0000	110.80	95.1	66.5	.276E-06
11	42	.00274	.105	6416.	0.0000	118.43	95.2	66.4	.294E-06
12	46	.00270	.108	7109.	0.0000	127.87	95.2	66.2	.294E-06
13	50	.00275	.111	7853.	0.0000	138.30	95.2	66.0	.282E-06
14	54	.00247	.113	8681.	0.0000	149.90	95.0	65.8	.153E-06
15	58	.00233	.121	9391.	0.0000	151.26	95.1	65.8	-.845E-08
16	62	.00230	.132	10116.	0.0000	149.95	95.1	65.8	-.264E-07
17	66	.00226	.141	10776.	0.0000	149.21	95.2	65.8	-.549E-08
18	70	.00225	.150	11465.	0.0000	149.16	95.2	65.8	.511E-09
19	74	.00221	.159	12134.	0.0000	149.55	95.3	65.8	.233E-08
20	78	.00218	.167	12792.	0.0000	149.93	95.3	65.8	.738E-08
21	82	.00214	.175	13488.	0.0000	150.25	95.2	65.8	.136E-07
22	86	.00215	.184	14167.	0.0000	150.85	95.2	65.8	.133E-07
23	90	.00219	.192	14839.	0.0000	151.39	95.2	65.8	.575E-08

STANTON NO. RUN - K=0.28E-6, F=0 - FIRST 6 PLATES UNHEATED
RUN = 042975 TDB = 74.00
TINFO = 67.40 TWB = 58.00

PL	X	ST	DEH2	REDEH2	F	UINF	TW	TINF	K
1	2	0.00000	0.000	0.	0.0000	87.10	68.6	67.0	-.121E-07
2	6	0.00000	0.000	0.	0.0000	86.91	68.4	67.0	-.549E-08
3	10	0.00000	0.000	0.	0.0000	86.93	68.1	67.0	-.389E-08
4	14	0.00000	0.000	0.	0.0000	86.84	68.0	67.0	-.154E-07
5	18	0.00000	0.000	0.	0.0000	86.57	68.2	67.0	.540E-07
6	22	0.00000	0.000	0.	0.0000	88.78	69.1	67.0	.216E-06
7	26	.00490	.010	471.	0.0000	93.38	95.0	67.0	.272E-06
8	30	.00369	.026	1315.	0.0000	98.67	95.1	66.9	.278E-06
9	34	.00349	.039	2075.	0.0000	104.43	94.9	66.8	.272E-06
10	38	.00328	.050	2820.	0.0000	110.82	95.0	66.7	.276E-06
11	42	.00321	.059	3579.	0.0000	118.45	95.0	66.6	.294E-06
12	46	.00313	.067	4376.	0.0000	127.89	95.1	66.4	.294E-06
13	50	.00311	.074	5238.	0.0000	138.33	95.1	66.2	.282E-06
14	54	.00280	.080	6122.	0.0000	149.92	95.0	66.0	.153E-06
15	58	.00261	.090	6949.	0.0000	151.28	95.1	65.9	-.845E-08
16	62	.00255	.101	7725.	0.0000	149.97	95.1	66.0	-.264E-07
17	66	.00247	.111	8492.	0.0000	149.24	95.1	66.0	-.549E-08
18	70	.00245	.121	9233.	0.0000	149.18	95.2	66.0	.511E-09
19	74	.00238	.130	9961.	0.0000	149.57	95.2	66.0	.233E-08
20	78	.00233	.139	10696.	0.0000	149.96	95.2	66.0	.738E-08
21	82	.00229	.149	11433.	0.0000	150.27	95.1	66.0	.136E-07
22	86	.00228	.157	12109.	0.0000	150.88	95.2	66.0	.133E-07
23	90	.00232	.165	12806.	0.0000	151.41	95.2	65.9	.575E-08

STANTON NO. RUN - KR=0.50E-3, F=0
RUN = 050875 TDB = 75.00
TINFO = 66.90 TWB = 61.00

PL	X	ST	DEH2	REDEH2	F	UINF	TW	TINF	KR
1	2	.00525	.011	453.	0.0000	83.69	95.6	66.5	-.200E-05
2	6	.00372	.028	1227.	0.0000	83.84	95.5	66.5	-.285E-05
3	10	.00328	.042	1830.	0.0000	83.73	95.6	66.5	-.345E-05
4	14	.00302	.055	2377.	0.0000	83.74	95.5	66.5	-.703E-05
5	18	.00288	.067	2880.	0.0000	83.69	95.6	66.5	.920E-04
6	22	.00284	.076	3390.	0.0000	86.57	95.5	66.5	.350E-03
7	26	.00296	.082	3932.	0.0000	93.19	95.5	66.4	.498E-03
8	30	.00286	.087	4521.	0.0000	101.34	95.5	66.3	.515E-03
9	34	.00284	.091	5148.	0.0000	109.75	95.4	66.2	.487E-03
10	38	.00274	.095	5800.	0.0000	118.58	95.5	66.0	.490E-03
11	42	.00275	.099	6493.	0.0000	128.33	95.5	65.9	.468E-03
12	46	.00264	.103	7232.	0.0000	137.29	95.5	65.7	.363E-03
13	50	.00265	.108	7967.	0.0000	144.65	95.6	65.5	.329E-03
14	54	.00243	.112	8755.	0.0000	152.43	95.6	65.4	.183E-03
15	58	.00231	.122	9530.	0.0000	153.19	95.5	65.4	-.987E-05
16	62	.00228	.132	10258.	0.0000	152.30	95.5	65.4	-.266E-04
17	66	.00225	.141	10925.	0.0000	151.91	95.6	65.4	-.130E-05
18	70	.00224	.150	11677.	0.0000	152.09	95.4	65.4	.747E-05
19	74	.00221	.158	12328.	0.0000	152.34	95.5	65.4	.879E-05
20	78	.00218	.167	13044.	0.0000	152.64	95.5	65.4	.110E-04
21	82	.00215	.176	13753.	0.0000	153.10	95.4	65.4	.174E-04
22	86	.00216	.184	14446.	0.0000	153.46	95.4	65.4	.920E-05
23	90	.00220	.192	15078.	0.0000	153.61	95.5	65.3	.964E-05

STANTON NO. RUN - VARIABLE UINF,F - STEPS IN F - TWALL CONSTANT
RUN = 051475 TDB = 77.00
TINFO = 65.10 TWB = 62.00

PL	X	ST	DEH2	REDEH2	F	UINF	TW	TINF	KR
1	2	.00521	.010	477.	0.0000	87.78	90.5	64.7	0.
2	6	.00367	.028	1292.	0.0000	87.77	90.3	64.7	-.566E-06
3	10	.00325	.042	1921.	0.0000	87.75	90.4	64.7	-.340E-05
4	14	.00301	.055	2501.	0.0000	87.68	90.3	64.7	-.109E-04
5	18	.00287	.067	3035.	0.0000	87.56	90.3	64.7	.653E-04
6	22	.00276	.076	3551.	0.0000	89.74	90.4	64.7	.249E-03
7	26	.00191	.088	4324.	.0037	94.58	90.6	64.6	.342E-03
8	30	.00165	.104	5417.	.0035	99.99	90.6	64.6	.343E-03
9	34	.00164	.118	6490.	.0033	105.47	90.6	64.5	.343E-03
10	38	.00158	.131	7580.	.0031	111.53	90.6	64.4	.350E-03
11	42	.00160	.142	8708.	.0030	117.87	90.6	64.3	.322E-03
12	46	.00160	.154	9848.	.0028	123.61	90.5	64.2	.264E-03
13	50	.00150	.165	10981.	.0027	128.60	90.5	64.1	.250E-03
14	54	.00150	.175	12164.	.0026	133.84	90.4	64.0	.205E-03
15	58	.00150	.187	13278.	.0026	137.03	90.5	63.9	.122E-03
16	62	.00142	.199	14365.	.0025	139.50	90.6	63.9	.105E-03
17	66	.00194	.206	15138.	0.0000	141.73	90.7	63.8	.109E-03
18	70	.00200	.213	15871.	0.0000	144.06	90.5	63.8	.102E-03
19	74	.00204	.217	16419.	0.0000	146.26	90.6	63.8	.793E-04
20	78	.00204	.223	17043.	0.0000	147.82	90.6	63.7	.671E-04
21	82	.00202	.229	17716.	0.0000	149.25	90.5	63.7	.612E-04
22	86	.00202	.235	18321.	0.0000	150.59	90.6	63.7	.377E-04
23	90	.00206	.243	18985.	0.0000	151.32	90.5	63.6	.209E-04

STANTON NO. RUN - VARIABLE UNIF,F - STEPS IN F,TWALL
RUN = 051475 TDB = 77.00
TINFO = 65.00 TWB = 62.00

PL	X	ST	DEH2	REDEH2	F	UINF	TW	TINF	KR
1	2	.00515	.010	471.	0.0000	87.78	90.7	64.7	0.
2	6	.00364	.028	1278.	0.0000	87.76	90.6	64.7	-.566E-06
3	10	.00323	.042	1908.	0.0000	87.75	90.6	64.7	-.340E-05
4	14	.00300	.054	2477.	0.0000	87.68	90.6	64.7	-.109E-04
5	18	.00284	.066	3004.	0.0000	87.56	90.6	64.7	.653E-04
6	22	.00274	.075	3524.	0.0000	89.73	90.6	64.7	.249E-03
7	26	.00186	.087	4293.	.0037	94.58	90.8	64.6	.342E-03
8	30	.00159	.103	5375.	.0035	99.99	90.8	64.5	.343E-03
9	34	.00161	.118	6445.	.0033	105.46	90.8	64.4	.343E-03
10	38	.00154	.130	7535.	.0031	111.52	90.8	64.4	.350E-03
11	42	.00155	.141	8633.	.0030	117.86	90.8	64.3	.322E-03
12	46	.00153	.152	9735.	.0028	123.61	90.8	64.2	.264E-03
13	50	.00196	.124	8269.	.0027	128.60	100.3	64.1	.250E-03
14	54	.00173	.136	9449.	.0026	133.84	100.5	64.0	.205E-03
15	58	.00165	.150	10640.	.0026	137.03	100.5	63.9	.122E-03
16	62	.00154	.163	11759.	.0025	139.49	100.7	63.9	.105E-03
17	66	.00210	.172	12640.	0.0000	141.72	100.8	63.8	.109E-03
18	70	.00217	.179	13350.	0.0000	144.06	100.6	63.8	.102E-03
19	74	.00220	.184	13957.	0.0000	146.25	100.7	63.7	.793E-04
20	78	.00217	.191	14637.	0.0000	147.82	100.7	63.7	.671E-04
21	82	.00214	.198	15288.	0.0000	149.25	100.7	63.7	.612E-04
22	86	.00213	.205	15968.	0.0000	150.58	100.7	63.6	.377E-04
23	90	.00216	.213	16686.	0.0000	151.32	100.6	63.6	.209E-04

TMEAN PROFILE - KR=0.15E-3, F=0.0000 RUN

RUN	= 040175	ST	= .00247
PLATE	= 9	DEH	= .843
X	= 34	DEH2	= .103
UINF	= 88.28	DE	= .806
TW	= 92.32	DE2	= .113
TINF	= 65.16	KR	= .532E-05
F	= 0.0000		

PT	Y	Y/DEH2	Y/DE2	T	TBAR
1	.014	.136	.124	79.49	.473
2	.019	.184	.168	78.95	.492
3	.026	.252	.230	78.43	.511
4	.034	.330	.301	77.86	.532
5	.044	.427	.389	77.23	.556
6	.060	.583	.531	76.53	.581
7	.080	.777	.708	75.81	.608
8	.105	1.019	.929	75.08	.635
9	.130	1.262	1.150	74.44	.658
10	.155	1.505	1.372	73.89	.678
11	.190	1.845	1.681	73.16	.705
12	.225	2.184	1.991	72.55	.728
13	.275	2.670	2.434	71.69	.759
14	.325	3.155	2.876	70.93	.788
15	.375	3.641	3.319	70.22	.814
16	.425	4.126	3.761	69.57	.838
17	.500	4.854	4.425	68.61	.873
18	.575	5.583	5.088	67.72	.906
19	.650	6.311	5.752	66.91	.935
20	.750	7.282	6.637	65.99	.970
21	.850	8.252	7.522	65.41	.991
22	.950	9.223	8.407	65.16	1.000
23	1.050	10.194	9.292	65.16	1.000

TMEAN PROFILE - KR=0.15E-3, F=0.0000 RUN

RUN	= 040175	ST	= .00242
PLATE	= 15	DEH	= 1.147
X	= 58	DEH2	= .149
UINF	= 97.97	DE	= 1.061
TW	= 92.39	DE2	= .127
TINF	= 64.91	KR	= .147E-03
F	= 0.0000		

PT	Y	Y/DEH2	Y/DE2	T	TBAR
1	.013	.087	.102	80.46	.434
2	.016	.107	.126	80.10	.447
3	.020	.134	.157	79.77	.459
4	.025	.168	.197	79.43	.471
5	.035	.235	.276	78.59	.502
6	.045	.302	.354	78.04	.522
7	.060	.403	.472	77.31	.549
8	.080	.537	.630	76.55	.576
9	.105	.705	.827	75.88	.601
10	.130	.872	1.024	75.20	.625
11	.155	1.040	1.220	74.65	.645
12	.190	1.275	1.496	73.98	.670
13	.225	1.510	1.772	73.31	.694
14	.275	1.846	2.165	72.48	.725
15	.350	2.349	2.756	71.44	.763
16	.425	2.852	3.346	70.58	.794
17	.500	3.356	3.937	69.78	.823
18	.600	4.027	4.724	68.76	.860
19	.700	4.698	5.512	67.92	.890
20	.800	5.369	6.299	67.09	.921
21	.900	6.040	7.087	66.38	.946
22	1.000	6.711	7.874	65.77	.969
23	1.150	7.718	9.055	65.19	.990
24	1.300	8.725	10.236	64.97	.998
25	1.450	9.732	11.417	64.91	1.000
26	1.600	10.738	12.598	64.91	1.000
27	1.750	11.745	13.780	64.91	1.000

TMEAN PROFILE - KR=0.15E-3, F=0.0000 RUN

RUN	= 040175	ST	= .00242
PLATE	= 17	DEH	= 1.217
X	= 66	DEH2	= .159
UINF	= 102.70	DE	= 1.119
TW	= 92.32	DE2	= .131
TINF	= 65.01	KR	= .153E-03
F	= 0.0000		

PT	Y	Y/DEH2	Y/DE2	T	TBAR
1	.013	.082	.099	80.79	.422
2	.016	.101	.122	80.42	.436
3	.020	.126	.153	79.91	.454
4	.025	.157	.191	79.54	.468
5	.035	.220	.267	78.96	.489
6	.045	.283	.344	78.26	.515
7	.060	.377	.458	77.71	.535
8	.080	.503	.611	76.92	.564
9	.105	.660	.802	76.09	.594
10	.130	.818	.992	75.53	.615
11	.155	.975	1.183	74.93	.637
12	.190	1.195	1.450	74.22	.663
13	.225	1.415	1.718	73.66	.683
14	.275	1.730	2.099	72.83	.713
15	.350	2.201	2.672	71.82	.751
16	.425	2.673	3.244	70.90	.784
17	.500	3.145	3.817	70.15	.812
18	.600	3.774	4.580	69.11	.850
19	.700	4.403	5.344	68.24	.881
20	.800	5.031	6.107	67.44	.911
21	.900	5.660	6.870	66.79	.935
22	1.000	6.289	7.634	66.11	.960
23	1.150	7.233	8.779	65.47	.983
24	1.300	8.176	9.924	65.13	.995
25	1.450	9.119	11.069	65.01	1.000
26	1.600	10.063	12.214	65.01	1.000
27	1.750	11.006	13.359	65.01	1.000

TMEAN PROFILE - KR=0.15E-3, F=0.0000 RUN

RUN	= 040175	ST	= .00242
PLATE	= 19	DEH	= 1.280
X	= 74	DEH2	= .170
UINF	= 107.55	DE	= 1.144
TW	= 92.66	DE2	= .130
TINF	= 64.98	KR	= .141E-03
F	= 0.0000		

PT	Y	Y/DEH2	Y/DE2	T	TBAR
1	.013	.076	.100	81.04	.420
2	.016	.094	.123	80.65	.434
3	.020	.118	.154	80.37	.444
4	.025	.147	.192	80.00	.457
5	.035	.206	.269	79.27	.484
6	.045	.265	.346	78.72	.504
7	.060	.353	.462	78.02	.529
8	.080	.471	.615	77.31	.555
9	.105	.618	.808	76.51	.583
10	.130	.765	1.000	75.92	.605
11	.155	.912	1.192	75.31	.627
12	.190	1.118	1.462	74.60	.653
13	.225	1.324	1.731	73.98	.675
14	.275	1.618	2.115	73.15	.705
15	.350	2.059	2.692	72.17	.740
16	.425	2.500	3.269	71.27	.773
17	.500	2.941	3.846	70.44	.803
18	.600	3.529	4.615	69.42	.840
19	.700	4.118	5.385	68.55	.871
20	.800	4.706	6.154	67.75	.900
21	.900	5.294	6.923	67.01	.927
22	1.000	5.882	7.692	66.39	.949
23	1.150	6.765	8.846	65.65	.976
24	1.300	7.647	10.000	65.22	.991
25	1.450	8.529	11.154	65.07	.997
26	1.600	9.412	12.308	64.98	1.000
27	1.750	10.294	13.462	64.98	1.000

TMEAN PROFILE - KR=0.15E-3, F=0.0000 RUN

RUN	= 040175	ST	= .00232
PLATE	= 22	DEH	= 1.349
X	= 86	DEH2	= .186
UINF	= 115.43	DE	= 1.192
TW	= 92.76	DE2	= .131
TINF	= 64.91	KR	= .139E-03
F	= 0.0000		

PT	Y	Y/DEH2	Y/DE2	T	TBAR
1	.013	.070	.099	81.40	.488
2	.016	.086	.122	81.04	.421
3	.020	.108	.153	80.79	.430
4	.025	.134	.191	80.36	.445
5	.035	.188	.267	79.60	.473
6	.045	.242	.344	79.10	.491
7	.060	.323	.458	78.36	.517
8	.080	.430	.611	77.65	.543
9	.105	.565	.802	76.91	.569
10	.130	.699	.992	76.26	.593
11	.155	.833	1.183	75.73	.612
12	.190	1.022	1.450	75.02	.637
13	.225	1.210	1.718	74.40	.659
14	.275	1.478	2.099	73.65	.686
15	.350	1.882	2.672	72.57	.725
16	.425	2.285	3.244	71.64	.758
17	.500	2.688	3.817	70.84	.787
18	.600	3.226	4.580	69.85	.823
19	.700	3.763	5.344	68.95	.855
20	.800	4.301	6.107	68.05	.887
21	.900	4.839	6.870	67.31	.914
22	1.000	5.376	7.634	66.63	.938
23	1.150	6.183	8.779	65.80	.968
24	1.300	6.989	9.924	65.31	.986
25	1.450	7.796	11.069	65.03	.996
26	1.600	8.602	12.214	64.91	1.000
27	1.750	9.409	13.359	64.91	1.000

TMEAN PROFILE - KR=0.29E-3, F=0.0000 RUN

RUN	= 022575	ST	= .00287
PLATE	= 5	DEH	= .531
X	= 18	DEH2	= .065
UINF	= 87.36	DE	= .496
TW	= 93.08	DE2	= .072
TINF	= 64.99	KR	= .722E-04
F	= 0.0000		

PT	Y	Y/DEH2	Y/DE2	T	TBAR
1	.013	.200	.181	79.30	.490
2	.016	.246	.222	78.88	.505
3	.020	.308	.278	78.40	.522
4	.025	.385	.347	77.92	.540
5	.031	.477	.431	77.47	.556
6	.038	.585	.528	77.05	.571
7	.045	.692	.625	76.59	.587
8	.054	.831	.750	76.08	.605
9	.064	.985	.889	75.66	.620
10	.076	1.169	1.056	75.11	.640
11	.090	1.385	1.250	74.56	.659
12	.110	1.692	1.528	73.90	.683
13	.130	2.000	1.806	73.20	.708
14	.150	2.308	2.083	72.59	.730
15	.175	2.692	2.431	71.88	.755
16	.200	3.077	2.778	71.21	.779
17	.225	3.462	3.125	70.57	.802
18	.250	3.846	3.472	70.01	.821
19	.275	4.231	3.819	69.43	.842
20	.300	4.615	4.167	68.93	.860
21	.325	5.000	4.514	68.41	.878
22	.350	5.385	4.861	67.88	.897
23	.380	5.846	5.278	67.36	.916
24	.410	6.308	5.694	66.80	.936
25	.450	6.923	6.250	66.13	.960
26	.500	7.692	6.944	65.51	.982
27	.550	8.462	7.639	65.18	.994
28	.600	9.231	8.333	64.99	1.000
29	.650	10.000	9.028	64.99	1.000

TMEAN PROFILE - KR=0.29E-3, F=0.0000 RUN

RUN	= 022575	ST	= .00271
PLATE	= 9	DEH	= .689
X	= 34	DEH2	= .091
UINF	= 102.31	DE	= .642
TW	= 92.94	DE2	= .078
TINF	= 64.74	KR	= .279E-03
F	= 0.0000		

PT	Y	Y/DEH2	Y/DE2	T	TBAR
1	.013	.143	.167	79.85	.464
2	.016	.176	.205	79.58	.474
3	.019	.209	.244	79.27	.485
4	.023	.253	.295	78.88	.499
5	.027	.297	.346	78.60	.509
6	.031	.341	.397	78.33	.518
7	.037	.407	.474	77.87	.534
8	.045	.495	.577	77.38	.552
9	.055	.604	.705	76.86	.570
10	.065	.714	.833	76.34	.589
11	.075	.824	.962	75.97	.602
12	.085	.934	1.090	75.58	.616
13	.100	1.099	1.282	74.96	.637
14	.115	1.264	1.474	74.48	.655
15	.130	1.429	1.667	74.01	.671
16	.150	1.648	1.923	73.46	.691
17	.175	1.923	2.244	72.75	.716
18	.200	2.198	2.564	72.14	.738
19	.225	2.473	2.885	71.52	.760
20	.250	2.747	3.205	71.00	.778
21	.275	3.022	3.526	70.48	.797
22	.310	3.407	3.974	69.80	.821
23	.350	3.846	4.487	69.09	.846
24	.400	4.396	5.128	68.25	.876
25	.450	4.945	5.769	67.51	.902
26	.500	5.495	6.410	66.77	.928
27	.550	6.044	7.051	66.15	.950
28	.600	6.593	7.692	65.63	.968
29	.650	7.143	8.333	65.26	.982
30	.750	8.242	9.615	64.75	1.000
31	.850	9.341	10.897	64.75	1.000
32	.950	10.440	12.179	64.74	1.000

TMEAN PROFILE - KR=0.29E-3, F=0.0000 RUN

RUN	= 022575	ST	= .00265
PLATE	= 11	DEH	= .702
X	= 42	DEH2	= .098
UINF	= 111.98	DE	= .658
TW	= 93.04	DE2	= .077
TINF	= 64.60	KR	= .280E-03
F	= 0.0000		

PT	Y	Y/DEH2	Y/DE2	T	TBAR
1	.013	.133	.169	80.13	.454
2	.016	.163	.208	79.67	.470
3	.019	.194	.247	79.42	.479
4	.023	.235	.299	79.08	.491
5	.027	.276	.351	78.75	.503
6	.031	.316	.403	78.50	.511
7	.037	.378	.481	78.13	.524
8	.045	.459	.584	77.67	.541
9	.055	.561	.714	77.17	.558
10	.065	.663	.844	76.62	.577
11	.075	.765	.974	76.25	.590
12	.085	.867	1.104	75.85	.605
13	.100	1.020	1.299	75.35	.622
14	.115	1.173	1.494	74.80	.641
15	.130	1.327	1.688	74.33	.658
16	.150	1.531	1.948	73.78	.677
17	.175	1.786	2.273	73.06	.702
18	.200	2.041	2.597	72.45	.724
19	.225	2.296	2.922	71.92	.743
20	.250	2.551	3.247	71.33	.763
21	.275	2.806	3.571	70.81	.782
22	.310	3.163	4.026	70.15	.805
23	.350	3.571	4.545	69.38	.832
24	.400	4.082	5.195	68.51	.862
25	.450	4.592	5.844	67.71	.891
26	.500	5.102	6.494	66.97	.917
27	.550	5.612	7.143	66.32	.939
28	.600	6.122	7.792	65.73	.960
29	.650	6.633	8.442	65.27	.976
30	.750	7.653	9.740	64.60	1.000
31	.850	8.673	11.039	64.60	1.000
32	.950	9.694	12.338	64.60	1.000

TMEAN PROFILE - KR=0.29E-3, F=0.0000 RUN

RUN	= 022575	ST	= .00261
PLATE	= 12	DEH	= .740
X	= 46	DEH2	= .104
UINF	= 117.33	DE	= .668
TW	= 92.97	DE2	= .077
TINF	= 64.56	KR	= .289E-03
F	= 0.0000		

PT	Y	Y/DEH2	Y/DE2	T	TBAR
1	.013	.125	.169	80.05	.455
2	.016	.154	.208	79.68	.468
3	.019	.183	.247	79.49	.474
4	.023	.221	.299	79.15	.486
5	.027	.260	.351	78.98	.495
6	.031	.298	.403	78.71	.502
7	.037	.356	.481	78.28	.517
8	.045	.433	.584	77.76	.535
9	.055	.529	.714	77.32	.551
10	.065	.625	.844	76.86	.567
11	.075	.721	.974	76.39	.583
12	.085	.817	1.104	76.05	.596
13	.100	.962	1.299	75.53	.614
14	.115	1.106	1.494	75.03	.632
15	.130	1.250	1.688	74.62	.646
16	.150	1.442	1.948	74.03	.667
17	.175	1.683	2.273	73.32	.692
18	.200	1.923	2.597	72.73	.712
19	.225	2.163	2.922	72.14	.733
20	.250	2.404	3.247	71.58	.753
21	.275	2.644	3.571	71.05	.771
22	.310	2.981	4.026	70.34	.797
23	.350	3.365	4.545	69.59	.823
24	.400	3.846	5.195	68.69	.854
25	.450	4.327	5.844	67.92	.882
26	.500	4.808	6.494	67.12	.910
27	.550	5.288	7.143	66.47	.933
28	.600	5.769	7.792	65.91	.952
29	.650	6.250	8.442	65.42	.970
30	.750	7.212	9.740	64.80	.991
31	.850	8.173	11.039	64.56	1.000
32	.950	9.135	12.338	64.56	1.000

TMEAN PROFILE - KR=0.29E-3, F=0.0000 RUN

RUN	= 022575	ST	= .00221
PLATE	= 19	DEH	= 1.091
X	= 74	DEH2	= .162
UINF	= 129.54	DE	= .989
TW	= 93.04	DE2	= .133
TINF	= 64.09	KR	= .107E-04
F	= 0.0000		

PT	Y	Y/DEH2	Y/DE2	T	TBAR
1	.014	.086	.105	81.02	.415
2	.017	.105	.128	80.78	.424
3	.020	.123	.150	80.50	.433
4	.025	.154	.188	80.25	.442
5	.035	.216	.263	79.54	.466
6	.045	.278	.338	79.04	.483
7	.060	.370	.451	78.37	.507
8	.080	.494	.602	77.77	.528
9	.100	.617	.752	77.15	.549
10	.130	.802	.977	76.40	.575
11	.170	1.049	1.278	75.52	.605
12	.220	1.358	1.654	74.65	.635
13	.270	1.667	2.030	73.80	.665
14	.320	1.975	2.406	73.05	.691
15	.395	2.438	2.970	71.97	.728
16	.470	2.901	3.534	70.88	.766
17	.570	3.519	4.286	69.55	.811
18	.670	4.136	5.038	68.23	.857
19	.795	4.907	5.977	66.67	.911
20	.920	5.679	6.917	65.36	.956
21	1.070	6.605	8.045	64.46	.987
22	1.220	7.531	9.173	64.15	.998
23	1.370	8.457	10.301	64.09	1.000
24	1.520	9.383	11.429	64.09	1.000

TMEAN PROFILE - KR=0.29E-3, F=0.0039 RUN

RUN	= 030875	ST	= .00145
PLATE	= 5	DEH	= .768
X	= 18	DEH2	= .108
UINF	= 87.00	DE	= .747
TW	= 97.67	DE2	= .117
TINF	= 65.93	KR	= .552E-04
F	= .0039		

PT	Y	Y/DEH2	Y/DE2	T	TBAR
1	.013	.120	.111	86.81	.342
2	.016	.148	.137	86.37	.356
3	.020	.185	.171	85.90	.371
4	.025	.231	.214	85.39	.387
5	.032	.296	.274	84.83	.404
6	.040	.370	.342	84.21	.424
7	.050	.463	.427	83.55	.445
8	.065	.602	.556	82.69	.472
9	.085	.787	.726	81.74	.502
10	.105	.972	.897	80.93	.527
11	.130	1.204	1.111	79.91	.559
12	.155	1.435	1.325	79.10	.585
13	.185	1.713	1.581	78.11	.616
14	.225	2.083	1.923	77.03	.650
15	.275	2.546	2.350	75.67	.693
16	.325	3.009	2.778	74.36	.734
17	.375	3.472	3.205	73.17	.772
18	.425	3.935	3.632	72.04	.807
19	.475	4.398	4.060	70.94	.842
20	.525	4.861	4.487	69.87	.876
21	.575	5.324	4.915	68.83	.909
22	.625	5.787	5.342	67.94	.937
23	.675	6.250	5.769	67.17	.961
24	.725	6.713	6.197	66.56	.980
25	.775	7.176	6.624	66.20	.991
26	.825	7.639	7.051	66.02	.997
27	.875	8.102	7.479	65.96	.999
28	.925	8.565	7.906	65.93	1.000
29	.975	9.028	8.333	65.93	1.000

TMEAN PROFILE - KR=0.29E-3, F=0.0039 RUN

RUN	= 030875	ST	= .00129
PLATE	= 9	DEH	= 1.047
X	= 34	DEH2	= .164
UINF	= 102.31	DE	= .962
TW	= 97.87	DE2	= .130
TINF	= 65.85	KR	= .284E-03
F	= .0039		

PT	Y	Y/DEH2	Y/DE2	T	TBAR
1	.013	.079	.100	87.58	.322
2	.016	.098	.123	87.19	.334
3	.019	.116	.146	86.89	.343
4	.023	.140	.177	86.59	.352
5	.027	.165	.208	86.35	.360
6	.032	.195	.246	85.81	.377
7	.039	.238	.300	85.15	.397
8	.046	.280	.354	84.88	.406
9	.055	.335	.423	84.28	.425
10	.065	.396	.500	83.71	.442
11	.075	.457	.577	83.29	.456
12	.087	.530	.669	82.66	.475
13	.100	.610	.769	82.08	.493
14	.115	.701	.885	81.57	.509
15	.130	.793	1.000	81.08	.524
16	.150	.915	1.154	80.36	.547
17	.170	1.037	1.308	79.76	.566
18	.195	1.189	1.500	79.12	.586
19	.220	1.341	1.692	78.45	.606
20	.255	1.555	1.962	77.63	.632
21	.295	1.799	2.269	76.73	.660
22	.340	2.073	2.615	75.78	.690
23	.390	2.378	3.000	74.72	.723
24	.440	2.683	3.385	73.80	.752
25	.490	2.988	3.769	72.89	.780
26	.550	3.354	4.231	71.91	.811
27	.625	3.811	4.808	70.71	.848
28	.700	4.268	5.385	69.61	.883
29	.800	4.878	6.154	68.26	.925
30	.900	5.488	6.923	67.13	.960
31	1.000	6.098	7.692	66.40	.983
32	1.100	6.707	8.462	66.03	.994
33	1.250	7.622	9.615	65.85	1.000
34	1.400	8.537	10.769	65.85	1.000
35	1.500	9.146	11.538	65.85	1.000

TMEAN PROFILE - KR=0.29E-3, F=0.0039 RUN

RUN	= 030875	ST	= .00132
PLATE	= 11	DEH	= 1.141
X	= 42	DEH2	= .188
UINF	= 111.95	DE	= 1.019
TW	= 97.70	DE2	= .131
TINF	= 65.56	KR	= .300E-03
F	= .0039		

PT	Y	Y/DEH2	Y/DE2	T	TBAR
1	.013	.069	.099	88.06	.300
2	.016	.085	.122	87.70	.311
3	.019	.101	.145	87.34	.322
4	.023	.122	.176	87.04	.332
5	.027	.144	.206	86.70	.342
6	.032	.170	.244	86.31	.354
7	.039	.207	.298	85.83	.369
8	.046	.245	.351	85.38	.383
9	.055	.293	.420	84.80	.401
10	.065	.346	.496	84.32	.416
11	.075	.399	.573	83.89	.430
12	.087	.463	.664	83.32	.447
13	.100	.532	.763	82.77	.464
14	.115	.612	.878	82.20	.482
15	.130	.691	.992	81.68	.498
16	.150	.798	1.145	81.01	.519
17	.170	.904	1.298	80.46	.536
18	.195	1.037	1.489	79.70	.560
19	.220	1.170	1.679	79.07	.580
20	.255	1.356	1.947	78.24	.605
21	.295	1.569	2.252	77.30	.635
22	.340	1.809	2.595	76.29	.666
23	.390	2.074	2.977	75.32	.696
24	.440	2.340	3.359	74.37	.726
25	.490	2.606	3.740	73.45	.754
26	.550	2.926	4.198	72.50	.784
27	.625	3.324	4.771	71.22	.824
28	.700	3.723	5.344	70.14	.857
29	.800	4.255	6.107	68.76	.900
30	.900	4.787	6.870	67.54	.938
31	1.000	5.319	7.634	66.62	.967
32	1.100	5.851	8.397	66.04	.985
33	1.250	6.649	9.542	65.65	.997
34	1.400	7.447	10.687	65.56	1.000
35	1.500	7.979	11.450	65.56	1.000

TMEAN PROFILE - KR=0.29E-3, F=0.0039 RUN

RUN	= 030875	ST	= .00125
PLATE	= 12	DEH	= 1.167
X	= 46	DEH2	= .197
UINF	= 117.67	DE	= 1.048
TW	= 97.98	DE2	= .131
TINF	= 65.75	KR	= .295E-03
F	= .0039		

PT	Y	Y/DEH2	Y/DE2	T	TBAR
1	.013	.066	.099	88.85	.308
2	.016	.081	.122	87.74	.318
3	.019	.096	.145	87.47	.326
4	.023	.117	.176	87.08	.338
5	.027	.137	.206	86.81	.347
6	.032	.162	.244	86.44	.358
7	.039	.198	.298	85.99	.372
8	.046	.234	.351	85.54	.386
9	.055	.279	.420	85.20	.397
10	.065	.330	.496	84.59	.415
11	.075	.381	.573	84.11	.430
12	.087	.442	.664	83.62	.446
13	.100	.508	.763	83.24	.457
14	.115	.584	.878	82.61	.477
15	.130	.660	.992	82.12	.492
16	.150	.761	1.145	81.51	.511
17	.170	.863	1.298	80.93	.529
18	.195	.990	1.489	80.23	.551
19	.220	1.117	1.679	79.64	.569
20	.255	1.294	1.947	78.79	.595
21	.295	1.497	2.252	77.81	.626
22	.340	1.726	2.595	76.93	.653
23	.390	1.980	2.977	75.94	.684
24	.440	2.234	3.359	74.91	.716
25	.490	2.487	3.740	74.02	.743
26	.550	2.792	4.198	72.98	.776
27	.625	3.173	4.771	71.72	.815
28	.700	3.553	5.344	70.59	.850
29	.800	4.061	6.107	69.24	.892
30	.900	4.569	6.870	68.01	.930
31	1.000	5.076	7.634	67.03	.960
32	1.100	5.584	8.397	66.36	.981
33	1.250	6.345	9.542	65.90	.995
34	1.400	7.107	10.687	65.75	1.000
35	1.500	7.614	11.450	65.75	1.000

TMEAN PROFILE - KR=0.29E-3, F=0.0039 RUN

RUN	= 030875	ST	= .00098
PLATE	= 19	DEH	= 1.761
X	= 74	DEH2	= .316
UINF	= 130.12	DE	= 1.576
TW	= 97.98	DE2	= .230
TINF	= 65.40	KR	= -.863E-05
F	= .0039		

PT	Y	Y/DEH2	Y/DE2	T	TBAR
1	.013	.041	.057	89.22	.269
2	.017	.054	.074	88.83	.281
3	.023	.073	.100	88.46	.292
4	.031	.098	.135	87.87	.310
5	.041	.130	.178	87.29	.328
6	.055	.174	.239	86.60	.349
7	.072	.228	.313	85.99	.368
8	.090	.285	.391	85.35	.388
9	.110	.348	.478	84.74	.406
10	.130	.411	.565	84.28	.420
11	.155	.491	.674	83.73	.437
12	.190	.601	.826	83.03	.459
13	.240	.759	1.043	82.23	.483
14	.290	.918	1.261	81.43	.508
15	.365	1.155	1.587	80.45	.538
16	.465	1.472	2.022	79.12	.579
17	.565	1.788	2.457	77.85	.618
18	.665	2.104	2.891	76.70	.653
19	.780	2.468	3.391	75.21	.699
20	.900	2.848	3.913	73.78	.743
21	1.050	3.323	4.565	71.93	.800
22	1.200	3.797	5.217	70.13	.855
23	1.400	4.430	6.087	67.94	.922
24	1.600	5.063	6.957	66.40	.969
25	1.800	5.696	7.826	65.64	.993
26	1.975	6.250	8.587	65.40	1.000
27	2.000	6.329	8.696	65.40	1.000

TMEAN PROFILE - K=0.28E-6, F=0.0000 RUN

RUN	= 050275	ST	= .00301
PLATE	= 4	DEH	= .448
X	= 14	DEH2	= .052
UINF	= 87.38	DE	= .423
TW	= 94.21	DE2	= .062
TINF	= 65.80	K	= -.154E-07
F	= 0.0000		

PT	Y	Y/DEH2	Y/DE2	T	TBAR
1	.015	.288	.242	79.27	.526
2	.020	.385	.323	78.67	.547
3	.027	.519	.435	78.12	.566
4	.035	.673	.565	77.46	.590
5	.045	.865	.726	76.80	.613
6	.057	1.096	.919	76.16	.635
7	.070	1.346	1.129	75.46	.660
8	.085	1.635	1.371	74.83	.682
9	.105	2.019	1.694	74.07	.709
10	.130	2.500	2.097	73.15	.741
11	.155	2.981	2.500	72.36	.769
12	.180	3.462	2.903	71.59	.796
13	.210	4.038	3.387	70.76	.825
14	.250	4.808	4.032	69.72	.862
15	.300	5.769	4.839	68.54	.904
16	.350	6.731	5.645	67.49	.941
17	.400	7.692	6.452	66.63	.971
18	.450	8.654	7.258	66.07	.990
19	.500	9.615	8.065	65.86	.998
20	.550	10.577	8.871	65.80	1.000
21	.600	11.538	9.677	65.80	1.000

TMEAN PROFILE - K=0.28E-6, F=0.0000 RUN

RUN	= 050275	ST	= .00288
PLATE	= 7	DEH	= .631
X	= 26	DEH2	= .081
UINF	= 93.93	DE	= .583
TW	= 94.28	DE2	= .076
TINF	= 65.59	K	= .272E-06
F	= 0.0000		

PT	Y	Y/DEH2	Y/DE2	T	TBAR
1	.013	.160	.171	80.76	.470
2	.017	.210	.224	80.18	.490
3	.022	.272	.289	79.64	.509
4	.029	.358	.382	79.03	.530
5	.038	.469	.500	78.25	.557
6	.048	.593	.632	77.64	.578
7	.060	.741	.789	77.01	.600
8	.075	.926	.987	76.34	.623
9	.100	1.235	1.316	75.31	.659
10	.130	1.605	1.711	74.42	.690
11	.160	1.975	2.105	73.54	.721
12	.200	2.469	2.632	72.53	.756
13	.250	3.086	3.289	71.37	.796
14	.300	3.704	3.947	70.35	.831
15	.350	4.321	4.605	69.43	.863
16	.425	5.247	5.592	68.16	.907
17	.500	6.173	6.579	67.03	.947
18	.575	7.099	7.566	66.17	.977
19	.650	8.025	8.553	65.71	.993
20	.725	8.951	9.539	65.50	1.000
21	.800	9.877	10.526	65.50	1.000

TMEAN PROFILE - K=0.28E-6, F=0.0000 RUN

RUN	= 050275	ST	= .00277
PLATE	= 9	DEH	= .673
X	= 34	DEH2	= .089
UINF	= 104.95	DE	= .626
TW	= 94.15	DE2	= .073
TINF	= 65.31	K	= .272E-06
F	= 0.0000		

PT	Y	Y/DEH2	Y/DE2	T	TBAR
1	.013	.146	.178	80.88	.460
2	.017	.191	.233	80.30	.480
3	.022	.247	.301	79.78	.498
4	.028	.315	.384	79.23	.517
5	.035	.393	.479	78.71	.535
6	.045	.506	.616	78.01	.560
7	.060	.674	.822	77.27	.585
8	.080	.899	1.096	76.35	.617
9	.105	1.180	1.438	75.46	.648
10	.130	1.461	1.781	74.57	.679
11	.155	1.742	2.123	73.81	.705
12	.190	2.135	2.603	72.79	.741
13	.225	2.528	3.082	71.96	.769
14	.275	3.090	3.767	70.89	.807
15	.325	3.652	4.452	69.93	.840
16	.375	4.213	5.137	69.03	.871
17	.450	5.056	6.164	67.86	.912
18	.525	5.899	7.192	66.82	.948
19	.600	6.742	8.219	66.05	.974
20	.675	7.584	9.247	65.59	.990
21	.750	8.427	10.274	65.37	.998
22	.825	9.270	11.301	65.31	1.000
23	.900	10.112	12.329	65.31	1.000
24	.975	10.955	13.356	65.31	1.000

TMEAN PROFILE - K=0.28E-6, F=0.0000 RUN

RUN	= 050275	ST	= .00274
PLATE	= 11	DEH	= .697
X	= 42	DEH2	= .895
UINF	= 119.12	DE	= .610
TW	= 94.15	DE2	= .069
TINF	= 64.98	K	= .294E-06
F	= 0.0000		

PT	Y	Y/DEH2	Y/DE2	T	TBAR
1	.013	.137	.188	80.83	.456
2	.017	.179	.246	80.37	.472
3	.022	.232	.319	79.79	.492
4	.028	.295	.406	79.26	.510
5	.035	.368	.507	78.82	.525
6	.045	.474	.652	78.17	.548
7	.060	.632	.870	77.43	.573
8	.080	.842	1.159	76.47	.606
9	.105	1.105	1.522	75.54	.638
10	.130	1.368	1.884	74.73	.666
11	.155	1.632	2.246	73.89	.695
12	.190	2.000	2.754	72.96	.726
13	.225	2.368	3.261	72.06	.757
14	.275	2.895	3.986	70.97	.795
15	.325	3.421	4.710	69.95	.830
16	.375	3.947	5.435	68.99	.863
17	.450	4.737	6.522	67.72	.906
18	.525	5.526	7.609	66.70	.941
19	.600	6.316	8.696	65.87	.970
20	.675	7.105	9.783	65.38	.986
21	.750	7.895	10.870	65.11	.996
22	.825	8.684	11.957	65.01	.999
23	.900	9.474	13.043	64.98	1.000
24	.975	10.263	14.130	64.98	1.000

TMEAN PROFILE - K=0.28E-6, F=0.0000 RUN

RUN	= 050275	ST	= .00270
PLATE	= 12	DEH	= .685
X	= 46	DEH2	= .898
UINF	= 128.60	DE	= .603
TW	= 94.18	DE2	= .065
TINF	= 64.79	K	= .294E-06
F	= 0.0000		

PT	Y	Y/DEH2	Y/DE2	T	TBAR
1	.013	.133	.200	80.94	.451
2	.017	.173	.262	80.53	.465
3	.022	.224	.338	80.00	.483
4	.028	.286	.431	79.56	.498
5	.035	.357	.538	79.03	.516
6	.045	.459	.692	78.28	.541
7	.060	.612	.923	77.53	.567
8	.080	.816	1.231	76.62	.598
9	.105	1.071	1.615	75.65	.631
10	.130	1.327	2.000	74.74	.661
11	.155	1.582	2.385	74.00	.687
12	.190	1.939	2.923	72.91	.724
13	.225	2.296	3.462	72.01	.755
14	.275	2.806	4.231	70.80	.796
15	.325	3.316	5.000	69.77	.831
16	.375	3.827	5.769	68.80	.864
17	.450	4.592	6.923	67.47	.909
18	.525	5.357	8.077	66.42	.945
19	.600	6.122	9.231	65.59	.973
20	.675	6.888	10.385	65.13	.988
21	.750	7.653	11.538	64.92	.996
22	.825	8.418	12.692	64.82	.999
23	.900	9.184	13.846	64.79	1.000
24	.975	9.949	15.000	64.79	1.000

UMEAN PROFILE - KR=0,F=0 RUN

RUN	=	010875	DE1	=	.079
PLATE	=	3	DE2	=	.049
X	=	10	H	=	1.61
UINF	=	86.70	G	=	6.79
CF/2	=	.00308	BETA	=	0.00
UTAU	=	4.81	REDE2	=	2199.
F	=	0.0000	REK	=	77.
DE	=	.342	KR	=	0.

PT	Y	Y/DE2	Y/DE	U	U/UINF
1	.006	.122	.018	28.86	.333
2	.007	.143	.020	29.24	.337
3	.009	.184	.026	31.60	.364
4	.012	.245	.035	34.12	.394
5	.016	.327	.047	36.94	.426
6	.020	.408	.058	39.11	.451
7	.025	.510	.073	41.38	.477
8	.030	.612	.088	43.33	.500
9	.037	.755	.108	45.56	.525
10	.045	.918	.132	47.73	.551
11	.055	1.122	.161	50.18	.579
12	.067	1.367	.196	52.87	.610
13	.080	1.633	.234	55.38	.639
14	.095	1.939	.278	58.11	.670
15	.110	2.245	.322	60.60	.699
16	.130	2.653	.380	64.06	.739
17	.150	3.061	.439	66.93	.772
18	.170	3.469	.497	69.78	.805
19	.190	3.878	.556	72.52	.836
20	.210	4.286	.614	74.98	.865
21	.235	4.796	.687	78.00	.900
22	.260	5.306	.760	80.56	.929
23	.285	5.816	.833	82.76	.955
24	.310	6.327	.906	84.53	.975
25	.340	6.939	.994	85.81	.990
26	.380	7.755	1.111	86.56	.998
27	.430	8.776	1.257	86.70	1.000
28	.480	9.796	1.404	86.70	1.000

UMEAN PROFILE - KR=0,F=0 RUN

RUN	=	010875	DE1	=	.113
PLATE	=	5	DE2	=	.072
X	=	18	H	=	1.57
UINF	=	86.90	G	=	6.67
CF/2	=	.00294	BETA	=	0.00
UTAU	=	4.71	REDE2	=	3230.
F	=	0.0000	REK	=	75.
DE	=	.497	KR	=	0.

PT	Y	Y/DE2	Y/DE	U	U/UINF
1	.006	.083	.012	28.97	.333
2	.007	.097	.014	29.68	.342
3	.009	.125	.018	31.41	.361
4	.012	.167	.024	33.41	.384
5	.016	.222	.032	35.64	.410
6	.021	.292	.042	37.87	.436
7	.028	.389	.056	40.55	.467
8	.035	.486	.070	42.49	.489
9	.045	.625	.091	45.03	.518
10	.057	.792	.115	47.31	.544
11	.070	.972	.141	49.57	.570
12	.085	1.181	.171	51.90	.597
13	.100	1.389	.201	54.10	.623
14	.115	1.597	.231	55.96	.644
15	.130	1.806	.262	58.00	.667
16	.150	2.083	.302	60.29	.694
17	.175	2.431	.352	63.02	.725
18	.200	2.778	.402	65.41	.753
19	.230	3.194	.463	68.46	.788
20	.260	3.611	.523	71.22	.820
21	.290	4.028	.584	73.80	.849
22	.325	4.514	.654	76.56	.881
23	.360	5.000	.724	79.26	.912
24	.400	5.556	.805	81.88	.942
25	.450	6.250	.905	84.39	.971
26	.500	6.944	1.006	86.01	.990
27	.550	7.639	1.107	86.65	.997
28	.600	8.333	1.207	86.90	1.000
29	.650	9.028	1.308	86.90	1.000

UMEAN PROFILE - KR=0,F=0 RUN

RUN	=	010875	DE1	=	.144
PLATE	=	7	DE2	=	.093
X	=	26	H	=	1.55
UINF	=	86.87	G	=	6.87
CF/2	=	.00269	BETA	=	0.00
UTAU	=	4.51	REDE2	=	4136.
F	=	0.0000	REK	=	72.
DE	=	.646	KR	=	0.

PT	Y	Y/DE2	Y/DE	U	U/UINF
1	.006	.065	.009	25.46	.293
2	.007	.075	.011	26.28	.303
3	.009	.097	.014	28.81	.332
4	.012	.129	.019	31.21	.359
5	.016	.172	.025	33.77	.389
6	.021	.226	.033	36.11	.416
7	.028	.301	.043	38.59	.444
8	.036	.387	.056	40.91	.471
9	.045	.484	.070	43.14	.497
10	.055	.591	.085	44.91	.517
11	.067	.720	.104	47.12	.542
12	.080	.860	.124	49.05	.565
13	.095	1.022	.147	50.89	.586
14	.110	1.183	.170	52.67	.606
15	.130	1.398	.201	54.79	.631
16	.150	1.613	.232	56.73	.653
17	.175	1.882	.271	59.12	.681
18	.200	2.151	.310	61.22	.705
19	.230	2.473	.356	63.80	.734
20	.265	2.849	.410	66.40	.764
21	.305	3.280	.472	69.42	.799
22	.350	3.763	.542	72.47	.834
23	.400	4.301	.619	75.54	.870
24	.450	4.839	.697	78.50	.904
25	.500	5.376	.774	80.93	.932
26	.550	5.914	.851	83.30	.959
27	.625	6.720	.967	85.58	.985
28	.700	7.527	1.084	86.57	.997
29	.775	8.333	1.200	86.87	1.000
30	.850	9.140	1.316	86.87	1.000

UMEAN PROFILE - KR=0,F=0 RUN

RUN	=	010875	DE1	=	.207
PLATE	=	12	DE2	=	.139
X	=	46	H	=	1.50
UINF	=	86.62	G	=	6.72
CF/2	=	.00244	BETA	=	0.00
UTAU	=	4.28	REDE2	=	6173.
F	=	0.0000	REK	=	68.
DE	=	1.015	KR	=	0.

PT	Y	Y/DE2	Y/DE	U	U/UINF
1	.006	.043	.006	25.23	.291
2	.007	.050	.007	26.11	.301
3	.009	.065	.009	28.24	.326
4	.012	.086	.012	30.36	.350
5	.016	.115	.016	32.58	.376
6	.021	.151	.021	34.99	.404
7	.028	.201	.028	37.50	.433
8	.036	.259	.035	39.61	.457
9	.045	.324	.044	41.56	.480
10	.055	.396	.054	43.44	.502
11	.067	.482	.066	45.36	.524
12	.080	.576	.079	46.91	.542
13	.095	.683	.094	48.47	.560
14	.112	.806	.110	50.21	.580
15	.130	.935	.128	51.96	.600
16	.155	1.115	.153	53.86	.622
17	.185	1.331	.182	56.11	.648
18	.220	1.583	.217	58.26	.673
19	.260	1.871	.256	60.42	.698
20	.310	2.230	.305	63.11	.729
21	.370	2.662	.365	66.04	.762
22	.445	3.201	.438	69.39	.801
23	.520	3.741	.512	72.58	.838
24	.595	4.281	.586	75.34	.870
25	.675	4.856	.665	78.08	.901
26	.775	5.576	.764	81.24	.938
27	.875	6.295	.862	83.64	.966
28	1.000	7.194	.985	85.58	.988
29	1.125	8.094	1.108	86.45	.998
30	1.275	9.173	1.256	86.62	1.000
31	1.425	10.252	1.404	86.62	1.000

UMEAN PROFILE - KR=0,F=0 RUN

RUN	= 010875	DE1	= .266
PLATE	= 17	DE2	= .182
X	= 66	H	= 1.46
UINF	= 86.53	G	= 6.53
CF/2	= .00234	BETA	= 0.00
UTAU	= 4.19	REDE2	= 8081.
F	= 0.0000	REK	= 67.
DE	= 1.352	KR	= 0.

PT	Y	Y/DE2	Y/DE	U	U/UINF
1	.006	.033	.004	23.87	.276
2	.007	.038	.005	25.06	.290
3	.009	.049	.007	27.03	.312
4	.012	.066	.009	29.26	.338
5	.016	.088	.012	31.77	.367
6	.021	.115	.016	33.86	.391
7	.028	.154	.021	36.54	.422
8	.036	.198	.027	38.73	.448
9	.046	.253	.034	40.62	.469
10	.060	.330	.044	43.08	.498
11	.077	.423	.057	45.62	.527
12	.095	.522	.070	47.42	.548
13	.115	.632	.085	49.59	.573
14	.130	.714	.096	50.87	.588
15	.155	.852	.115	52.62	.608
16	.190	1.044	.141	54.70	.632
17	.240	1.319	.178	57.52	.665
18	.300	1.648	.222	60.02	.694
19	.375	2.060	.277	62.87	.727
20	.450	2.473	.333	65.72	.760
21	.550	3.022	.407	68.61	.793
22	.675	3.709	.499	72.50	.838
23	.800	4.396	.592	75.68	.875
24	.950	5.220	.703	79.40	.918
25	1.100	6.044	.814	82.42	.953
26	1.250	6.868	.925	84.68	.979
27	1.450	7.967	1.072	86.06	.995
28	1.650	9.066	1.220	86.39	.998
29	1.850	10.165	1.368	86.53	1.000
30	2.050	11.264	1.516	86.53	1.000

UMEAN PROFILE - KR=0,F=0 RUN

RUN	= 010875	DE1	= .321
PLATE	= 22	DE2	= .223
X	= 86	H	= 1.44
UINF	= 86.60	G	= 6.44
CF/2	= .00226	BETA	= 0.00
UTAU	= 4.12	REDE2	= 9905.
F	= 0.0000	REK	= 66.
DE	= 1.698	KR	= 0.

PT	Y	Y/DE2	Y/DE	U	U/UINF
1	.006	.027	.004	24.44	.282
2	.007	.031	.004	25.25	.292
3	.010	.045	.006	27.76	.321
4	.014	.063	.008	30.38	.351
5	.020	.090	.012	32.99	.381
6	.027	.121	.016	35.43	.409
7	.035	.157	.021	37.72	.436
8	.045	.202	.027	39.95	.461
9	.057	.256	.034	42.00	.485
10	.070	.314	.041	44.04	.509
11	.085	.381	.050	45.50	.525
12	.105	.471	.062	47.88	.553
13	.130	.583	.077	49.70	.574
14	.165	.740	.097	51.90	.599
15	.210	.942	.124	54.56	.630
16	.260	1.166	.153	57.23	.661
17	.310	1.390	.183	58.87	.680
18	.385	1.726	.227	61.44	.709
19	.470	2.108	.277	63.78	.736
20	.570	2.556	.336	66.54	.768
21	.670	3.004	.395	69.06	.797
22	.770	3.453	.453	71.36	.824
23	.920	4.126	.542	74.73	.863
24	1.070	4.798	.630	77.55	.895
25	1.220	5.471	.718	80.27	.927
26	1.420	6.368	.836	83.01	.959
27	1.620	7.265	.954	85.19	.984
28	1.820	8.161	1.072	86.23	.996
29	2.020	9.058	1.190	86.60	1.000
30	2.120	9.507	1.249	86.60	1.000

UMEAN PROFILE - KR=0.15E-3, F=0.0000 RUN

RUN	=	033175	DE1	=	.127
PLATE	=	6	DE2	=	.083
X	=	22	H	=	1.54
UINF	=	87.92	G	=	6.71
CF/2	=	.00276	BETA	=	-.01
UTAU	=	4.62	REDE2	=	3740.
F	=	0.0000	REK	=	74.
DE	=	.577	KR	=	.780E-05

PT	Y	Y/DE2	Y/DE	U	U/UINF
1	.006	.072	.010	29.08	.331
2	.008	.096	.014	31.13	.354
3	.011	.133	.019	33.46	.381
4	.014	.169	.024	35.20	.400
5	.018	.217	.031	37.25	.424
6	.023	.277	.040	39.10	.445
7	.030	.361	.052	41.42	.471
8	.040	.482	.069	44.16	.502
9	.050	.602	.087	46.20	.525
10	.065	.783	.113	48.92	.556
11	.085	1.024	.147	51.71	.588
12	.105	1.265	.182	54.27	.617
13	.130	1.566	.225	57.38	.653
14	.155	1.867	.269	59.71	.679
15	.180	2.169	.312	62.39	.710
16	.210	2.530	.364	64.95	.739
17	.240	2.892	.416	67.41	.767
18	.275	3.313	.477	70.49	.802
19	.325	3.916	.563	74.25	.845
20	.375	4.518	.650	77.67	.883
21	.425	5.120	.737	80.97	.921
22	.475	5.723	.823	83.59	.951
23	.525	6.325	.910	85.65	.974
24	.600	7.229	1.040	87.32	.993
25	.675	8.133	1.170	87.92	1.000
26	.775	9.337	1.343	87.92	1.000

UMEAN PROFILE - KR=0.15E-3, F=0.0000 RUN

RUN	=	033175	DE1	=	.173
PLATE	=	9	DE2	=	.114
X	=	34	H	=	1.52
UINF	=	87.30	G	=	6.84
CF/2	=	.00250	BETA	=	-.02
UTAU	=	4.37	REDE2	=	5106.
F	=	0.0000	REK	=	70.
DE	=	.806	KR	=	.840E-05

PT	Y	Y/DE2	Y/DE	U	U/UINF
1	.006	.053	.007	28.15	.322
2	.008	.070	.010	29.80	.341
3	.011	.096	.014	31.68	.363
4	.014	.123	.017	33.33	.382
5	.019	.167	.024	35.53	.407
6	.026	.228	.032	38.05	.436
7	.034	.298	.042	40.20	.460
8	.044	.386	.055	42.59	.488
9	.060	.526	.074	45.38	.520
10	.080	.702	.099	48.14	.551
11	.105	.921	.130	51.13	.586
12	.130	1.140	.161	53.74	.616
13	.155	1.360	.192	55.57	.637
14	.190	1.667	.236	58.39	.669
15	.225	1.974	.279	60.75	.696
16	.275	2.412	.341	64.21	.736
17	.325	2.851	.403	66.98	.767
18	.375	3.289	.465	69.97	.801
19	.425	3.728	.527	72.83	.834
20	.500	4.386	.620	76.50	.876
21	.575	5.044	.713	79.87	.915
22	.650	5.702	.806	82.69	.947
23	.750	6.579	.931	85.51	.979
24	.850	7.456	1.055	86.85	.995
25	.950	8.333	1.179	87.30	1.000
26	1.050	9.211	1.303	87.30	1.000

UMEAN PROFILE - KR=0.15E-3, F=0.0000 RUN

RUN	=	033175	DE1	=	.182
PLATE	=	12	DE2	=	.126
X	=	46	H	=	1.45
UINF	=	91.34	G	=	6.12
CF/2	=	.00258	BETA	=	-.40
UTAU	=	4.64	REDE2	=	5909.
F	=	0.0000	REK	=	74.
DE	=	.963	KR	=	.143E-03

PT	Y	Y/DE2	Y/DE	U	U/UINF
1	.006	.048	.006	30.82	.337
2	.008	.063	.008	32.50	.356
3	.010	.079	.010	34.19	.374
4	.013	.103	.013	36.00	.394
5	.017	.135	.018	38.40	.420
6	.022	.175	.023	40.48	.443
7	.029	.230	.030	43.22	.473
8	.037	.294	.038	45.20	.495
9	.047	.373	.049	47.74	.523
10	.060	.476	.062	50.09	.548
11	.080	.635	.083	52.99	.580
12	.105	.833	.109	55.82	.611
13	.130	1.032	.135	58.29	.638
14	.155	1.230	.161	60.18	.659
15	.190	1.508	.197	62.79	.687
16	.225	1.786	.234	64.82	.710
17	.275	2.183	.286	67.82	.743
18	.350	2.778	.363	71.37	.781
19	.425	3.373	.441	74.64	.817
20	.500	3.968	.519	77.92	.853
21	.575	4.563	.597	80.83	.885
22	.650	5.159	.675	83.27	.912
23	.725	5.754	.753	85.70	.938
24	.825	6.548	.857	88.36	.967
25	.925	7.341	.961	89.99	.985
26	1.025	8.135	1.064	91.03	.997
27	1.125	8.929	1.168	91.34	1.000
28	1.225	9.722	1.272	91.34	1.000

UMEAN PROFILE - KR=0.15E-3, F=0.0000 RUN

RUN	=	033175	DE1	=	.178
PLATE	=	15	DE2	=	.127
X	=	58	H	=	1.41
UINF	=	97.06	G	=	5.66
CF/2	=	.00265	BETA	=	-.39
UTAU	=	5.00	REDE2	=	6318.
F	=	0.0000	REK	=	80.
DE	=	1.061	KR	=	.144E-03

PT	Y	Y/DE2	Y/DE	U	U/UINF
1	.006	.047	.006	34.01	.350
2	.008	.063	.008	35.90	.370
3	.010	.079	.009	37.40	.385
4	.013	.102	.012	39.31	.405
5	.016	.126	.015	40.67	.419
6	.020	.157	.019	42.95	.443
7	.025	.197	.024	45.07	.464
8	.035	.276	.033	48.15	.496
9	.045	.354	.042	51.14	.527
10	.060	.472	.057	54.21	.559
11	.080	.630	.075	57.83	.596
12	.105	.827	.099	60.99	.628
13	.130	1.024	.123	63.93	.659
14	.155	1.220	.146	66.03	.680
15	.190	1.496	.179	68.84	.709
16	.225	1.772	.212	71.38	.735
17	.275	2.165	.259	74.09	.763
18	.350	2.756	.330	77.84	.802
19	.425	3.346	.401	80.74	.832
20	.500	3.937	.471	83.48	.860
21	.600	4.724	.566	86.79	.894
22	.700	5.512	.660	89.59	.923
23	.800	6.299	.754	91.95	.947
24	.900	7.087	.848	94.06	.969
25	1.000	7.874	.943	95.48	.984
26	1.150	9.055	1.084	96.64	.996
27	1.300	10.236	1.225	97.06	1.000
28	1.450	11.417	1.367	97.06	1.000
29	1.600	12.598	1.508	97.06	1.000

UMEAN PROFILE - KR=0.15E-3, F=0.0000 RUN

RUN	=	033175	DE1	=	.183
PLATE	=	17	DE2	=	.131
X	=	66	H	=	1.40
UINF	=	102.04	G	=	5.58
CF/2	=	.00266	BETA	=	-.40
UTAU	=	5.26	REDE2	=	6854.
F	=	0.0000	REK	=	84.
DE	=	1.119	KR	=	.146E-03

PT	Y	Y/DE2	Y/DE	U	U/UINF
1	.006	.046	.005	34.26	.336
2	.008	.061	.007	36.29	.356
3	.010	.076	.009	38.11	.373
4	.013	.099	.012	40.31	.395
5	.016	.122	.014	42.33	.415
6	.020	.153	.018	44.62	.437
7	.025	.191	.022	46.99	.461
8	.035	.267	.031	50.63	.496
9	.045	.344	.040	53.42	.524
10	.060	.458	.054	56.90	.558
11	.080	.611	.071	60.41	.592
12	.105	.802	.094	64.24	.630
13	.130	.992	.116	67.41	.661
14	.155	1.183	.139	69.52	.681
15	.190	1.450	.170	72.44	.710
16	.225	1.718	.201	75.01	.735
17	.275	2.099	.246	78.02	.765
18	.350	2.672	.313	81.72	.801
19	.425	3.244	.380	84.92	.832
20	.500	3.817	.447	87.66	.859
21	.600	4.580	.536	90.82	.890
22	.700	5.344	.626	93.43	.916
23	.800	6.107	.715	95.93	.940
24	.900	6.870	.804	98.06	.961
25	1.000	7.634	.894	99.65	.977
26	1.150	8.779	1.028	101.28	.993
27	1.300	9.924	1.162	101.72	.997
28	1.450	11.069	1.296	102.04	1.000
29	1.600	12.214	1.430	102.04	1.000

UMEAN PROFILE - KR=0.15E-3, F=0.0000 RUN

RUN	=	033175	DE1	=	.182
PLATE	=	19	DE2	=	.130
X	=	74	H	=	1.40
UINF	=	107.33	G	=	5.62
CF/2	=	.00257	BETA	=	-.41
UTAU	=	5.44	REDE2	=	7193.
F	=	0.0000	REK	=	87.
DE	=	1.144	KR	=	.145E-03

PT	Y	Y/DE2	Y/DE	U	U/UINF
1	.006	.046	.005	36.40	.339
2	.008	.062	.007	38.33	.357
3	.010	.077	.009	40.16	.374
4	.013	.100	.011	42.62	.397
5	.016	.123	.014	44.78	.417
6	.020	.154	.017	46.95	.437
7	.025	.192	.022	49.49	.461
8	.035	.269	.031	53.52	.499
9	.045	.346	.039	56.61	.527
10	.060	.462	.052	60.00	.559
11	.080	.615	.070	64.00	.596
12	.105	.808	.092	67.81	.632
13	.130	1.000	.114	71.01	.662
14	.155	1.192	.135	73.42	.684
15	.190	1.462	.166	77.02	.718
16	.225	1.731	.197	79.29	.739
17	.275	2.115	.240	82.54	.769
18	.350	2.692	.306	86.24	.804
19	.425	3.269	.372	89.50	.834
20	.500	3.846	.437	92.52	.862
21	.600	4.615	.524	95.69	.892
22	.700	5.385	.612	98.35	.916
23	.800	6.154	.699	100.92	.940
24	.900	6.923	.787	102.86	.958
25	1.000	7.692	.874	104.59	.974
26	1.150	8.846	1.005	106.31	.990
27	1.300	10.000	1.136	107.11	.998
28	1.450	11.154	1.267	107.33	1.000
29	1.600	12.308	1.399	107.33	1.000

UMEAN PROFILE - KR=0.15E-3, F=0.0000 RUN

RUN	=	033175	DE1	=	.181
PLATE	=	22	DE2	=	.131
X	=	86	H	=	1.38
UINF	=	113.89	G	=	5.41
CF/2	=	.00263	BETA	=	-.38
UTAU	=	5.84	REDE2	=	7643.
F	=	0.0000	REK	=	93.
DE	=	1.192	KR	=	.139E-03

PT	Y	Y/DE2	Y/DE	U	U/UINF
1	.006	.046	.005	39.84	.350
2	.008	.061	.007	41.86	.368
3	.010	.076	.008	43.72	.384
4	.013	.099	.011	46.09	.405
5	.016	.122	.013	48.33	.424
6	.020	.153	.017	50.77	.446
7	.025	.191	.021	53.64	.471
8	.035	.267	.029	57.50	.505
9	.045	.344	.038	60.86	.534
10	.060	.458	.050	64.53	.567
11	.080	.611	.067	68.86	.605
12	.105	.802	.088	72.80	.639
13	.130	.992	.109	76.11	.668
14	.155	1.183	.130	79.08	.694
15	.190	1.450	.159	82.16	.721
16	.225	1.718	.189	84.85	.745
17	.275	2.099	.231	88.01	.773
18	.350	2.672	.294	92.15	.809
19	.425	3.244	.357	95.58	.839
20	.500	3.817	.419	98.27	.863
21	.600	4.580	.503	101.73	.893
22	.700	5.344	.587	104.42	.917
23	.800	6.107	.671	106.89	.939
24	.900	6.870	.755	108.96	.957
25	1.000	7.634	.839	110.67	.972
26	1.150	8.779	.965	112.36	.987
27	1.300	9.924	1.091	113.29	.995
28	1.450	11.069	1.216	113.89	1.000
29	1.600	12.214	1.342	113.89	1.000

UMEAN PROFILE - KR=0.29E-3, F=0.0000 RUN

RUN	=	020675	DE1	=	.081
PLATE	=	3	DE2	=	.051
X	=	10	H	=	1.61
UINF	=	88.18	G	=	6.72
CF/2	=	.00315	BETA	=	-.04
UTAU	=	4.95	REDE2	=	2317.
F	=	0.0000	REK	=	80.
DE	=	.348	KR	=	.364E-05

PT	Y	Y/DE2	Y/DE	U	U/UINF
1	.006	.118	.017	28.97	.329
2	.008	.157	.023	31.26	.355
3	.011	.216	.032	33.99	.385
4	.014	.275	.040	36.11	.410
5	.017	.333	.049	37.98	.431
6	.020	.392	.057	39.76	.451
7	.025	.490	.072	41.89	.475
8	.031	.608	.089	43.96	.499
9	.038	.745	.109	46.32	.525
10	.045	.882	.129	48.08	.545
11	.055	1.078	.158	50.64	.574
12	.067	1.314	.193	53.31	.605
13	.080	1.569	.230	55.85	.633
14	.095	1.863	.273	58.56	.664
15	.112	2.196	.322	61.47	.697
16	.130	2.549	.374	64.63	.733
17	.150	2.941	.431	67.79	.769
18	.175	3.431	.503	71.03	.806
19	.200	3.922	.575	74.41	.844
20	.225	4.412	.647	77.38	.878
21	.250	4.902	.718	80.28	.910
22	.275	5.392	.790	82.74	.938
23	.300	5.882	.862	84.88	.963
24	.330	6.471	.948	86.63	.982
25	.370	7.255	1.063	87.76	.995
26	.420	8.235	1.207	88.18	1.000
27	.470	9.216	1.351	88.18	1.000

UMEAN PROFILE - KR=0.29E-3, F=0.0000 RUN

RUN	=	020675	DE1	=	.115
PLATE	=	5	DE2	=	.073
X	=	18	H	=	1.57
UINF	=	88.76	G	=	6.93
CF/2	=	.00273	BETA	=	-.01
UTAU	=	4.64	REDE2	=	3386.
F	=	0.0000	REK	=	75.
DE	=	.501	KR	=	.786E-05

PT	Y	Y/DE2	Y/DE	U	U/UINF
1	.006	.082	.012	28.76	.324
2	.008	.110	.016	30.82	.347
3	.011	.151	.022	33.01	.372
4	.014	.192	.028	34.96	.394
5	.017	.233	.034	36.57	.412
6	.020	.274	.040	38.14	.430
7	.025	.342	.050	40.00	.451
8	.031	.425	.062	41.95	.473
9	.038	.521	.076	44.04	.496
10	.045	.616	.090	45.62	.514
11	.054	.740	.108	47.59	.536
12	.064	.877	.128	49.43	.557
13	.076	1.041	.152	51.46	.580
14	.090	1.233	.180	53.62	.604
15	.110	1.507	.220	56.37	.635
16	.130	1.781	.259	58.99	.665
17	.155	2.123	.309	61.55	.693
18	.180	2.466	.359	64.38	.725
19	.205	2.808	.409	67.08	.756
20	.230	3.151	.459	69.44	.782
21	.255	3.493	.509	71.57	.806
22	.280	3.836	.559	74.10	.835
23	.305	4.178	.609	76.24	.859
24	.330	4.521	.659	78.36	.883
25	.355	4.863	.709	80.19	.903
26	.390	5.342	.778	82.65	.931
27	.430	5.890	.858	84.99	.958
28	.480	6.575	.958	87.13	.982
29	.530	7.260	1.058	88.32	.995
30	.580	7.945	1.158	88.69	.999
31	.630	8.630	1.257	88.76	1.000
32	.680	9.315	1.357	88.76	1.000

UMEAN PROFILE - KR=0.29E-3, F=0.0000 RUN

RUN	=	020675	DE1	=	.115
PLATE	=	7	DE2	=	.077
X	=	26	H	=	1.49
UINF	=	93.92	G	=	5.92
CF/2	=	.00309	BETA	=	-.42
UTAU	=	5.22	REDE2	=	3773.
F	=	0.0000	REK	=	84.
DE	=	.579	KR	=	.281E-03

PT	Y	Y/DE2	Y/DE	U	U/UINF
1	.006	.078	.010	30.75	.327
2	.008	.104	.014	33.02	.352
3	.010	.130	.017	35.21	.375
4	.012	.156	.021	37.18	.396
5	.014	.182	.024	38.88	.414
6	.017	.221	.029	40.83	.435
7	.020	.260	.035	42.57	.453
8	.023	.299	.040	44.21	.471
9	.027	.351	.047	45.96	.489
10	.032	.416	.055	47.79	.509
11	.039	.506	.067	49.79	.530
12	.047	.610	.081	52.07	.554
13	.057	.740	.098	54.31	.578
14	.070	.909	.121	56.92	.606
15	.085	1.104	.147	59.32	.632
16	.100	1.299	.173	61.61	.656
17	.115	1.494	.199	63.39	.675
18	.130	1.688	.225	64.97	.692
19	.150	1.948	.259	67.27	.716
20	.175	2.273	.302	69.71	.742
21	.200	2.597	.345	71.79	.764
22	.230	2.987	.397	74.47	.793
23	.265	3.442	.458	77.04	.820
24	.300	3.896	.518	79.51	.847
25	.340	4.416	.587	82.12	.874
26	.390	5.065	.674	85.05	.906
27	.440	5.714	.760	87.84	.935
28	.490	6.364	.846	90.14	.960
29	.540	7.013	.933	91.95	.979
30	.590	7.662	1.019	93.09	.991
31	.640	8.312	1.105	93.73	.998
32	.690	8.961	1.192	93.92	1.000
33	.740	9.610	1.278	93.92	1.000

UMEAN PROFILE - KR=0.29E-3, F=0.0000 RUN

RUN	=	022275	DE1	=	.112
PLATE	=	9	DE2	=	.078
X	=	34	H	=	1.44
UINF	=	102.61	G	=	5.56
CF/2	=	.00306	BETA	=	-.41
UTAU	=	5.68	REDE2	=	4154.
F	=	0.0000	REK	=	92.
DE	=	.642	KR	=	.279E-03

PT	Y	Y/DE2	Y/DE	U	U/UINF
1	.006	.077	.009	37.91	.369
2	.008	.103	.012	40.19	.392
3	.010	.128	.016	42.09	.410
4	.013	.167	.020	44.61	.435
5	.016	.205	.025	46.42	.452
6	.019	.244	.030	48.17	.469
7	.023	.295	.036	50.38	.491
8	.027	.346	.042	52.14	.508
9	.031	.397	.048	53.68	.523
10	.037	.474	.058	55.90	.545
11	.045	.577	.070	58.01	.565
12	.055	.705	.086	60.71	.592
13	.065	.833	.101	62.99	.614
14	.075	.962	.117	64.82	.632
15	.085	1.090	.132	66.57	.649
16	.100	1.282	.156	68.92	.672
17	.115	1.474	.179	70.85	.690
18	.130	1.667	.202	72.94	.711
19	.150	1.923	.234	75.53	.736
20	.175	2.244	.273	77.83	.759
21	.200	2.564	.312	80.23	.782
22	.225	2.885	.350	82.48	.804
23	.250	3.205	.389	84.43	.823
24	.275	3.526	.428	86.13	.839
25	.310	3.974	.483	88.60	.863
26	.350	4.487	.545	91.04	.887
27	.400	5.128	.623	93.69	.913
28	.450	5.769	.701	95.98	.935
29	.500	6.410	.779	97.91	.954
30	.550	7.051	.857	99.73	.972
31	.600	7.692	.935	100.84	.983
32	.650	8.333	1.012	101.73	.991
33	.750	9.615	1.168	102.37	.998
34	.850	10.897	1.324	102.55	.999
35	.950	12.179	1.480	102.61	1.000
36	1.100	14.103	1.713	102.61	1.000

UMEAN PROFILE - KR=0.29E-3, F=0.0000 RUN

RUN	=	022275	DE1	=	.111
PLATE	=	11	DE2	=	.077
X	=	42	H	=	1.43
UINF	=	110.77	G	=	5.46
CF/2	=	.00307	BETA	=	-.41
UTAU	=	6.14	REDE2	=	4466.
F	=	0.0000	REK	=	99.
DE	=	.658	KR	=	.282E-03

PT	Y	Y/DE2	Y/DE	U	U/UINF
1	.006	.078	.009	41.59	.375
2	.008	.104	.012	43.70	.395
3	.010	.130	.015	45.83	.414
4	.013	.169	.020	48.22	.435
5	.016	.208	.024	50.31	.454
6	.019	.247	.029	52.31	.472
7	.023	.299	.035	54.53	.492
8	.027	.351	.041	56.51	.510
9	.031	.403	.047	58.05	.524
10	.037	.481	.056	60.70	.548
11	.045	.584	.068	63.39	.572
12	.055	.714	.084	66.28	.598
13	.065	.844	.099	68.61	.619
14	.075	.974	.114	70.88	.640
15	.085	1.104	.129	72.63	.656
16	.100	1.299	.152	74.84	.676
17	.115	1.494	.175	77.34	.698
18	.130	1.688	.198	79.48	.718
19	.150	1.948	.228	82.01	.740
20	.175	2.273	.266	85.00	.767
21	.200	2.597	.304	87.32	.788
22	.225	2.922	.342	89.52	.808
23	.250	3.247	.380	91.57	.827
24	.275	3.571	.418	93.38	.843
25	.310	4.026	.471	95.91	.866
26	.350	4.545	.532	98.32	.888
27	.400	5.195	.608	101.16	.913
28	.450	5.844	.684	103.65	.936
29	.500	6.494	.760	105.62	.954
30	.550	7.143	.836	107.24	.968
31	.600	7.792	.912	108.64	.981
32	.650	8.442	.988	109.54	.989
33	.750	9.740	1.140	110.50	.998
34	.850	11.039	1.292	110.77	1.000
35	.950	12.338	1.444	110.77	1.000
36	1.100	14.286	1.672	110.77	1.000

UMEAN PROFILE - KR=0.29E-3, F=0.0000 RUN

RUN	=	022275	DE1	=	.110
PLATE	=	12	DE2	=	.077
X	=	46	H	=	1.43
UINF	=	117.33	G	=	5.33
CF/2	=	.00315	BETA	=	-.40
UTAU	=	6.59	REDE2	=	4732.
F	=	0.0000	REK	=	106.
DE	=	.668	KR	=	.287E-03

PT	Y	Y/DE2	Y/DE	U	U/UINF
1	.006	.078	.009	44.03	.375
2	.008	.104	.012	46.65	.398
3	.010	.130	.015	48.91	.417
4	.013	.169	.019	51.80	.441
5	.016	.208	.024	54.15	.462
6	.019	.247	.028	55.89	.476
7	.023	.299	.034	58.51	.499
8	.027	.351	.040	60.84	.519
9	.031	.403	.046	62.37	.532
10	.037	.481	.055	64.61	.551
11	.045	.584	.067	67.56	.576
12	.055	.714	.082	70.21	.598
13	.065	.844	.097	72.86	.621
14	.075	.974	.112	75.15	.641
15	.085	1.104	.127	77.16	.658
16	.100	1.299	.150	79.75	.680
17	.115	1.494	.172	82.18	.700
18	.130	1.688	.195	84.53	.720
19	.150	1.948	.225	87.21	.743
20	.175	2.273	.262	90.21	.769
21	.200	2.597	.299	92.54	.789
22	.225	2.922	.337	95.13	.811
23	.250	3.247	.374	97.38	.830
24	.275	3.571	.412	99.20	.845
25	.310	4.026	.464	101.72	.867
26	.350	4.545	.524	104.36	.889
27	.400	5.195	.599	107.26	.914
28	.450	5.844	.674	109.68	.935
29	.500	6.494	.749	111.71	.952
30	.550	7.143	.823	113.42	.967
31	.600	7.792	.898	114.84	.979
32	.650	8.442	.973	115.85	.987
33	.750	9.740	1.123	116.93	.997
34	.850	11.039	1.272	117.33	1.000
35	.950	12.338	1.422	117.33	1.000
36	1.100	14.286	1.647	117.33	1.000

UMEAN PROFILE - KR=0.29E-3, F=0.0000 RUN

RUN	=	020675	DE1	=	.134
PLATE	=	15	DE2	=	.090
X	=	58	H	=	1.49
UINF	=	128.59	G	=	6.71
CF/2	=	.00238	BETA	=	-.01
UTAU	=	6.27	REDE2	=	5984.
F	=	0.0000	REK	=	101.
DE	=	.739	KR	=	.397E-05

PT	Y	Y/DE2	Y/DE	U	U/UINF
1	.006	.067	.008	41.16	.320
2	.008	.089	.011	44.13	.343
3	.010	.111	.014	46.63	.363
4	.012	.133	.016	48.70	.379
5	.014	.156	.019	50.49	.393
6	.017	.189	.023	52.81	.411
7	.020	.222	.027	54.38	.423
8	.025	.278	.034	57.58	.448
9	.030	.333	.041	59.81	.465
10	.037	.411	.050	63.04	.490
11	.045	.500	.061	66.41	.516
12	.055	.611	.074	69.47	.540
13	.065	.722	.088	72.39	.563
14	.077	.856	.104	75.73	.589
15	.090	1.000	.122	78.45	.610
16	.105	1.167	.142	81.54	.634
17	.120	1.333	.162	84.48	.657
18	.130	1.444	.176	86.32	.671
19	.150	1.667	.203	89.33	.695
20	.170	1.889	.230	92.15	.717
21	.195	2.167	.264	95.48	.743
22	.225	2.500	.304	99.06	.770
23	.260	2.889	.352	102.69	.799
24	.300	3.333	.406	106.51	.828
25	.350	3.889	.474	110.74	.861
26	.400	4.444	.541	114.10	.887
27	.475	5.278	.643	118.50	.922
28	.575	6.389	.778	122.94	.956
29	.675	7.500	.913	126.05	.980
30	.775	8.611	1.049	127.74	.993
31	.875	9.722	1.184	128.59	1.000
32	.975	10.833	1.319	128.59	1.000

UMEAN PROFILE - KR=0.29E-3, F=0.0000 RUN

RUN	=	020675	DE1	=	.200
PLATE	=	19	DE2	=	.133
X	=	74	H	=	1.50
UINF	=	128.50	G	=	6.78
CF/2	=	.00243	BETA	=	-.00
UTAU	=	6.33	REDE2	=	8847.
F	=	0.0000	REK	=	102.
DE	=	.989	KR	=	.900E-06

PT	Y	Y/DE2	Y/DE	U	U/UINF
1	.006	.045	.006	36.96	.288
2	.008	.060	.008	39.90	.311
3	.010	.075	.010	42.23	.329
4	.012	.090	.012	44.15	.344
5	.014	.105	.014	45.93	.357
6	.017	.128	.017	47.71	.371
7	.020	.150	.020	50.16	.390
8	.025	.188	.025	52.87	.411
9	.035	.263	.035	57.24	.445
10	.045	.338	.046	60.74	.473
11	.060	.451	.061	64.69	.503
12	.080	.602	.081	69.36	.540
13	.100	.752	.101	73.28	.570
14	.130	.977	.131	77.31	.602
15	.170	1.278	.172	82.54	.642
16	.220	1.654	.222	87.30	.679
17	.270	2.030	.273	91.98	.716
18	.320	2.406	.324	95.78	.745
19	.395	2.970	.399	101.32	.788
20	.470	3.534	.475	105.92	.824
21	.570	4.286	.576	111.83	.870
22	.670	5.038	.677	117.08	.911
23	.795	5.977	.804	122.25	.951
24	.920	6.917	.930	125.96	.980
25	1.070	8.045	1.082	128.05	.996
26	1.220	9.173	1.234	128.50	1.000
27	1.370	10.301	1.385	128.50	1.000

UMEAN PROFILE - KR=0.29E-3, F=0.0039 RUN

RUN	=	030475	DE1	=	.132
PLATE	=	3	DE2	=	.075
X	=	10	H	=	1.77
UINF	=	86.52	G	=	11.00
CF/2	=	.00157	BETA	=	.02
UTAU	=	3.43	REDE2	=	3343.
F	=	.0039	REK	=	55.
DE	=	.463	KR	=	-.572E-05

PT	Y	Y/DE2	Y/DE	U	U/UINF
1	.006	.080	.013	19.70	.228
2	.008	.107	.017	21.54	.249
3	.011	.147	.024	23.96	.277
4	.015	.200	.032	26.35	.305
5	.020	.267	.043	28.63	.331
6	.027	.360	.058	31.16	.360
7	.035	.467	.076	33.64	.389
8	.045	.600	.097	36.34	.420
9	.057	.760	.123	38.78	.448
10	.070	.933	.151	41.40	.479
11	.090	1.200	.194	44.91	.519
12	.110	1.467	.238	47.86	.553
13	.130	1.733	.281	50.88	.588
14	.150	2.000	.324	53.74	.621
15	.175	2.333	.378	57.11	.660
16	.200	2.667	.432	60.54	.700
17	.235	3.133	.508	64.99	.751
18	.275	3.667	.594	69.76	.806
19	.325	4.333	.702	75.45	.872
20	.375	5.000	.810	80.25	.928
21	.425	5.667	.918	83.91	.970
22	.475	6.333	1.026	85.92	.993
23	.525	7.000	1.134	86.52	1.000
24	.575	7.667	1.242	86.52	1.000

UMEAN PROFILE - KR=0.29E-3, F=0.0039 RUN

RUN	=	030475	DE1	=	.205
PLATE	=	5	DE2	=	.117
X	=	18	H	=	1.76
UINF	=	87.07	G	=	11.71
CF/2	=	.00136	BETA	=	-.41
UTAU	=	3.21	REDE2	=	5264.
F	=	.0039	REK	=	52.
DE	=	.747	KR	=	.680E-04

PT	Y	Y/DE2	Y/DE	U	U/UINF
1	.006	.051	.008	18.35	.211
2	.008	.068	.011	20.12	.231
3	.010	.085	.013	21.23	.244
4	.013	.111	.017	22.95	.264
5	.016	.137	.021	24.24	.278
6	.020	.171	.027	25.78	.296
7	.025	.214	.033	27.38	.314
8	.032	.274	.043	29.32	.337
9	.040	.342	.054	31.25	.359
10	.050	.427	.067	33.22	.382
11	.065	.556	.087	35.97	.413
12	.085	.726	.114	38.78	.445
13	.105	.897	.141	41.40	.475
14	.130	1.111	.174	44.13	.507
15	.155	1.325	.207	46.50	.534
16	.185	1.581	.248	49.45	.568
17	.225	1.923	.301	53.40	.613
18	.275	2.350	.368	57.69	.663
19	.325	2.778	.435	61.93	.711
20	.375	3.205	.502	66.01	.758
21	.425	3.632	.569	69.97	.804
22	.475	4.060	.636	73.72	.847
23	.525	4.487	.703	77.17	.886
24	.575	4.915	.770	80.33	.923
25	.625	5.342	.837	82.92	.952
26	.675	5.769	.904	85.03	.977
27	.725	6.197	.971	86.12	.989
28	.775	6.624	1.037	86.70	.996
29	.825	7.051	1.104	87.00	.999
30	.875	7.479	1.171	87.07	1.000
31	.925	7.906	1.238	87.07	1.000

UMEAN PROFILE - KR=0.29E-3, F=0.0039 RUN

RUN	=	030475	DE1	=	.208
PLATE	=	7	DE2	=	.129
X	=	26	H	=	1.61
UINF	=	92.64	G	=	9.34
CF/2	=	.00164	BETA	=	-1.44
UTAU	=	3.75	REDE2	=	6196.
F	=	.0039	REK	=	61.
DE	=	.876	KR	=	.284E-03

PT	Y	Y/DE2	Y/DE	U	U/UINF
1	.006	.047	.007	22.26	.240
2	.008	.062	.009	24.02	.259
3	.010	.078	.011	25.74	.278
4	.013	.101	.015	27.71	.299
5	.016	.124	.018	29.44	.318
6	.020	.155	.023	31.76	.343
7	.025	.194	.029	33.67	.363
8	.032	.248	.037	35.88	.387
9	.040	.310	.046	38.04	.411
10	.050	.388	.057	40.09	.433
11	.065	.504	.074	43.21	.466
12	.085	.659	.097	46.55	.502
13	.105	.814	.120	49.19	.531
14	.130	1.008	.148	52.05	.562
15	.155	1.202	.177	54.42	.587
16	.185	1.434	.211	56.86	.614
17	.225	1.744	.257	59.94	.647
18	.275	2.132	.314	63.43	.685
19	.325	2.519	.371	66.98	.723
20	.375	2.907	.428	70.04	.756
21	.450	3.488	.514	74.50	.804
22	.525	4.070	.599	78.65	.849
23	.600	4.651	.685	82.78	.894
24	.675	5.233	.771	86.09	.929
25	.750	5.814	.856	89.02	.961
26	.825	6.395	.942	90.93	.982
27	.900	6.977	1.027	92.08	.994
28	.975	7.558	1.113	92.64	1.000
29	1.050	8.140	1.199	92.64	1.000

UMEAN PROFILE - KR=0.29E-3, F=0.0039 RUN

RUN	=	030475	DE1	=	.200
PLATE	=	9	DE2	=	.130
X	=	34	H	=	1.54
UINF	=	101.66	G	=	8.92
CF/2	=	.00154	BETA	=	-1.45
UTAU	=	3.99	REDE2	=	6843.
F	=	.0039	REK	=	64.
DE	=	.962	KR	=	.278E-03

PT	Y	Y/DE2	Y/DE	U	U/UINF
1	.006	.046	.006	25.83	.254
2	.008	.062	.008	27.74	.273
3	.010	.077	.010	29.78	.293
4	.013	.100	.014	31.93	.314
5	.016	.123	.017	33.80	.332
6	.019	.146	.020	35.42	.348
7	.023	.177	.024	37.32	.367
8	.027	.208	.028	39.03	.384
9	.032	.246	.033	41.08	.404
10	.039	.300	.041	43.43	.427
11	.046	.354	.048	45.39	.446
12	.055	.423	.057	47.67	.469
13	.065	.500	.068	50.21	.494
14	.075	.577	.078	52.04	.512
15	.087	.669	.090	53.96	.531
16	.100	.769	.104	56.10	.552
17	.115	.885	.120	58.08	.571
18	.130	1.000	.135	60.26	.593
19	.150	1.154	.156	62.27	.613
20	.170	1.308	.177	64.42	.634
21	.195	1.500	.203	66.76	.657
22	.220	1.692	.229	68.92	.678
23	.255	1.962	.265	71.64	.705
24	.295	2.269	.307	74.10	.729
25	.340	2.615	.353	77.20	.759
26	.390	3.000	.405	80.20	.789
27	.440	3.385	.457	82.67	.813
28	.490	3.769	.509	85.24	.838
29	.550	4.231	.572	88.09	.867
30	.625	4.808	.650	91.38	.899
31	.700	5.385	.728	94.27	.927
32	.800	6.154	.832	97.46	.959
33	.900	6.923	.936	99.73	.981
34	1.000	7.692	1.040	101.16	.995
35	1.100	8.462	1.143	101.55	.999
36	1.250	9.615	1.299	101.66	1.000

UMEAN PROFILE - KR=0.29E-3, F=0.0039 RUN

RUN	=	030475	DE1	=	.197
PLATE	=	11	DE2	=	.131
X	=	42	H	=	1.50
UINF	=	111.25	G	=	8.35
CF/2	=	.00161	BETA	=	-1.44
UTAU	=	4.46	REDE2	=	7524.
F	=	.0039	REK	=	72.
DE	=	1.019	KR	=	.294E-03

PT	Y	Y/DE2	Y/DE	U	U/UINF
1	.006	.046	.006	30.33	.273
2	.008	.061	.008	32.20	.289
3	.010	.076	.010	33.64	.302
4	.013	.099	.013	36.24	.326
5	.016	.122	.016	38.20	.343
6	.019	.145	.019	39.97	.359
7	.023	.176	.023	42.13	.379
8	.027	.206	.026	44.08	.396
9	.032	.244	.031	46.24	.416
10	.039	.298	.038	48.40	.435
11	.046	.351	.045	50.89	.457
12	.055	.420	.054	53.58	.482
13	.065	.496	.064	56.13	.505
14	.075	.573	.074	58.05	.522
15	.087	.664	.085	60.74	.546
16	.100	.763	.098	63.25	.569
17	.115	.878	.113	65.41	.588
18	.130	.992	.128	67.66	.608
19	.150	1.145	.147	70.18	.631
20	.170	1.298	.167	72.23	.649
21	.195	1.489	.191	74.82	.673
22	.220	1.679	.216	77.15	.693
23	.255	1.947	.250	80.00	.719
24	.295	2.252	.289	82.84	.745
25	.340	2.595	.334	85.96	.773
26	.390	2.977	.383	88.74	.798
27	.440	3.359	.432	91.57	.823
28	.490	3.740	.481	94.12	.846
29	.550	4.198	.540	96.86	.871
30	.625	4.771	.613	99.90	.898
31	.700	5.344	.687	102.68	.923
32	.800	6.107	.785	105.72	.950
33	.900	6.870	.883	108.28	.973
34	1.000	7.634	.981	109.88	.988
35	1.100	8.397	1.079	110.67	.995
36	1.250	9.542	1.227	111.25	1.000
37	1.400	10.687	1.374	111.25	1.000

UMEAN PROFILE - KR=0.29E-3, F=0.0039 RUN

RUN	=	030475	DE1	=	.195
PLATE	=	12	DE2	=	.131
X	=	46	H	=	1.49
UINF	=	116.62	G	=	7.97
CF/2	=	.00171	BETA	=	-1.36
UTAU	=	4.82	REDE2	=	7888.
F	=	.0039	REK	=	78.
DE	=	1.048	KR	=	.297E-03

PT	Y	Y/DE2	Y/DE	U	U/UINF
1	.006	.046	.006	32.10	.275
2	.008	.061	.008	34.09	.292
3	.010	.076	.010	36.26	.311
4	.013	.099	.012	38.45	.330
5	.016	.122	.015	40.97	.351
6	.019	.145	.018	42.53	.365
7	.023	.176	.022	44.76	.384
8	.027	.206	.026	46.87	.402
9	.032	.244	.031	48.78	.418
10	.039	.298	.037	52.07	.446
11	.046	.351	.044	53.92	.462
12	.055	.420	.052	56.36	.483
13	.065	.496	.062	59.03	.506
14	.075	.573	.072	61.21	.525
15	.087	.664	.083	64.27	.551
16	.100	.763	.095	66.74	.572
17	.115	.878	.110	69.04	.592
18	.130	.992	.124	70.89	.608
19	.150	1.145	.143	73.83	.633
20	.170	1.298	.162	76.49	.656
21	.195	1.489	.186	79.14	.679
22	.220	1.679	.210	81.56	.699
23	.255	1.947	.243	84.24	.722
24	.295	2.252	.281	87.79	.753
25	.340	2.595	.324	90.44	.776
26	.390	2.977	.372	93.72	.804
27	.440	3.359	.420	96.59	.828
28	.490	3.740	.468	98.84	.848
29	.550	4.198	.525	101.59	.871
30	.625	4.771	.596	104.89	.899
31	.700	5.344	.668	107.53	.922
32	.800	6.107	.763	110.53	.948
33	.900	6.870	.859	113.00	.969
34	1.000	7.634	.954	114.88	.985
35	1.100	8.397	1.050	115.90	.994
36	1.250	9.542	1.193	116.62	1.000

UMEAN PROFILE - KR=0.29E-3, F=0.0039 RUN

RUN	=	030475	DE1	=	.239
PLATE	=	15	DE2	=	.155
X	=	58	H	=	1.54
UINF	=	128.18	G	=	11.27
CF/2	=	.00097	BETA	=	-.21
UTAU	=	3.99	REDE2	=	10251.
F	=	.0039	REK	=	64.
DE	=	1.220	KR	=	.210E-04

PT	Y	Y/DE2	Y/DE	U	U/UINF
1	.006	.039	.005	31.29	.244
2	.008	.052	.007	33.07	.258
3	.010	.065	.008	34.91	.272
4	.013	.084	.011	36.95	.288
5	.017	.110	.014	40.14	.313
6	.022	.142	.018	42.51	.332
7	.030	.194	.025	46.35	.362
8	.040	.258	.033	50.11	.391
9	.052	.335	.043	54.18	.423
10	.065	.419	.053	57.93	.452
11	.080	.516	.066	61.46	.479
12	.095	.613	.078	65.07	.508
13	.110	.710	.090	68.06	.531
14	.130	.839	.107	71.44	.557
15	.155	1.000	.127	75.15	.586
16	.185	1.194	.152	79.11	.617
17	.225	1.452	.184	83.29	.650
18	.275	1.774	.225	87.82	.685
19	.325	2.097	.266	92.77	.724
20	.375	2.419	.307	96.51	.753
21	.450	2.903	.369	101.56	.792
22	.525	3.387	.430	105.71	.825
23	.600	3.871	.492	109.90	.857
24	.700	4.516	.574	114.18	.891
25	.800	5.161	.656	117.92	.920
26	.925	5.968	.758	121.83	.950
27	1.050	6.774	.861	124.53	.972
28	1.200	7.742	.984	126.71	.989
29	1.350	8.710	1.107	127.54	.995
30	1.500	9.677	1.230	127.88	.998
31	1.650	10.645	1.352	128.18	1.000
32	1.800	11.613	1.475	128.18	1.000

UMEAN PROFILE - KR=0.29E-3, F=0.0039 RUN

RUN	=	030475	DE1	=	.372
PLATE	=	19	DE2	=	.230
X	=	74	H	=	1.62
UINF	=	128.68	G	=	12.11
CF/2	=	.00099	BETA	=	.09
UTAU	=	4.05	REDE2	=	15263.
F	=	.0039	REK	=	65.
DE	=	1.576	KR	=	-.611E-05

PT	Y	Y/DE2	Y/DE	U	U/UINF
1	.006	.026	.004	25.35	.197
2	.008	.035	.005	26.86	.209
3	.010	.043	.006	28.56	.222
4	.013	.057	.008	30.75	.239
5	.017	.074	.011	33.43	.260
6	.023	.100	.015	36.61	.285
7	.031	.135	.020	39.77	.309
8	.041	.178	.026	43.43	.338
9	.055	.239	.035	47.48	.369
10	.072	.313	.046	51.36	.399
11	.090	.391	.057	55.25	.429
12	.110	.478	.070	58.08	.451
13	.130	.565	.082	61.54	.478
14	.155	.674	.098	64.04	.498
15	.190	.826	.121	67.13	.522
16	.240	1.043	.152	72.45	.563
17	.290	1.261	.184	75.69	.588
18	.365	1.587	.232	80.68	.627
19	.465	2.022	.295	86.91	.675
20	.565	2.457	.359	92.36	.718
21	.665	2.891	.422	97.55	.758
22	.780	3.391	.495	103.31	.803
23	.900	3.913	.571	108.48	.843
24	1.050	4.565	.666	114.24	.888
25	1.200	5.217	.761	119.46	.928
26	1.400	6.087	.888	124.77	.970
27	1.600	6.957	1.015	127.59	.992
28	1.800	7.826	1.142	128.68	1.000
29	2.000	8.696	1.269	128.68	1.000

UMEAN PROFILE - K=0.28E-6, F=0.0000 RUN

RUN	=	043075	DE1	=	.097
PLATE	=	4	DE2	=	.062
X	=	14	H	=	1.57
UINF	=	87.63	G	=	6.85
CF/2	=	.00280	BETA	=	.02
UTAU	=	4.64	REDE2	=	2813.
F	=	0.0000	REK	=	75.
DE	=	.423	K	=	-.153E-07

PT	Y	Y/DE2	Y/DE	U	U/UINF
1	.006	.097	.014	31.08	.355
2	.008	.129	.019	32.53	.371
3	.011	.177	.026	34.60	.395
4	.015	.242	.035	36.86	.421
5	.020	.323	.047	39.14	.447
6	.027	.435	.064	42.00	.479
7	.035	.565	.083	44.33	.506
8	.045	.726	.106	46.95	.536
9	.057	.919	.135	49.50	.565
10	.070	1.129	.165	51.92	.592
11	.085	1.371	.201	54.40	.621
12	.105	1.694	.248	57.48	.656
13	.130	2.097	.307	60.68	.692
14	.155	2.500	.366	64.04	.731
15	.180	2.903	.426	67.01	.765
16	.210	3.387	.496	70.24	.802
17	.250	4.032	.591	74.49	.850
18	.300	4.839	.709	79.18	.904
19	.350	5.645	.827	82.94	.946
20	.400	6.452	.946	85.94	.981
21	.450	7.258	1.064	87.25	.996
22	.500	8.065	1.182	87.63	1.000
23	.550	8.871	1.300	87.63	1.000

UMEAN PROFILE - K=0.28E-6, F=0.0000 RUN

RUN	=	043075	DE1	=	.111
PLATE	=	7	DE2	=	.076
X	=	26	H	=	1.46
UINF	=	93.37	G	=	5.83
CF/2	=	.00295	BETA	=	-.49
UTAU	=	5.07	REDE2	=	3681.
F	=	0.0000	REK	=	81.
DE	=	.583	K	=	.270E-06

PT	Y	Y/DE2	Y/DE	U	U/UINF
1	.006	.079	.010	33.37	.357
2	.008	.105	.014	36.04	.386
3	.010	.132	.017	38.00	.407
4	.013	.171	.022	40.41	.433
5	.017	.224	.029	42.78	.458
6	.022	.289	.038	45.36	.486
7	.029	.382	.050	48.12	.515
8	.038	.500	.065	50.94	.546
9	.048	.632	.082	53.59	.574
10	.060	.789	.103	56.12	.601
11	.075	.987	.129	58.80	.630
12	.100	1.316	.172	62.32	.667
13	.130	1.711	.223	65.79	.705
14	.160	2.105	.274	68.72	.736
15	.200	2.632	.343	72.25	.774
16	.250	3.289	.429	76.05	.815
17	.300	3.947	.515	79.40	.850
18	.350	4.605	.600	82.68	.886
19	.425	5.592	.729	86.81	.930
20	.500	6.579	.858	90.12	.965
21	.575	7.566	.986	92.27	.988
22	.650	8.553	1.115	93.11	.997
23	.725	9.539	1.244	93.37	1.000
24	.800	10.526	1.372	93.37	1.000

UMEAN PROFILE - K=0.28E-6, F=0.0000 RUN

RUN	=	043075	DE1	=	.105
PLATE	=	9	DE2	=	.073
X	=	34	H	=	1.43
UINF	=	104.02	G	=	5.44
CF/2	=	.00305	BETA	=	-.50
UTAU	=	5.74	REDE2	=	3933.
F	=	0.0000	REK	=	92.
DE	=	.626	K	=	.272E-06

PT	Y	Y/DE2	Y/DE	U	U/UINF
1	.006	.082	.010	38.74	.372
2	.008	.110	.013	41.24	.396
3	.010	.137	.016	43.32	.416
4	.013	.178	.021	45.85	.441
5	.017	.233	.027	48.52	.466
6	.022	.301	.035	51.71	.497
7	.028	.384	.045	54.69	.526
8	.035	.479	.056	57.39	.552
9	.045	.616	.072	60.51	.582
10	.060	.822	.096	64.42	.619
11	.080	1.096	.128	68.65	.660
12	.105	1.438	.168	72.58	.698
13	.130	1.781	.208	75.85	.729
14	.155	2.123	.248	78.91	.759
15	.190	2.603	.304	82.28	.791
16	.225	3.082	.359	85.25	.820
17	.275	3.767	.439	88.79	.854
18	.325	4.452	.519	92.03	.885
19	.375	5.137	.599	94.82	.912
20	.450	6.164	.719	98.20	.944
21	.525	7.192	.839	100.91	.970
22	.600	8.219	.958	102.57	.986
23	.675	9.247	1.078	103.53	.995
24	.750	10.274	1.198	103.82	.998
25	.825	11.301	1.318	104.02	1.000
26	.900	12.329	1.438	104.02	1.000

UMEAN PROFILE - K=0.28E-6, F=0.0000 RUN

RUN	=	043075	DE1	=	.098
PLATE	=	11	DE2	=	.069
X	=	42	H	=	1.42
UINF	=	117.61	G	=	5.33
CF/2	=	.00305	BETA	=	-.57
UTAU	=	6.50	REDE2	=	4189.
F	=	0.0000	REK	=	104.
DE	=	.610	K	=	.292E-06

PT	Y	Y/DE2	Y/DE	U	U/UINF
1	.006	.087	.010	46.11	.392
2	.008	.116	.013	47.97	.408
3	.010	.145	.016	50.09	.426
4	.013	.188	.021	52.87	.450
5	.017	.246	.028	56.29	.479
6	.022	.319	.036	59.67	.507
7	.028	.406	.046	63.28	.538
8	.035	.507	.057	66.28	.564
9	.045	.652	.074	70.17	.597
10	.060	.870	.098	74.56	.634
11	.080	1.159	.131	79.40	.675
12	.105	1.522	.172	83.91	.713
13	.130	1.884	.213	87.65	.745
14	.155	2.246	.254	91.25	.776
15	.190	2.754	.311	94.85	.806
16	.225	3.261	.369	98.23	.835
17	.275	3.986	.451	102.19	.869
18	.325	4.710	.533	105.53	.897
19	.375	5.435	.615	108.48	.922
20	.450	6.522	.738	111.89	.951
21	.525	7.609	.861	114.47	.973
22	.600	8.696	.984	116.23	.988
23	.675	9.783	1.107	117.16	.996
24	.750	10.870	1.230	117.41	.998
25	.825	11.957	1.352	117.61	1.000
26	.900	13.043	1.475	117.61	1.000

UMEAN PROFILE - K=0.28E-6, F=0.0000 RUN

RUN	=	043075	DE1	=	.091
PLATE	=	12	DE2	=	.065
X	=	46	H	=	1.40
UINF	=	126.72	G	=	5.09
CF/2	=	.00313	BETA	=	-.56
UTAU	=	7.09	REDE2	=	4242.
F	=	0.0000	REK	=	113.
DE	=	.603	K	=	.292E-06

PT	Y	Y/DE2	Y/DE	U	U/UINF
1	.006	.092	.010	50.83	.401
2	.008	.123	.013	53.64	.423
3	.010	.154	.017	56.21	.444
4	.013	.200	.022	59.53	.470
5	.017	.262	.028	63.28	.499
6	.022	.338	.036	67.15	.530
7	.028	.431	.046	70.32	.555
8	.035	.538	.058	73.87	.583
9	.045	.692	.075	78.06	.616
10	.060	.923	.100	83.14	.656
11	.080	1.231	.133	88.27	.697
12	.105	1.615	.174	93.18	.735
13	.130	2.000	.216	97.03	.766
14	.155	2.385	.257	100.41	.792
15	.190	2.923	.315	104.35	.823
16	.225	3.462	.373	107.76	.850
17	.275	4.231	.456	111.67	.881
18	.325	5.000	.539	115.00	.908
19	.375	5.769	.622	117.93	.931
20	.450	6.923	.746	121.39	.958
21	.525	8.077	.871	123.74	.976
22	.600	9.231	.995	125.39	.990
23	.675	10.385	1.119	126.14	.995
24	.750	11.538	1.244	126.52	.998
25	.825	12.692	1.368	126.72	1.000
26	.900	13.846	1.493	126.72	1.000

REYNOLDS STRESS TENSOR COMPONENTS - KR=0.29E-3, F=0.0039 RUN

RUN	=	030675	CF/2	=	.00161	DE1	=	.197	BETA	=	-1.44
PLATE	=	11	UTAU	=	4.44	DE2	=	.131	REDE2	=	7524.
X	=	42	F	=	.0039	H	=	1.50	REK	=	72.
UINF	=	110.67	DE	=	1.019	G	=	8.35	KR	=	.294E-03

Y	Y/DE	U	UP2/UI2	VP2/UI2	WP2/UI2	-UV/UI2	Q2/UI2	RUV	RQ2
.008	.008	33.06	.00836						
.013	.013	36.92	.00889						
.023	.023	42.63	.00969						
.032	.031	46.28	.01031						
.046	.045	50.88	.01088						
.065	.064	56.16	.01135						
.075	.074	58.21	.01141						
.087	.085	60.64	.01147						
.100	.098	62.89	.01145						
.115	.113	65.44	.01136						
.130	.128	67.73	.01117	.00318	.00525	.00271	.01960	.455	.138
.150	.147	70.15	.01091	.00301	.00513	.00269	.01905	.469	.141
.195	.191	74.68	.01000	.00304	.00463	.00261	.01767	.473	.148
.295	.289	82.75	.00813	.00270	.00381	.00224	.01464	.478	.153
.390	.383	88.60	.00667	.00215	.00314	.00186	.01196	.491	.156
.550	.540	96.44	.00452	.00167	.00233	.00133	.00852	.484	.156
.700	.687	102.38	.00297	.00118	.00158	.00089	.00573	.475	.155
.900	.883	107.80	.00122	.00070	.00065	.00037	.00257	.400	.144
1.100	1.079	110.24	.00024	.00024	.00015	.00007	.00063	.292	.111

REYNOLDS STRESS TENSOR COMPONENTS - K=0.28E-6, F=0.0000 RUN

RUN	=	050375	CF/2	=	.00305	DE1	=	.098	BETA	=	-.57
PLATE	=	11	UTAU	=	6.42	DE2	=	.069	REDE2	=	4189.
X	=	42	F	=	0.0000	H	=	1.42	REK	=	104.
UINF	=	116.23	DE	=	.610	G	=	5.33	K	=	.292E-06

Y	Y/DE	U	UP2/UI2	VP2/UI2	WP2/UI2	-UV/UI2	Q2/UI2	RUV	RQ2
.006	.010	45.74	.00768						
.010	.016	50.22	.00801						
.017	.028	56.04	.00865						
.028	.046	62.70	.00922						
.035	.057	65.95	.00932						
.045	.074	69.77	.00931						
.060	.098	74.29	.00911						
.080	.131	79.03	.00869						
.105	.172	83.47	.00808						
.130	.213	87.43	.00742	.00208	.00309	.00185	.01259	.471	.147
.155	.254	90.56	.00677	.00175	.00282	.00164	.01134	.476	.145
.190	.311	94.55	.00581	.00156	.00249	.00145	.00986	.482	.147
.225	.369	97.68	.00494	.00159	.00219	.00131	.00872	.467	.150
.275	.451	101.69	.00391	.00128	.00181	.00102	.00700	.456	.146
.325	.533	104.88	.00306	.00097	.00144	.00080	.00547	.464	.146
.375	.615	107.61	.00236	.00082	.00109	.00063	.00427	.453	.148
.450	.738	110.82	.00156	.00053	.00067	.00040	.00276	.440	.145
.525	.861	113.34	.00087	.00040	.00043	.00024	.00170	.407	.141
.600	.984	114.85	.00041						

UNLIMITED RELEASE

INITIAL DISTRIBUTION

T. B. Lane, 1280
R. C. Maydew, 1330, Attn: S. McAlees, 1333
E. D. Reed, 2000, Attn: W. J. Spencer, 2100
K. J. Touryan, 5260
T. B. Cook, Jr., 8000, Attn: C. H. DeSelm, 8200,
W. C. Scrivner, 8400
L. Gutierrez, 8100, Attn: W. E. Alzheimer, 8120,
D. E. Gregson, 8150,
R. D. Cozine, 8160,
C. S. Selvage, 8180
A. N. Blackwell, 8110, Attn: A. F. Baker, 8111,
C. W. Robinson, 8116
H. W. Coleman, 8115
D. L. Hartley, 8115 (2)
B. F. Murphey, 8300
J. L. Wirth, 8340
A. R. Willis, 8344
J. F. Barham, 8360, Attn: G. R. Otey, 8362
Technical Publications and Art Division, 8265, for TIC (2)
F. J. Cupps, 8265/Classification and Technical Library Processing Division, 3141
Classification and Technical Library Processing Division, 3141 (4)
Library and Security Classification Division, 8266-2 (5)

HWC:8115:sh